

1 **Referee#1**

2 ---

3 General comments:

4

5 A better knowledge of the radiative influence of the aerosols on the Mediterranean climate is  
6 important to estimate their impact on the global warming. The Mediterranean region is rich in a  
7 variety of particles from both continental and marine sources. This paper presents the first results  
8 of an ambitious experimental campaign, based on surface and aircraft observations that propose a  
9 rather complete view of the physiochemical and optical properties of the Mediterranean aerosol.  
10 In addition, the data analysis takes benefit of the expertise from a large group of recognized  
11 scientists. Although we could discuss of the relevance of such a long paper, this manuscript brings  
12 valuable advanced results on the aerosol properties across the Mediterranean basin. However,  
13 some questions arise when reading the manuscript. First of all, if the objectives of the  
14 ChArMEx/ADRI MED project are well-presented in the introduction, the aim and the borders of the  
15 paper should be better précised, more particularly in view of the fact that the authors continuously  
16 refer along the paper to other published results on the same topics (for instance, Section 5.4.1  
17 mainly deals with the results of Nicolas et al. (2015) and Meloni et al. (2015)). Few parts of the  
18 manuscript looks like a compilation of results which could have been more synthesized. In  
19 particular, our understanding would gain a lot if the authors could provide a synthesis of the  
20 different results they obtained to make the reader see how to relate them, as for the AOD data in  
21 Section 5.2 or for estimates of the radiative forcing reported in Section 5.4. In addition, the authors  
22 present the analysis of the aerosol composition in Section 5.1.4 and the CHIMERE calculations in  
23 Section 6.2, but any link is made between the two sections. By the way, the comparison between  
24 the different regional models reported in Section 6 does not seem really useful for this paper since  
25 all models did not take into account aerosol species in a similar way. I also think that the  
26 manuscript could be improved thanks to a more rigorous comparison between the aerosol  
27 characteristics at the different sites. To my opinion, the major interest of the paper deals with the  
28 estimates of the local radiative forcing and the large dataset concerning the aerosol extinction  
29 provided using different instruments and methods. It is clear that this paper merits publication in  
30 ACP. I would recommend, however, a revision of the manuscript in view of the comments that I  
31 have listed below.

32 ***First, we'd like to thank the reviewer for these constructive remarks and comments on the article. We***  
33 ***have tried to take into account most of the comments to improve the resubmitted manuscript. The***  
34 ***detailed answers are provided hereafter.***

35

36 Major concerns:

37

38 p. 19642: The description of the general meteorological conditions seems incomplete. In spite of  
39 the figure 8, too small and providing pressure by the way, the wind speed, which is the key  
40 parameter of the aerosol transport is not really given with a sufficient precision in any part of the  
41 text.

42 ***The wind intensity and direction were indicated in the Figure 7 for three different stations and in the***  
43 ***Figure 8 at the altitude of 700 hPa but we agree that this important meteorological parameter should be***  
44 ***more detailed. In that sense, we have included in the revised manuscript the vertical profiles of the wind***  
45 ***intensity at the three different stations (Ersa, Lampedusa and Minorca) in the new Figure 8 for all the***  
46 ***ChArMEx/ADRI MED period. In addition, a new paragraph discussing the wind speed intensity during the***  
47 ***observed period of important sea-spray concentration at Ersa has been included (part 5.2.1).***

48

49 p. 19645: The comparison between the two coastal sites, i.e., Lampedusa and Ersa indicates a  
50 significantly higher mass concentration in Lampedusa. One can expect that the surplus in aerosol

51 concentrations measured in Lampedusa is rather due to height above the sea of the aerosol  
52 acquisition, which was closer to the sea surface in Lampedusa than in Ersa. In particular, if we  
53 consider that the sea-spray aerosols issued from breaking waves can largely contribute to the  
54 PM10 concentrations in the lower layer in such marine environments, a correction factor could be  
55 easily used for an accurate comparison by assuming an exponential decay of aerosol  
56 concentrations with altitude. The vertical profiles of aerosol concentrations can be then modelled  
57 using Toba (1965) as a kernel. The authors can also use the work of Piazzola et al. (2015) who  
58 approached the concentrations decay with altitude by a logarithmic law using vertical aerosol  
59 profiles measured in the Indian Ocean compared to data obtained from the CALIOP level2  
60 operational products. I would suggest the authors to use this kind of corrective factor to ensure an  
61 accurate comparison between the two sites. This remarks can also be considered for the  
62 comparison between the volume distributions at four different sites reported in p. 19646.

63 ***Thank you for this interesting remark; this is effectively right and we have now used the logarithm law***  
64 ***proposed by Piazzola et al. (2015) for estimating the concentration of aerosols at the Ersa station for an***  
65 ***altitude of 50 m, which is close to the altitude of Lampedusa (45 m). The calculation has been made using***  
66 ***the value of 0.75 for the coefficient  $s$  (that corresponds to particle sizes higher than  $0.5 \mu\text{m}$ , see the Figure***  
67 ***8 of Piazzola et al., 2015) for sea-spray aerosols. By applying this correction, the corrected mean PM10***  
68 ***aerosol mass concentration is  $12 \mu\text{g m}^{-3}$ , closer to the value observed at the Lampedusa station. We have***  
69 ***now indicated this point in the text and in the new figure (including one additional curve).***

70  
71 ***In addition, we have now also added a new paragraph on this specific point in the section 5.1.1: "In order***  
72 ***to take into account the difference of altitudes between the two sites of Lampedusa and Ersa, we have***  
73 ***applied a correction factor to PM10 observed at Ersa (530 m) for estimating a new PM10 concentration***  
74 ***corresponding to the altitude of Lampedusa. In that sense, we have applied the logarithmic law reported***  
75 ***by Piazzola et al. (2015) using a value of 0.75 for the factor  $s$  to correct the mass concentration of sea***  
76 ***spray aerosols only. The calculated mean value of PM10 at 45 m is about  $12 \mu\text{g m}^{-3}$  (Figure 13), closer to***  
77 ***the mean value observed at Lampedusa ( $21 \mu\text{g m}^{-3}$ ). A new caption has also been added for the Figure 13.***

78  
79 ***It should be noted that the same corrections have been now applied to the concentration of the coarse***  
80 ***mode estimated from sun-photometer observations at Ersa. The value is now reported in the Table 6,***  
81 ***using the value of 0.75 for the coefficient  $s$ . This point is now also mentioned in the text in the section***  
82 ***5.1.2.***

83  
84 p. 19646: The impact of the convective processes on the concentrations of anthropogenic aerosols  
85 could have been evaluated through the survey of the air-sea temperature difference. This induces  
86 a seasonal variation of the anthropogenic aerosols which can explain the differences noted with  
87 the ESCOMPTE campaign. This should be included in the analysis of meteorological conditions to  
88 produce large concentrations of polluted-smoke particles.

89 ***To our point of view, this aspect is already discussed in the parts 4.1 and 4.2 of the article, where we have***  
90 ***demonstrated that the meteorological field (surface temperature, synoptic situations) observed during***  
91 ***the SOP-1a campaign were not favourable to produce large concentration of secondary polluted or smoke***  
92 ***aerosols. Such meteorological situations are indeed very different with those observed during the***  
93 ***ESCOMPTE campaign, where AOD as large as 0.3-0.5 (in the visible range) has been observed due to the***  
94 ***important concentration of anthropogenic-polluted particles. This point has now been reinforced in the***  
95 ***part 5.1.4 of the new version, where comparisons with the ESCOMPTE observations are mentioned.***

96  
97 p. 19648-49 : By the way, the comparison of the Ersa and Lampedusa chemical analysis with the  
98 data reported during the ESCOMPTE campaign does not seems appropriate. The authors should  
99 rather compare their results to sites with quite similar character, whether it is located in the  
100 Eastern (see, Eleftheriadis et al. 2006; Bardouki et al. 2003) or in the Western Mediterranean (e.g.,  
101 Piazzola et al., 2012; Sellegri et al., 2001).

102 ***This is effectively right and we have now included some comparisons with the data reported in the***

103 *different references listed by the reviewer, which are more appropriated than those obtained during the*  
104 *ESCOMPTE project. However and as mentioned in the article, we have chosen to focus our discussions on*  
105 *the BC and OC mass size distribution as such measurements are original and scarce over the*  
106 *Mediterranean compared to other aerosol species (as sulphates, sea-salt, nitrates or ammonium) largely*  
107 *referenced. In that sense, we did not use the Bardouki et al. and Sellegri et al. papers, which are mainly*  
108 *focused on inorganic species but we used the Eleftheriadis et al. (2006) work, which reports BC*  
109 *concentration at the Finokalia remote coastal site and onboard the R/V “Aegaeon”. We have also used*  
110 *the Piazzola et al. (2012) and Mallet et al. (2011) works, which report aerosol mass size distributions of BC*  
111 *and OC aerosols at the Porquerolles coastal island (southeast France). Comparisons are focused on the*  
112 *different modes of the BC and OC mass size distributions. This point is now integrated in the article in the*  
113 *part 5.1.4. The following sentence has been added:*

114 *“It should be also noted that the EC concentrations observed at the Ersa station are logically (due at least*  
115 *to the altitude of the station and the absence of intense pollution during the SOP-1a, see section 4) lower*  
116 *(0.39  $\mu\text{g.m}^{-3}$ ) than EC concentrations (PM<sub>2.1</sub>) reported by Eleftheriadis et al. (2006) from the eastern*  
117 *Mediterranean during the summer season (0.60  $\mu\text{g.m}^{-3}$ ) in July 2000. The same ascertainment is obtained*  
118 *on OC concentrations with higher values (4.2  $\mu\text{g.m}^{-3}$ ) reported by Eleftheriadis et al. (2006) compared to*  
119 *observations in Ersa (1.5  $\mu\text{g.m}^{-3}$ ). Concerning the modes of the OC and EC particle mass size distributions,*  
120 *the two identified modes detected in Ersa are consistent with those reported by Mallet et al. (2011) at the*  
121 *Porquerolles coastal island (south eastern France), who also detected two (fine and coarse) different*  
122 *modes of the mass size distributions for EC (0.3-0.4  $\mu\text{m}$  and 4-6  $\mu\text{m}$ ) and OC (0.3  $\mu\text{m}$  and 5-6  $\mu\text{m}$ ) aerosol*  
123 *particles.”*

124

125 P. 19653: The authors explained the low values of the SSA measured in Lampedusa by the  
126 contribution of the coarse mode to the total size distribution, which is attributed to the dust  
127 aerosols. Would it be possible that the sea-spray production at the air-sea interface (see next  
128 comment) also contributes to the decrease of the SSA through the injection of coarse and giant  
129 particles in the MABL?

130 *This is effectively right and the presence of the coarse mode of sea salt aerosols could effectively*  
131 *contribute to the decrease of SSA in the solar spectral region. We have now added this specific point in*  
132 *the new version.*

133

134 p. 19657: The southwest episodes allowing dust transport in the Northern Mediterranean is also  
135 often characterized by the occurrence of strong sea-spray injection in the lower part of the Marine  
136 Atmospheric Layer through breaking waves in addition to deposition fluxes of the dust particles  
137 advected from the Saharan region. This is confirmed by the LNG surface observations reported in  
138 Section 5.3.2. Can we consider that the AOD values measured in these conditions should be due  
139 the combination of dust and strong sea-spray flux occurring at the sea surface? Could the authors  
140 use more the Angstrom coefficient to provide a better analysis?

141 *Effectively, the AOD measured on 19 June and presented in the Section 5.3.2 using LNG observations is the*  
142 *combination of sea-salt aerosols produced at the sea surface associated with the presence of mineral dust*  
143 *transported above the MBL. This point is mentioned in the document:*

144 *“The aerosol extinction is found to be significant around 41 to 41.5° N that could be due to sea-salt*  
145 *particles generated in south Corsica Island due to the local acceleration of the wind occurring between*  
146 *the Corsica and Sardinia islands (not shown). This increase of the aerosol loading in the MBL associated*  
147 *with dust aerosol transported to higher altitudes results in an increase of total AOD at these latitudes.”*

148

149 *In addition, the remark of the reviewer is interesting as we can effectively observe a difference in the*  
150 *daily Angstrom Exponent (AE, calculated between 440 and 870 nm) between the Ersa (AE of 1.0) and the*  
151 *Minorca (AE of 0.5) stations, which are affected by this dust event. However pure sea salt and desert dust*  
152 *have AE in the same range (<0.5) and we cannot conclude that such a difference is due to a larger*  
153 *contribution of sea-salt at Ersa.*

154

155 p. 19666: The main objectives of ten ChArMex project is to investigate how the modifications of  
156 the radiative budget due to aerosols affect the sea-surface evaporation fluxes. Concerning the sea-  
157 spray aerosols, could the impact on the sea-surface evaporation fluxes and relative humidity  
158 profiles be estimated ?

159 ***This interesting question is difficult to answer. To our point of view, the AOD contribution due to sea-salt***  
160 ***is likely too moderate on average for affecting significantly the sea surface temperature, O-A fluxes and***  
161 ***relative humidity profiles, but a firm conclusion would need an important work with specific simulations***  
162 ***which we consider outside of the scope of this paper. The possible impact of sea-salt radiative forcing on***  
163 ***the sea-surface evaporation fluxes and relative humidity profiles should indeed be studied using specific***  
164 ***simulations including only marine aerosols in a coupled Ocean-Atmosphere model.***  
165

166 P. 19658 If a strong contribution of dust aerosols is indeed noted all along the campaign, do these  
167 results allowed to say if it is different from the past, especially if we consider that the  
168 measurement period is known to be the good one (with the autumn season) for Saharan dust  
169 intrusion in the Northern Mediterranean.

170 ***The representativity of our observations obtained during the 2013 summer period compared to other***  
171 ***years and seasons is an interesting scientific question. A specific work-package of the ChArMEX project***  
172 ***dedicated to the variability and trends over the Mediterranean is on-going to investigate this point.***  
173 ***Nevertheless and as mentioned in the part 4.2 of the article, we have integrated the AOD anomalies of***  
174 ***summer 2013 compared to summer AOD derived from MODIS and MISR data (for the 2000 to 2013***  
175 ***period). Our conclusions were that the aerosol concentrations observed during the SOP-1a were slightly***  
176 ***lower but in the same range of magnitude that usually observed during summer period over the western***  
177 ***Mediterranean. This point is now detailed in the section 4.2.***  
178

179 p. 19651: The results reported in Section 5.2.1, 5.2.2 and 5.2.3 should deserve to be synthesized.  
180 ***As much as possible, we have tried to synthesize and reduce the size of the three different sections in the***  
181 ***new version.***  
182

183 p. 19663: The comparison of the COSMO-MUSCAT with other regional models which does not have  
184 the same characteristics (Table 8) seems inappropriate since all models did not take into account  
185 aerosol species in a similar way. I am not sure that this part of the paper is very useful.

186 ***We propose to let in place this part related to the COSMO-MUSCAT model in the article. We understand***  
187 ***the remark but although COSMO-MUSCAT doesn't take into account all aerosol species (especially***  
188 ***secondary inorganic), this model simulated the dust sources, emission fluxes, size distribution, vertical***  
189 ***profiles and (dry/wet) deposition of dust aerosols (which are the major species in most of the SOP-1a***  
190 ***aerosol events) in a different way than the two other RCM (RegCM and ALADIN) or the CTM CHIMERE***  
191 ***models. In that context, it appears important to us presenting the results obtained with this regional***  
192 ***model.***  
193

194 p. 19669: Some question also deals with the radiative impact of Mediterranean aerosols, the TOA  
195 simulations presented in Fig. 29 at the end of the manuscript, we could expect the authors to  
196 relate their results to the potential changes of the radiative budget due to aerosols in the  
197 Mediterranean or compare them to the work of Nicolas et al. (2015) and Meloni et al. (2015).

198 ***This is a very interesting remark and we have now added some comparisons with the results obtained***  
199 ***from 1-D radiative transfer calculations. In that sense, we focused our discussion on the Nicolas et al.***  
200 ***(2015) work, who performed different simulations using different surface albedo based on the ATR-42***  
201 ***flights above the Balearic islands (flight 29) and the Granada (flight 30) station, which are characterized***  
202 ***by two distinct surface albedo. The inclusion of high surface albedo (0.27 at 870 nm) in the 1-D radiative***  
203 ***transfer model compared to sea-surface albedo (0.02 at 870 nm) decreases the Top Of Atmosphere***  
204 ***radiative effect from forcings weakly (-4 W m<sup>-2</sup>) to significant negative (-10 W m<sup>-2</sup>) values, for the***  
205 ***Granada and Minorca simulations, respectively. Such results are consistent with the 3-D simulations***  
206 ***presented in Fig. 29 and we have now added a sentence on this point in the part 6.5.2:***

207 ***"Such results are consistent with the study of Nicolas et al. (in prep.), who performed two different***  
208 ***simulations using different surface albedo (from marine to continental), based on the ATR-42***  
209 ***observations above the Balearic Islands and the Granada station. The inclusion of high surface albedo***  
210 ***(0.27 at 870 nm) in the 1-D radiative transfer model compared to low sea-surface albedo (0.02 at 870 nm)***  
211 ***contributes to decrease the TOA radiative effect at Granada."***

212

213 p. 19671: The authors concluded "Non negligible aerosol extinctions (about 50 Mm<sup>-1</sup>) have also  
214 been observed within the Marine Boundary Layer (MBL), due to the presence of polluted or  
215 marine aerosols." Maybe I have missed something, but I did not see anything in the manuscript  
216 that permits this conclusion.

217 ***This is effectively right and we have now modified this sentence by removing the term "polluted" and***  
218 ***including the possible contribution of sea-spray aerosols to the aerosol extinction in the MBL. The new***  
219 ***sentence is the following:***

220 ***"Aerosol extinctions measured on-board the ATR-42 show local maxima reaching up to 150 Mm<sup>-1</sup> within***  
221 ***the dust plume, associated to extinctions of about 50 Mm<sup>-1</sup> within the Marine Boundary Layer (MBL)***  
222 ***possibly due to the presence of sea-spray aerosols."***

223

224 Minor concerns:

225

226 p. 19619 and others: I would replace "sea-salt" by "sea-spray."

227 ***This is now done in the new version.***

228

229 p. 19635: A comparison of the aerosol extinction vertical profiles with satellite data, as the CALIOP  
230 outputs could have been interesting.

231 ***This specific comparison is proposed in the work of Nicolas et al. (in prep. in this special issue), which will***  
232 ***be submitted to the ChArMEx special issue as well as the Léon et al. (2015), which will be re-submitted.***

233

234 p. 19646: In parallel, the lowest concentrations are observed at the Ersa station, near the  
235 anthropogenic sources of the southern France and Italy. This is well consistent with the absence of  
236 intense polluted photochemical or smoke aerosol events during the SOP-1a.

237 ***This sentence was effectively not very clear. We have now rephrased it in the new version: "In parallel, the***  
238 ***lowest concentrations are observed at the Ersa station due to the absence of intense polluted***  
239 ***photochemical or smoke aerosol events over southern France and Italy during the SOP-1a."***

240

241 p. 19699: I don't know if it is due to my printed version of the manuscript, but the figures are too  
242 small to be clear.

243 ***We think this is due to the printed version. All the figures have been provided in .eps or .pdf, with an***  
244 ***adapted format.***

245

246 References

247

248 Bardouki, H., Liakakou, H., Economou, C., Scafare, J., Smolik, J., Zdimal, V., Eleftheriadis, K.,  
249 Lazaridis, M., Dye, C., Mihalopoulos, N., 2003. Chemical composition of size resolved atmospheric  
250 aerosols in the eastern Mediterranean during summer and winter. Atmospheric Environment, 37,  
251 195-208.

252

253 Eleftheriadis, K., I. Colbeck, I., C. Housiadaa, C., M. Lazaridis, M., N. Mihalopoulos, N., C. Mitsakou,  
254 C., J. Smolá'sk, J., and V. Zdá'smal, V. (2006). Size distribution, composition and origin of the  
255 submicron aerosol in the marine boundary layer during the eastern Mediterranean "SUB-AERO"  
256 experiment. Atmospheric Environment, 40, 6245–6260.

257

258 Meloni, D., Junkermann, W., di Sarra, A., Cacciani, M., De Silvestri, L., Di Iorio, T., Estellés, V.,  
259 Gómez-Amo, J. L., Pace, G., and Sferlazzo, D. M.: Altitude-resolved shortwave and longwave  
260 radiative effects of desert dust in the Mediterranean during the GAMARF campaign: indications of  
261 a net daily cooling in the dust layer, *J. Geophys. Res.-Atmos.*, 120, doi:10.1002/2014JD022312,  
262 2015.

263

264 Nicolas, J., Mallet, M., Roberts, G., Denjean, C., Formenti, P., Fresney, E., Sellegri, K., Borgniez, G.,  
265 Bourriane, T., Pignatelli, B., Torres, B., Dubuisson, P., and Dulac, F.: Aerosol direct radiative forcing at  
266 a regional scale over the western Mediterranean in summer within the ADRIMED project: airborne  
267 observations compared to GAME simulations, *Atmos. Chem. Phys. Discuss.*, in preparation, 2015.

268

269 Piazzola, J., Tedeschi, G., Demoisson, A., 2015. A Model for the Transport of Sea- Spray Aerosols in  
270 the Coastal Zone, *Bound-Lay. Meteorol.* Vol. 155, Issue 2, pp. 329-350, doi10.1007/s10546-014-  
271 9994-3.

272

273 Piazzola, J., Sellegri, K., Bourcier, L., Mallet, M., Tedeschi, G. Missamou, T., 2012. Physicochemical  
274 characteristics of aerosols measured in the spring time in the Mediterranean coastal zone. *Atmos.*  
275 *Environment*, 54, 545–556. doi:10.1016/j.atmosenv.2012.02.057.

276

277 Sellegri, K., Gourdeau, J. ; Putaud, J.-P. ; Despiou, S. 2001 Chemical composition of marine aerosol  
278 in a Mediterranean coastal zone during the FETCH experiment *J. Geophys. Res.* Vol. 106 , No. D11 ,  
279 p. 12023-12038 HTML DOI 10.1029/2000JD900629.

280

281 Toba Y (1965) On the giant sea-salt particles in the atmosphere: II Theory of the Vertical  
282 Distribution in the 10-m Layer Over the Ocean. *Tellus* 17:365-382

283

284

285

286

287

288

289

290

291

292

293

294

295

296

297

298

299

300

301

302

303

304

305

306

307 **Referee#2**

308 ---

309 Review of the submitted paper to ACP “Overview of the Chemistry-Aerosol Mediterranean  
310 Experiment/Aerosol Direct Radiative Forcing on the Mediterranean Climate (ChArMEx/ADRMED)  
311 summer 2013 campaign” by Mallet et al.

312

313 The authors present the overview of the ChArMEx/ADRMED campaign, which investigates the  
314 properties and the radiative effects of aerosols Mediterranean region (mostly Western and Central  
315 parts of it). Unfortunately, during the campaign period no major aerosol events/plumes occurred in  
316 the region in terms of AOD. This manuscript mostly paves the way to the other papers of the way,  
317 so in its current status is light in term of scientific findings, although there is presentation of a lot of  
318 material from different observations/models mostly as capability examples but not necessarily  
319 connected between them (as they refer to different events/periods in general) or answering  
320 specific scientific questions. Thus, at the end the reader is wondering why this paper should be  
321 published. Personally, as a reviewer I see two ways that could improve the paper in order to make  
322 it suitable for publication in ACP. Either strengthen the Introduction section by expanding  
323 significantly the discussion about the rationale of the campaign and the open scientifically  
324 questions that it tries to tackle together with a Conclusion section about the outcomes of the  
325 whole campaign (at least till now) and not just the main findings of this manuscript only. Or  
326 provide more scientific results in sections 5 and 6, which are connected together and not just sub-  
327 sections of the type ‘the instrument/model observed/ simulated this and more deep analysis can  
328 be found in that paper’. I encourage the authors to do the respective work in order to improve the  
329 quality of their paper and see it published.

330

331 *First, we'd like to thank the reviewer for these remarks and comments on the article. We tried to take into*  
332 *account most of the comments to improve the manuscript. In that sense, we have now (i) included two*  
333 *important paragraphs in the introduction (see below), (ii) reinforced the scientific questions and the*  
334 *originality of this project in a broader context and (iii) rephrased the abstract and conclusion parts in that*  
335 *sense. Secondly, we have added different paragraphs in the sections 5 and 6 to provide more scientific*  
336 *results, especially in terms of original aerosol chemical observations (SP2 aircraft measurements of black*  
337 *carbon concentrations), aerosol size distribution (especially for mineral dust aerosols) but also SW and LW*  
338 *radiative fluxes for the estimation of the heating rate vertical profiles. The different answers are detailed*  
339 *in the following parts.*

340

341 Major comments

342

343 1. Page 19621, Line 17-18: “Numerous studies have documented the AOD for polluted  
344 anthropogenic Mediterranean aerosols ...” Why in the introduction there is an overview of the  
345 literature only for AOD? What about other properties of aerosols like single scattering albedo  
346 (SSA), vertical distribution, etc., there is no information about them, but there are also important.

347

348 *This is effectively right and we have now added a large number of references in the new introduction of*  
349 *the manuscript for documenting these two important aerosol properties, which are the aerosol single*  
350 *scattering albedo and the vertical profiles, as mentioned by the reviewer.*

351

352 *1) Concerning the SSA derived over the Mediterranean region, we have now integrated the following*  
353 *paragraphs in the introduction:*

354 *“In addition to AOD, the knowledge of SSA is essential to estimate the aerosol direct and semi-direct*  
355 *radiative forcing. Concerning mineral dust particles observed over the Mediterranean, it should be noted*  
356 *that significant variations in SSA are reported, with values near 1 for purely scattering aerosols, and quite*  
357 *remarkable low values (0.74, 0.77 or 0.81) at Lampedusa (Pace et al., 2006; Meloni et al., 2003). At the*

358 *high altitude Alpine Jungfrauoch station, SSA values are generally higher than 0.9 in case of African dust*  
359 *but occasional SSA as low as 0.75-0.80 are reported by Collaud-Coen et al. (2004). Intermediate values*  
360 *(0.85-0.92) have been also reported over the Mediterranean basin (Kubilay et al., 2003; Meloni et al.,*  
361 *2004; Tafuro et al., 2006; Saha et al., 2008). These estimates clearly indicate that significantly different*  
362 *SSA values are obtained following the dust particle origins and/or possible mixing of mineral dust with*  
363 *other species. For example, Kubilay et al. (2003) underlined the importance of mixing, showing SSA values*  
364 *clearly lower (0.85-0.90) in case of mineral dust transport coincident with urban-industrial aerosols as*  
365 *compared to pure dust (0.96-0.97).*  
366

367 *In addition, SSA observed in case of urban/industrial regimes has been also well documented over the*  
368 *Mediterranean Sea and coastal regions. In most cases, moderate or low SSA (0.78-0.94) is observed due to*  
369 *emissions containing absorbing black carbon aerosols. Over southeastern France, optical computations*  
370 *performed by Saha et al. (2008) and Mallet et al. (2004) indicate SSA values of 0.83 and 0.85 (at 550 nm)*  
371 *near the cities of Marseille and Toulon, respectively. Aircraft observations performed over the*  
372 *Marseille/Etang de Berre area during the ESCOMPTE campaign show values ranging between 0.88 and*  
373 *0.93 (at 550 nm) in the PBL (Mallet et al., 2005). These SSA values are close to those observed in South*  
374 *Spain (0.86-0.90) by Horvarth et al. (2002). Over southeastern Italy, Tafuro et al. (2007) reported a value*  
375 *of 0.94 during summer time corresponding to anthropogenic particles. Finally, polluted particles*  
376 *transported over the Mediterranean basin have also relatively low values as reported by Markowick et al.*  
377 *(2002) over Crete Island (0.87) and by Di Iorio et al. (2003) (0.79-0.83) over the Lampedusa Island for two*  
378 *cases (25 and 27 May 1999) of “aged” anthropogenic aerosols originating from Europe.*  
379

380 *As opposed to dust and polluted aerosols, few studies have derived the biomass burning SSA over the*  
381 *Mediterranean Sea. One estimate has been obtained during STAAARTE-MED by Formenti et al (2002) who*  
382 *reported a mean dry SSA of 0.89 (at 500 nm) for aged smoke from North America. Meloni et al. (2006)*  
383 *report estimations at Lampedusa with values of  $0.82 \pm 0.04$  (at 415 nm) for smoke aerosols over the*  
384 *Mediterranean region. The observed differences between SSA values could be due to the fact that the*  
385 *smoke events described by Meloni et al. (2006) are more “local” and not (or somewhat less) mixed with*  
386 *other secondary species, as compared to biomass burning particles documented by Formenti et al. (2002),*  
387 *which were issued from very distant Canadian fires. Finally, at Palencia (Spain), Cachorro et al. (2008)*  
388 *reported a column-integrated SSA of 0.88 (at 440 nm) for a biomass burning event occurring in July 28,*  
389 *2004. It should be remained that most estimations of SSA over the Mediterranean have been obtained*  
390 *from surface in-situ or remote-sensing techniques. In that sense, this project provides interesting and*  
391 *original observations of 3-D aerosol SSA, allowing investigating changes in its important optical property*  
392 *during the transport of aerosols over the Mediterranean.”*  
393

394 *2) In a second time and for the aerosol vertical profiles, we have now included the following paragraph in*  
395 *the introduction:*

396 *” Concerning the aerosol vertical profiles and apart from a few airborne in-situ measurements (Formenti*  
397 *et al., 2002), most of the available information in the Mediterranean region comes from lidar*  
398 *observations, which provide highly resolved vertical profiles of aerosol backscattering at one or more*  
399 *wavelengths and, depending on the complexity of the instrumental setup, particles depolarization and*  
400 *extinction. Several sites are equipped with aerosol lidar systems and carry out regular observations in a*  
401 *coordinated way within the European aerosol research lidar network EARLINET (Papayannis et al., 2008;*  
402 *Wang et al., 2014).*  
403

404 *Numerous studies have been specifically dedicated to the vertical distribution of Saharan dust during*  
405 *extended time periods and/or selected events from various Mediterranean regions, mainly from ground-*  
406 *based lidar systems: (i) the eastern basin in Thessaloniki (Hamonou et al., 1999; Balis et al., 2004), Crete*  
407 *(Gobbi et al., 2000; Balis et al., 2006), the Aegean sea (Dulac et al., 2003), and Athens plus Thessaloniki*  
408 *(Papayannis et al., 2005; Balis et al., 2006); (ii) the central basin in Lampedusa (Di Sarra et al., 2001;*  
409 *Di Iorio et al., 2003; Meloni et al., 2004), Lecce (Tafuro et al., 2006), and at Etna (Tafuro et al., 2006); and*  
410 *(iii) across the western basin with the first spaceborne lidar (Berthier et al., 2006) and at Observatoire de*  
411 *Haute Provence (Hamonou et al., 1999), and Barcelona (Pérez et al., 2006). Finally, using data from 20*



412 ***EARLINET lidar stations, Papayannis et al. (2008) indicate that African dust transport over the***  
413 ***Mediterranean basin is layered. Their analysis confirms early observations by Hamonou et al. (1999) that***  
414 ***not only different dust layers are superimposed at different altitudes, but that these layers have different***  
415 ***source regions. The dust layers were generally detected between 1.8 and 9 km altitude.***  
416

417 ***Not only desert dust, however, can be transported above the marine atmospheric boundary layer. Balis et***  
418 ***al. (2004) report non-dust aerosols within elevated layers over Thessaloniki, and Formenti et al. (2002)***  
419 ***report a forest fire haze layer from Canada observed from airborne measurements between***  
420 ***approximately 1 and 3.5 km above the northeastern Mediterranean in August 1998. Pérez et al. (2004)***  
421 ***describe the complex interaction among orography, sea-breeze and pollution that cause the recirculation***  
422 ***of pollutants and produce a strong layering with pollution aerosol layers above the boundary layer in the***  
423 ***region of Barcelona. In addition, aerosol plumes are emitted sporadically in the Mediterranean free***  
424 ***troposphere by Etna volcano. Such plumes have been observed to travel at altitudes between 4 and 5 km***  
425 ***(Pappalardo et al., 2004) or above (Sellitto et al., 2015) at relatively short distance from Etna. To***  
426 ***summarize, the lidar observations clearly show that only part of the aerosol transport occurs in the MBL***  
427 ***demonstrating the need of using aircraft observations within the aerosol plume to determine the aerosol***  
428 ***microphysical-chemical and optical properties of particles transported in altitude and so not detectable at***  
429 ***the surface. Indeed, although lidar observations provide obviously crucial information on the aerosol***  
430 ***vertical profiles, most of lidar systems cannot derive information on the aerosol size distribution, optical***  
431 ***properties and chemical composition along the vertical. Such observations can only be obtained using in-***  
432 ***situ aircraft vertical profiles as proposed in this ChArMEx/ADRIMED experiment. As an example, this***  
433 ***project provides interesting and unique observations of 3-D aerosol size distribution during the transport***  
434 ***over the Mediterranean basin, allowing us to investigate changes in size distribution between mixed and***  
435 ***pure mineral dust. “***  
436

437 ***We have now replaced all those information with associated references in a larger context to underline***  
438 ***the interest of building such intensive experimental campaign.***  
439

440 2. Page 19626, Line 1-9: Which are the open scientific questions addressed by the campaign? From  
441 the three main objectives, the first is general applicable to every campaign and the second has  
442 been addressed already in the literature, so which are the novelties except from the application to  
443 a new dataset (although may be more extensive)? The third objective seems more original;  
444 however there is no citing paper in the manuscript trying to explore the questions of this objective.  
445 Someone may say that it is rather early to tackle these questions, something that future papers will  
446 do. However, there is not indication about that in the current manuscript. In any way it is not clear  
447 why this campaign was/had to be organized, except for the obvious reason of providing a new  
448 extensive dataset.

449  
450 ***This remark is effectively right and we did not enough detail this aspect in the previous version. We have***  
451 ***now brought more details in the new version of the article. In that sense, we have now included different***  
452 ***paragraphs before listing the different objectives of the ChArMEX/ADRIMED project to argue for***  
453 ***developing such an intensive experimental campaign over the Western Mediterranean. The two different***  
454 ***paragraphs included in the introduction are the following:***  
455

456 ***1) “It should be remained that most estimations of SSA over the Mediterranean have been obtained from***  
457 ***surface in-situ or remote-sensing techniques. In that sense, this project provides interesting and original***  
458 ***observations of 3-D aerosol SSA, allowing investigating changes in its important optical property during***  
459 ***the transport of aerosols over the Mediterranean.”***  
460

461 ***2) “To summarize, the lidar observations clearly show that only part of the aerosol transport occurs in the***  
462 ***MBL demonstrating the need of using aircraft observations within the aerosol plume to determine the***  
463 ***aerosol microphysical-chemical and optical properties of particles transported in altitude and so not***  
464 ***detectable at the surface. Indeed, although lidar observations provide obviously crucial information on***

465 *the aerosol vertical profiles, most of lidar systems cannot derive information on the aerosol size*  
466 *distribution, optical properties and chemical composition along the vertical. Such observations can only*  
467 *be obtained using in-situ aircraft vertical profiles as proposed in this ChArMEX/ADRIMED experiment. As*  
468 *an example, this project provides interesting and unique observations of 3-D aerosol size distribution*  
469 *during the transport over the Mediterranean basin, allowing us to investigate changes in size distribution*  
470 *between mixed and pure mineral dust.”*

471  
472 *Concerning the third mentioned objectives, we agree with the reviewer that this original aspect was not*  
473 *enough detailed in the previous version and we have now introduced more details and some results*  
474 *based especially on the work of Nabat et al. (2015a). For that, we have now included a new paragraph in*  
475 *the section 6.4 to present some results of the climatic simulation conducted for the 2003 to 2009 period by*  
476 *Nabat et al. (2015a). This simulation uses, for the first time to our knowledge in the Mediterranean*  
477 *region, a regional Ocean-Atmosphere (O-A) coupled system model for investigating the effect of aerosol*  
478 *radiative forcing on the Sea Surface Temperature (SST), O-A fluxes (especially latent heat fluxes) and*  
479 *hydrological cycle over the Mediterranean. A new figure (Figure 29), showing changes in SST, AO fluxes*  
480 *and precipitations between two simulations (including or not aerosols) has been included in the new*  
481 *version. We have also mentioned this original result in the introduction and in the conclusion.*

482  
483 *The new paragraph is the following:*  
484 *“Using CNRM-RCSM with the new AOD monthly climatology over the period 2003-2009 (Nabat et al.,*  
485 *2013), Nabat et al. (2015a) have notably highlighted the response of the Mediterranean SST to the*  
486 *aerosol forcing. Figure 29a presents the annual average difference in SST over the period 2003-2009*  
487 *between a simulation ensemble including aerosols and a second one without any aerosol. Aerosols are*  
488 *found to induce an average decrease in SST by 0.5°C, because of the scattering and absorption of incident*  
489 *radiation. As a consequence, the latent heat loss is also reduced by aerosols (Figure 29b), as well as*  
490 *precipitation (Figure 29c). This result also underlines the importance of taking into account the ocean-*  
491 *atmosphere coupling in regional aerosol-climate studies over the Mediterranean.”*

492  
493 3. Which of the results summarized in the Conclusions section is new or even important for the  
494 Mediterranean region? Just by comparing with the existing references used in the Introduction and  
495 the other sections of the manuscript it is not clear what this paper adds on the existing literature.

496  
497 *As mentioned above, most of previous observations of aerosol microphysical, chemical and optical*  
498 *properties have been made in the Mediterranean region using remote-sensing techniques or surface in-*  
499 *situ observations (except the STAAARTE-MED and MINOS experiments in the eastern basin). In that*  
500 *context, such a new campaign offers a unique 3-D distribution of aerosol properties over the western*  
501 *Mediterranean using fully-equipped aircraft and surface observations. More particularly, this project has*  
502 *allowed us to derive the vertical structure of aerosol optical properties (real and imaginary part of*  
503 *refractive index, asymmetry parameter, single scattering albedo and mass extinction efficiency for*  
504 *different aerosol cases, which was really new over the Mediterranean. This database allows one (i) to*  
505 *investigate the variability of dust SSA obtained during the experiment and (ii) to make comparisons*  
506 *between SSA obtained during the transport of dust over the Mediterranean basin and those referenced*  
507 *near dust sources. Those different points are now reinforced in the abstract and conclusion of the new*  
508 *version.*

509  
510 *Added-value also concerns the characterization of the aerosol size distribution. Indeed, the*  
511 *ChArMEX/ADRIMED project has allowed us investigating (i) the vertical structure of the aerosol size*  
512 *distribution, (ii) the changes in the size distribution between mixed and pure dust particles, especially in*  
513 *terms of fine and coarse mode effective diameter during the transport over the Mediterranean and finally*  
514 *(iii) to compare the dust size distribution obtained over the Mediterranean with those referenced over*  
515 *dust source regions (FENNEC, SAMUM1 and AMMA projects), as well as measurements in the Atlantic*  
516 *Ocean at Cape-Verde region (SAMUM-2) and at Puerto-Rico (PRIDE). Such observations can also provide*  
517 *some information on the CCN and IN properties of mineral dust for the modelling community. As for the*

518 *aerosol optical properties, this specific point is now reinforced in the introduction, conclusion and in a*  
519 *new paragraph of the section 5.1.3.*

520 *In terms of aerosol direct forcing, an original aspect of this project concerns the estimation of the SW and*  
521 *LW heating rate along the vertical, which are directly deduced from observations of downward and*  
522 *upward radiative fluxes on board the ATR-42 aircraft. Our observations reveal instantaneous SW heating*  
523 *rate of about 5°K per day within the mineral dust layer, associated to a cooling (2-3 °K per day) in the LW*  
524 *spectral region. An interesting perspective is now to investigate the ability of the different models*  
525 *involved in the ChArMEx/ADRIMED project to reproduce this important radiative property, which controls,*  
526 *for a part, the semi-direct effect of mineral dust. This point is now more detailed in the abstract and*  
527 *conclusion of the new version. In addition, a specific section (5.4.4) associated to a new figure (Figure 28)*  
528 *have been added in the discussion to show an example of SW and LW heating rate profiles estimated for*  
529 *the 22 June. This case has been chosen as already discussed (see the Figure 21) in the text.*

530

531 *Another originality of this project concerns the SP2 observations deployed onboard the ATR-42 aircraft.*  
532 *This point was not enough detailed in the previous version and we have now provided a new paragraph*  
533 *of results of rBC concentrations obtained during the SOP-1a campaign in the section 5.1.4. A new figure*  
534 *(Figure 17), showing the vertical profiles of rBC concentration for five different regions, has been added in*  
535 *the new version.*

536

537 *Finally, the last original aspect of this project concerns the observations of aerosol chemical properties*  
538 *estimated from the C-TOF-AMS and PM10-PILS measurements at the Lampedusa and Ersa stations. The*  
539 *analysis and results of these instrumentations are not detailed in the new version but we have clearly*  
540 *mentioned the link with dedicated articles (Claeys et al., and Formenti et al.) which analysed these*  
541 *observations.*

542

543 *To our knowledge and in addition to “classical” observations over the Mediterranean, all those mentioned*  
544 *information listed above are really new and original. In that sense, those aspects are now reinforced in*  
545 *the abstract and conclusion as well as in different paragraphs of the new version.*

546

547 Minor comments

548

549 1. Page 19621, Line 22: AOD value of 0.1 you do not call it moderate but low, please rephrase.  
550 ***This is now changed in the text by including “low to moderate...”***

551

552 2. Page 19621, Line 27-28: “... only few studies have been dedicated to biomass burning aerosols  
553 ...”. I do not think it is the case, see e.g. Amiridis et al. (2012), Baldassarre et al. (2015), Barnaba et  
554 al. (2011), Kaskaoutis et al. (2011), Liu et al. (2009), Markowicz et al. (2002 – which is cited in the  
555 manuscript), Ravetta et al. (2007). Please rephrase and add references accordingly.  
556 ***Thank you for this remark. This is now changed in the text and all references have been added.***

557

558 3. Page 19624, Lines 4-11: Additional papers dealing with the radiative effects of smoke aerosols  
559 are: Markowicz et al. (2002), di Sarra et al. (2008) (both of them cited in the manuscript) and  
560 Kaskaoutis et al. (2011). Please rephrase and add references accordingly.  
561 ***Thank you. This is now changed in the text of the new version.***

562

563 4. Page 19626, Line 2: “... an innovative database ...” I agree that the database is rich, but what is  
564 the innovation about it?  
565 ***We agree that the term “innovative” is not adapted. In that sense, we modified this part to moderate our***  
566 ***message and underline what is really original and new to our point of view. As mentioned above, the new***  
567 ***paragraph is the following:***  
568 ***“In that context, the main objectives of the ADRIMED/ChArMEx project are the following:***  
569 ***- to conduct an experimental campaign, based on surface and aircraft observations, for creating a huge 3-***

570 ***D database of physical, chemical and optical properties of the main Mediterranean aerosols, including (i)***  
571 ***original in-situ aircraft observations of extinction coefficients, size distribution, black carbon***  
572 ***concentrations as well as (SW and LW) radiative fluxes and associated heating rates, (ii) balloons***  
573 ***observations of aerosol size distribution and (iii) surface measurements including original***  
574 ***characterization of chemical properties***  
575 ***- to investigate how the aerosol size distribution and optical (especially SSA) properties evolve along the***  
576 ***vertical, between the MBL and elevated layers, and during the transport over the Mediterranean***  
577 ***- to use experimental surface and aircraft observations to estimate the 1D-local DRF and forcing efficiency***  
578 ***of different aerosols at the surface, TOA and within the atmospheric layer***  
579 ***- to investigate how the modifications of the radiative budget due to aerosols affect the sea-surface***  
580 ***evaporation fluxes, relative humidity profiles, cloud-cover, precipitation and more largely the***  
581 ***Mediterranean hydrological cycle”***  
582  
583 5. Page 19627, Lines 18-20: “The Capre Corsica ... in-situ measurements”. Please rephrase as the  
584 statements “remote site” and “important local anthropogenic sources” are contradictory.  
585 ***This sentence is now changed in the new version: “The Cape Corsica peninsula is a remote site ensuring***  
586 ***that the in-situ measurements are not contaminated by local anthropogenic pollution.”***  
587  
588 6. Page 19633, Line 22: “... see also description in Dubovik et al., 2011”. This paper is not relevant  
589 to currently available AERONET products, as it is about spectral multiangle polarimetric satellite  
590 observations from POLDER/PARASOL.  
591 ***This is effectively right and this reference is now removed in the new version.***  
592  
593 7. Page 19634, Lines 11-25: What’s the point of the EARLINET/ACTRIS network section as the 4  
594 stations operated only for 1-2 days during the campaign and none of their data is presented in the  
595 manuscript. I suggest either to eliminate or to reduce significantly.  
596 ***If the reviewer agrees, we prefer keeping this part in the article as a study is ongoing to compare aircraft***  
597 ***observations with lidar retrievals. However, we agree that the part was too long and in that sense, we***  
598 ***have now reduced it in the new version.***  
599  
600 8. Page 19638, Line 24: Not all the balloons had ozone sondes, modify accordingly.  
601 ***This is effectively right and now modified in the text: “... respectively coupled, for certain flights (see***  
602 ***Tables 4 and 5***, to an ozone electrochemical sonde (Gheusi et al., in prep. in this special issue)...”  
603  
604 9. Page 19639, Line 26: Add references for the satellite retrievals.  
605 ***All the references; Tanré et al. (1997), Tanré et al. (2011), Khan et al. (2010) and Thieleux et al. (2005)***  
606 ***have now been cited for the MODIS, PARASOL, MISR and SEVIRI sensors, respectively.***  
607  
608 10. Page 19640, Line 9: “... anthropogenic aerosols over the Mediterranean.” Delete as in the  
609 subsequent discussion in this section there is nothing about anthropogenic aerosols. Otherwise  
610 add some text.  
611 ***This part is now removed in the new version.***  
612  
613 11. Page 19640, Line 23, Page 19641, Line 3 and Line 21: Provide AOD values for SEVIRI.  
614 ***AOD SEVIRI values are now added in the new version.***  
615  
616 12. Page 19642, Line 6 and 25: Provide references for NCEP reanalysis and CRU data.  
617 ***The two references for NCEP (Kalnay et al., 1996) and CRU (Harris et al., 2013) data are now included in***  
618 ***the text.***  
619  
620 ***Kalnay et al., The NCEP/NCAR 40-year reanalysis project, Bull. Amer. Meteor. Soc., 77, 437-470, 1996.***  
621 ***Harris I, Jones P, Osborn T, Lister D., Updated high-resolution grids of monthly climatic observations—the***

622 *cru ts3.10 dataset. Int J Climatol 34:623–642. doi:10.1002/joc.3711, 2013.*  
623

624 13. Page 19643, Lines 19-21: State explicitly the period for which the anomalies have been  
625 calculated, i.e. 2000-2013?  
626 ***The anomaly has been effectively calculated for the period 2000-2013. This is now included in the text.***  
627

628 14. Page 19643, Line 27: Why unexpected? Both Formenti et al. (2002) (cited in the manuscript)  
629 and Ravetta et al. (2007) presented similar cases.  
630 ***We used “unexpected” to refer to aerosols event which was not one of the main objectives of ADRIMED,***  
631 ***but the term is not adapted. We have now removed it in the new version.***  
632

633 15. Page 19645, Line 5: Why there are gaps for the observations of PM10 at Ersa in Fig. 13?  
634 ***This is unfortunately due to a problem of data acquisition on this instrument. This has been specified in***  
635 ***the figure legend.***  
636

637 16. Page 19645, Lines 8-10: Give the values of PM10 at Lampedusa as done for Ersa and not PM40.  
638 ***This is effectively a good remark. We have now changed it to indicate PM10 concentrations.***  
639

640 17. Page 19645, Line 11: Add “of PM40” after “significant peak”.  
641 ***This is now included.***  
642

643 18. Page 19646, Lines 11-15: Why the number of samples is not the same for the Ersa and Cap d’En  
644 Font stations in Fig. 14 and Tab. 6 ?  
645 ***There was effectively an error. This is now modified in the Table 6.***  
646

647 19. Page 19647, Lines 6-8: It is not evident why at Lampedusa there is important variability for the  
648 size of the coarse mode. The other sites have similar variability. Be more specific and may be add  
649 some text.  
650 ***The variability in the coarse mode size is about  $\pm 0.05 \mu\text{m}$  at Lampedusa, which is slightly higher compared***  
651 ***to Cagliari and Cap d’En Font ( $\pm 0.03 \mu\text{m}$ ) or Ersa ( $\pm 0.01 \mu\text{m}$ ) stations. This is certainly due to the proximity***  
652 ***of this station to dust sources compared to the other sites. Anyway, we agree that the term “important” is***  
653 ***not adapted and we remove it in the new version. The standard deviation of the derived coarse mode is***  
654 ***now indicated in the text.***  
655

656 20. Page 19652, Lines 8-10: Why present data for these AERONET stations?  
657 ***This was effectively not very clear. The idea is to use different observations for AERONET/PHOTONS***  
658 ***stations located within the “ADRIMED domain” and characterized by different aerosol regimes (see Table***  
659 ***2) in order to (i) characterize the aerosol optical properties over the studied region, (ii) to use such***  
660 ***observations for evaluating the different models involved in this project (see Menut et al., 2015). We have***  
661 ***now added a paragraph to argue about the use of these stations in the new version. The new paragraph***  
662 ***is the following:***  
663 ***“These AERONET/PHOTONS stations have been chosen as located in a domain encompassing most of the***  
664 ***ADRIMED in-situ and remote sensing observations (Figure 3) and they are characterized by different***  
665 ***aerosol regimes (see Table 2).”***  
666

667 21. Page 19652, Lines 8-10: The following AERONET stations Oujda, Cagliari, Cap d’En Font,  
668 Ouarzazate, Frioul and Majorque while appear in Figs. 18 and 25, there are missing from Tab. 2.  
669 ***This is effectively true and we have now completed the Table 2.***  
670

671 22. Page 19653, Line 8: Delete Tab.7 as the all the information exists in Fig. 19.  
672 ***This is effectively right and we have now removed the Table 7.***

673

674 23. Page 19656, Lines 15-18: Certainly the wavelength dependence is lower than below the 2 km,  
675 but it is not very small, as someone can see just above and below the peak at about 3 km. Why this  
676 happens?

677 *The reviewer correctly remarks that there is a relatively large variability in the backscattering coefficient*  
678 *wavelength dependence at the altitudes where desert dust is expected. This is apparent in figure 22 b),*  
679 *with layers characterized by high values of backscattering coefficient displaying a small wavelength*  
680 *dependence, and intermediate layers with a moderate dependence. This suggests a variability in the*  
681 *aerosol size distribution and/or refractive index/shape. We do not have additional information that*  
682 *allows us to interpret this variability. In any case, all the particles below approximately 2 km display a*  
683 *significantly larger wavelength dependence, suggesting markedly different optical properties. A similar*  
684 *vertical variability of the wavelength dependence is observed, for instance, in figure 20 for the scattering*  
685 *coefficient profile measured over Lampedusa on 22 June; as discussed in section 5.2.3, particles of*  
686 *different origin and optical properties may be identified at the various altitudes.*

687

688 24. Page 19657, Lines 6-8: Is the LNG cross section in Fig. 23 correct? It seems from the text and  
689 the AOD figure below that the latitude axis is inverted.

690 *There was effectively a mistake and the Figure 23 corresponds to the flight from Sardinia to the Gulf of*  
691 *Genoa. This is now changed in the text.*

692

693 25. Page 19661, Line 15: An AOD of 0.28 is not moderately high, especially for Lampedusa. Delete  
694 the word "high".

695 *This is now modified in the new version.*

696

697 26. Page 19666, Line 24: Provide the information of the visible range wavelengths for each of the  
698 models in Figure 27.

699 *This information is now provided in the new version.*

700

701 27. Page 19669, Line 20: Delete "vegetation fires", as no fires occurred during the campaign  
702 according to the previous sections of the manuscript.

703 *These terms are now removed in the new version.*

704

705 28. Page 19670, Lines 24-27: As it is written the phrase does not make sense to me, while I am  
706 looking at Fig. 29. Please provide more explicitly the type of surface (desert, sea, vegetation) after  
707 the word "TOA".

708 *The sentence was effectively not so explicit. We have now modified it in the new version. The sentence is*  
709 *now the following: "Due to this gradient in the surface albedo, moderate absorbing dust aerosols emitted*  
710 *over Northern Africa (characterized by high surface albedo) decrease the shortwave radiations reflected*  
711 *at TOA, compared to a non-turbid atmosphere. When advected above low surface reflectance as marine*  
712 *or dense forest over Europe, dust aerosols increase the upward SW radiations at TOA, leading to a cooling*  
713 *effect."*

714

715 29. Homogenize the boundaries of the maps in Figs. 1, 5, 6, 7, 9, 10, 11, 12, 27 and 29. The same  
716 for Figs. 2, 3 and 4.

717 *This is unfortunately quite difficult to homogenize all the figures as they have been prepared by using*  
718 *different products (models, satellites) with different horizontal resolutions and domains (for instance*  
719 *TRMM is limited to 50°N). For every figure, we have tried to represent as most as possible a similar*  
720 *domain, integrating the entire Mediterranean basin. If this is acceptable, we propose to keep the different*  
721 *figures in the present configuration.*

722

723 Technical comments

724  
725 1. Page 19621, Line 20: Crete is a Greek island, please modify accordingly.  
726 ***This is now modified in the introduction.***  
727 2. Page 19622, Line 19: The citation Kubilay et al. (2003) is missing from the References.  
728 ***This is effectively right and now added in the references.***  
729  
730 3. Page 19623, Lines 19 and 27, Page 19624, Line 1, Page 19625, Line 6, Page 19659, Line 7, Page  
731 19660, Line 16: Delete “D” from the citation “D. Meloni et al., 2015” and write to which of the two  
732 papers you are referring.  
733 ***This is now corrected in the text. We have now distinguished the Meloni et al. (2015) paper to the article***  
734 ***in preparation in the ChArMEx special issue; referenced as Meloni et al. (in prep. in this special issue).***  
735  
736 4. Page 19623, Line 21: di Sarra et al. (2011) examine dust aerosols not polluted, so delete.  
737 ***This is now removed.***  
738  
739 5. Page 19624, Line 15, Page 19661, Line 6: Nabat et al. (2015), which of the three?  
740 ***This is now indicated: Nabat et al. (2015a).***  
741  
742 6. Page 19628, Line 12: Insert “in” between “reported” and “Table 1”.  
743 ***This is now inserted.***  
744  
745 7. Page 19629, Line 11, Page 19652, Line 6: The citation Formenti et al. (2015) is missing from the  
746 References.  
747 ***This reference is now added in the new version.***  
748  
749 8. Page 19636, Line 11: The citation Petzold et al. (2013) is missing from the References.  
750 ***This citation is now added in the new version.***  
751  
752 9. Page 19636, Lines 15-16: The citation Moonsmuller et al. (2012) is missing from the References.  
753 ***This citation is now added in the new version. We did a mistake, the good reference is:***  
754 ***Moosmüller, H., Chakrabarty, R.K., Arnott, W.P.: Aerosol light absorption and its measurement: A review,***  
755 ***Journal of Quantitative Spectroscopy & radiative transfer, 100, 844-878, 2009.***  
756  
757 10. Page 19636, Line 22: The citation Karol et al. (2013) is missing from the References.  
758 ***This citation is now added.***  
759  
760 11. Page 19638, Line 28: The citation Vialard et al. (2015) is missing from the References.  
761 ***The correct citation is Vialard et al. (2009) and is referenced at the end of the manuscript.***  
762  
763 12. Page 19647, Line 26: Renard et al. (2015), which of the two?  
764 ***This corresponds to Renard et al. (2015b). This is now indicated in the text.***  
765  
766 13. Page 19651, Line 12: The citation Vaishya et al. (2012) is missing from the References.  
767 ***This reference is now added in the new version.***  
768  
769 14. Page 19653, Line 25: Change “Fig. 13” with “Fig. 14”.  
770 ***This is changed.***  
771  
772 15. Page 19656, Line 24: Provide the wavelengths for the “Angstrom exponent”.  
773 ***The Angstrom exponent has been calculated from the AOD at 440 and 870 nm. This is now indicated in***  
774 ***the text.***

775  
776 16. Delete the papers Sicard et al. (2006, 2011) and Ramanathan et al. (2009) from the References  
777 as they do not appear in the text.  
778 **We have now removed the two Sicard et al. (2006, 2011) references. For the other one, the reference is**  
779 **Ramanathan et al., 2001, which is referenced in the text.**  
780  
781 17. In Tab. 1 (2nd column) change the wavelength of the Leosphere lidar from 350 to 355 nm.  
782 **This point is corrected.**  
783  
784 18. In Tab. 2 the number of observations should be hours (or 15 mins periods), but not days.  
785 **This is effectively true. We have removed this column in the new version.**  
786  
787 19. In Tab. 5 for 16 Jun, 09:58 replace “LOA” by “LOAC” in the 2nd column.  
788 **Thank you, this point is now corrected.**  
789  
790 20. Rotate Fig. 8.  
791 **This is done in the new version.**  
792  
793 References  
794  
795 Amiridis, V., Zerefos, C., Kazadzis, S., Gerasopoulos, E., Eleftheratos, K., Vrekoussis, M., Stohl, A.,  
796 Mamouri, R.E., Kokkalis, P., Papayannis, A., Eleftheriadis, K., Diapouli, E., Keramitsoglou, I., Kontoes,  
797 C., Kotroni, V., Lagouvardos, K., Marinou, E., Giannakaki, E., Kostopoulou, E., Giannakopoulos, C.,  
798 Richter, A., Burrows, J.P., Mihalopoulos, N.: Impact of the 2009 Attica wild fires on the air quality in  
799 urban Athens, Atmos. Environ. 46, 536–544, 2012.  
800  
801 Baldassarre, G., Pozzoli, L., Schmidt, C. C., Unal, A., Kindap, T., Menzel, W. P., Whitburn, S., Coheur,  
802 P.-F., Kavgaci, A., and Kaiser, J. W.: Using SEVIRI fire observations to drive smoke plumes in the  
803 CMAQ air quality model: a case study over Antalya in 2008, Atmos. Chem. Phys., 15, 8539-8558,  
804 doi:10.5194/acp-15-8539-2015, 2015.  
805  
806 Barnaba, F., Angelini, F., Curci, G., and Gobbi, G. P.: An important fingerprint of wildfires on the  
807 European aerosol load, Atmos. Chem. Phys., 11, 10487-10501, doi:10.5194/acp-11-10487-2011,  
808 2011.  
809  
810 Kaskaoutis, D. G., Kharol, S. K., Sifakis, N., Nastos, P. T., Sharma, A. R., Badarinath, K. V. S., and  
811 Kambezidis, H. D.: Satellite monitoring of the biomass-burning aerosols during the wildfires of  
812 August 2007 in Greece: Climate implications, Atmospheric Environment, 45, 716–726,  
813 doi:10.1016/j.atmosenv.2010.09.043, 2011.  
814  
815 Liu, Y., Kahn, R. A., Chaloulakou, A., and Koutrakis, P.: Analysis of the impact of the forest fires in  
816 August 2007 on air quality of Athens using multi-sensor aerosol remote sensing data, meteorology  
817 and surface observations, Atmospheric Environment, 43, 3310–3318, 2009.  
818  
819 Ravetta, F., Ancellet, G., Colette, A., and Schlager, H.: Long-range transport and tropospheric ozone  
820 variability in the western Mediterranean region during the Intercontinental Transport of Ozone and  
821 Precursors (ITOP-2004) campaign, Journal of Geophysical Research, 112,  
822 doi:10.1029/2006JD007724, 2007.  
823  
824



825 **Dear Referees,**  
826 **Here you will find a version, where the corrections/modifications linked with the major and**  
827 **most of the minor comments are indicated in red and blue, respectively.**  
828 **Thank you again for your different remarks,**  
829 **With my best regards,**  
830 **Dr. Marc Mallet**

831 ---

832

833 Overview of the Chemistry-Aerosol Mediterranean Experiment/Aerosol Direct Radiative  
834 Forcing on the Mediterranean Climate (ChArMEx/ADRMED) summer 2013 campaign.

835

836 *Mallet M.<sup>1</sup>, F. Dulac<sup>2</sup>, P. Formenti<sup>3</sup>, P. Nabat<sup>4</sup>, J. Sciare<sup>2,5</sup>, G. Roberts<sup>4</sup>, J. Pelon<sup>6</sup>, G. Ancellet<sup>6</sup>, D. Tarré<sup>7</sup>, F.*  
837 *Parol<sup>7</sup>, C. Denjean<sup>4</sup>, G. Brogniez<sup>7</sup>, A. di Sarra<sup>8</sup>, L. Alados<sup>9</sup>, J. Arndt<sup>10</sup>, F. Auriol<sup>7</sup>, L. Blarel<sup>7</sup>, T. Bourriane<sup>5</sup>, P.*  
838 *Chazette<sup>2</sup>, S. Chevaillier<sup>3</sup>, M. Claeys<sup>5</sup>, B. D'Anna<sup>11</sup>, Y. Derimian<sup>7</sup>, K. Desboeufs<sup>3</sup>, T. Di Iorio<sup>8</sup>, J.-F. Doussin<sup>3</sup>, P.*  
839 *Durand<sup>1</sup>, A. Féron<sup>3</sup>, E. Freney<sup>13</sup>, C. Gaimoz<sup>3</sup>, P. Goloub<sup>7</sup>, J. L. Gómez-Amo<sup>8</sup>, M. J. Granados-Muñoz<sup>9</sup>, N. Grand<sup>3</sup>,*  
840 *E. Hamonou<sup>2</sup>, I. Jankowiak<sup>7</sup>, M. Jeannot<sup>14</sup>, J.-F. Léon<sup>1</sup>, M. Maillé<sup>3</sup>, S. Mailler<sup>15</sup>, D. Meloni<sup>8</sup>, L. Menut<sup>15</sup>, G.*  
841 *Momboisse<sup>5</sup>, J. Nicolas<sup>11</sup>, T. Podvin<sup>7</sup>, V. Pont<sup>1</sup>, G. Rea<sup>15</sup>, J.-B. Renard<sup>14</sup>, L. Roblou<sup>1</sup>, K. Schepanski<sup>16</sup>, A.*  
842 *Schwarzenboeck<sup>13</sup>, K. Sellegri<sup>13</sup>, M. Sicard<sup>17</sup>, F. Solmon<sup>18</sup>, S. Somot<sup>5</sup>, B. Torres<sup>7</sup>, J. Totems<sup>1</sup>, S. Triquet<sup>3</sup>, N.*  
843 *Verdier<sup>19</sup>, C. Verwaerde<sup>7</sup>, J. Wenger<sup>10</sup> and P. Zapf<sup>2</sup>.*

844

845 1 Laboratoire d'Aérodynamique, Observatoire Midi-Pyrénées, 14 Avenue Edouard Belin, 31400 Toulouse, France

846 2 LSCE-CEA/IPSL, CEA Saclay 701, 91191 Gif-sur-Yvette, France

847 3 Laboratoire Inter-Universitaire des Systèmes Atmosphériques (LISA), UMR CNRS 7583, Université Paris Est  
848 Créteil et Université Paris Diderot, Institut Pierre Simon Laplace, Créteil, France

849 4 Météo-France, CNRM-GAME, Centre national de recherches météorologiques, UMR3589, Toulouse,  
850 France

851 5 The Cyprus Institute, Energy Environment and Water Research Center, Nicosia, Cyprus

852 6 LATMOS-ISPL, UPMC Univ. Paris 06; Université Versailles St-Quentin; CNRS/INSU, Paris, France

853 7 LOA, Université Lille 1, Villeneuve d'Ascq, France

854 8 ENEA, Laboratory for Earth Observations and Analyses, Via Anguillarese 301, 00123 Roma, Italy

855 9 Department of Applied Physic, University of Granada, 18071, Granada, Spain

856 10 Department of Chemistry and Environmental Research Institute, University College Cork, Ireland

857 11 Institute de recherches sur la catalyse et l'environnement de Lyon (IRCE Lyon), University of Lyon, 69100  
858 Villeurbanne, France

859 12 Leibniz Institute for Tropospheric Research (TROPOS), Permoserstraße 15, 04318, Leipzig, Germany

860 13 Laboratoire de Météorologie Physique CNRS UMR6016, Observatoire de Physique du Globe de Clermont-  
861 Ferrand, Université Blaise Pascal, 63171 Aubière, France

862 14 LPC2E-CNRS/Université d'Orléans, 3A avenue de la recherche scientifique, 45071 Orléans, France

863 15 LMD, IPSL, CNRS, Ecole Polytechnique, École Normale Supérieure, Université Paris 6, UMR8539 91128  
864 Palaiseau CEDEX, France

865 16 Leibniz Institute for Tropospheric - Research - Permoserstr. 15, 04318 Leipzig, Germany

866 17 RSLab/CTE-CRAE-IEEC, Universitat Politècnica de Catalunya, Barcelona, Spain

867 18 The Abdus Salam International Center for Theoretical Physics, Strada Costiera 11, 34100 Trieste, Italy

868 19 Centre National d'Etudes Spatiales (CNES), DCT/BL/NB, 18 avenue Edouard Belin, 31401 Toulouse CEDEX  
869 9, France

870

871

872

873

874

875

876

877 **Abstract**

878

879 The Chemistry-Aerosol Mediterranean Experiment (ChArMEx; <http://charmex.lsce.ipsl.fr>) is a collaborative  
880 research program federating international activities to investigate Mediterranean regional chemistry-climate  
881 interactions. A special observing period (SOP-1a) including intensive airborne measurements was performed  
882 in the framework of the Aerosol Direct Radiative Forcing on the Mediterranean Climate (ADRIMED) project  
883 during the Mediterranean dry season over the western and central Mediterranean basins, with a focus on  
884 aerosol-radiation measurements and their modeling. The SOP-1a took place from 11 June to 05 July 2013.  
885 Airborne measurements were made by both the ATR-42 and F-20 French research aircraft operated from  
886 Sardinia (Italy) and instrumented for in situ and remote-sensing measurements, respectively, and by  
887 sounding and drifting balloons, launched in Minorca. The experimental set-up also involved several ground-  
888 based measurement sites on islands including two ground-based reference stations in Corsica and  
889 Lampedusa and secondary monitoring sites in Minorca and Sicily. Additional measurements including lidar  
890 profiling were also performed on alert during aircraft operations at EARLINET/ACTRIS stations at Granada  
891 and Barcelona in Spain, and in southern Italy. Remote sensing aerosol products from satellites (MSG/SEVIRI,  
892 MODIS) and from the AERONET/PHOTONS network were also used. Dedicated meso-scale and regional  
893 modelling experiments were performed in relation to this observational effort. We provide here an  
894 overview of the different surface and aircraft observations deployed during the ChArMEx/ADRIMED period  
895 and of associated modeling studies together with an analysis of the synoptic conditions that determined the  
896 aerosol emission and transport. Meteorological conditions observed during this campaign (moderate  
897 temperatures and southern flows) were not favorable to produce high level of atmospheric pollutants nor  
898 intense biomass burning events in the region. However, numerous mineral dust plumes were observed  
899 during the campaign with main sources located in Morocco, Algeria and Tunisia, leading to aerosol optical  
900 depth (AOD) values ranging between 0.2 to 0.6 (at 440 nm) over the western and central Mediterranean  
901 basins. One important point of this experiment concerns the direct observations of aerosol extinction on-  
902 board the ATR-42, using CAPS system, showing local maxima reaching up to  $150 \text{ Mm}^{-1}$  within the dust  
903 plume. Non negligible aerosol extinction (about  $50 \text{ Mm}^{-1}$ ) was also been observed within the Marine  
904 Boundary Layer (MBL). By combining the ATR-42 extinction coefficient observations with absorption and

905 scattering measurements, we performed a complete optical closure revealing excellent agreement with  
906 estimated optical properties. This additional information on extinction properties has allowed calculating  
907 the dust single scattering albedo (SSA) with a high level of confidence over the Western Mediterranean. Our  
908 results show a moderate variability from 0.90 to 1.00 (at 530 nm) for all flights studied that is contrary to  
909 the available literature on this optical parameter. Our results underline also a relatively low difference in SSA  
910 with values derived near dust sources. In parallel, active remote-sensing observations from the surface and  
911 onboard the F-20 aircraft suggest a complex vertical structure of particles and distinct aerosol layers with  
912 sea-spray and pollution located within the MBL, and mineral dust and/or aged north American smoke  
913 particles located above (up to 6-7 km in altitude). Aircraft and balloon-borne observations allow to  
914 investigate the vertical structure of aerosol size distribution showing particles characterized by large size  
915 (>10  $\mu\text{m}$  in diameter) within dust plumes. In most of cases, a coarse mode characterized by an effective  
916 diameter ranging between 5 and 10  $\mu\text{m}$ , has been detected above the MBL. In terms of shortwave (SW)  
917 direct forcing, in-situ surface and aircraft observations have been merged and used as inputs in 1-D radiative  
918 transfer codes for calculating the direct radiative forcing (DRF). Results show significant surface SW  
919 instantaneous forcing (up to  $-90 \text{ W m}^{-2}$  at noon). Aircraft observations provide also original estimates of the  
920 vertical structure of SW and LW radiative heating revealing significant instantaneous values of about  $5^\circ\text{K per}$   
921 day(in the solar spectrum (for a solar angle of  $30^\circ$ ) within the dust layer. Associated 3-D modeling studies  
922 from regional climate (RCM) and chemistry transport (CTM) models indicate a relatively good agreement for  
923 simulated AOD compared with observations from the AERONET/PHOTONS network and satellite data,  
924 especially for long-range dust transport. Calculations of the 3-D SW (clear-sky) surface DRF indicate an  
925 average of about  $-10$  to  $-20 \text{ W m}^{-2}$  (for the whole period) over the Mediterranean Sea together with maxima  
926 ( $-50 \text{ W m}^{-2}$ ) over northern Africa. The top of the atmosphere (TOA) DRF is shown to be highly variable within  
927 the domain, due to moderate absorbing properties of dust and changes in the surface albedo. Indeed, 3-D  
928 simulations indicate negative forcing over the Mediterranean Sea and Europe and positive forcing over  
929 northern Africa. Finally, a multi-year climatic simulation, performed for the 2003 to 2009 period and  
930 including an ocean-atmosphere (O-A) coupling, underlines the impact of the aerosol direct radiative forcing  
931 on the sea surface temperature, O-A fluxes and the hydrological cycle over the Mediterranean.

932 **1. Introduction**

933 The Mediterranean region has been identified as one of the most prominent “Hot-Spots” in future climate  
934 change projections (Giorgi and Lionello, 2008). It is characterized by its vulnerability to changes in the water  
935 cycle (e.g. Chenoweth et al., 2011; García-Ruiz et al., 2011). General Circulation Model (GCM) and Regional  
936 Climate Model (RCM) simulations show a substantial precipitation decrease and a warming of the region,  
937 especially in the long warm and dry Mediterranean season. At the end of 21<sup>st</sup> century, the average of the  
938 model outputs predicts a significant loss of freshwater (+40% for the period 2070-2090 compared to 1950-  
939 1999; Sanchez-Gomez et al, 2009) over the Mediterranean region. More recently, Mariotti et al. (2015) have  
940 used the newly available Coupled Model Intercomparison Project-Phase 5 (CMIP5) experiments and show a  
941 significant increase of the projected surface air temperature (by ~+ 2-3 °C) for the 2071-2098 period  
942 compared to 1980-2005. These results need to be put in the context of an increasing anthropogenic  
943 pressure on the Mediterranean region, with an expected doubling of the population in countries around the  
944 Mediterranean basin in the next decades, with a contrast between a small decrease in European countries  
945 and a strong increase in African and Middle-East countries (Brauch, 2003). However, as highlighted by  
946 Mariotti et al. (2008), despite the high degree of model consistency, the results concerning the future  
947 climate projections for the Mediterranean Sea water budget from the global coupled models are still  
948 uncertain due to their horizontal spatial resolutions that are not capable of resolving the local to regional  
949 Mediterranean specific processes (air-sea exchanges, coastline, topography, north-south gradient of  
950 albedo). Indeed, the Mediterranean climate is affected by local processes induced by the complex  
951 physiography of the region and the presence of a large body of water (the Mediterranean Sea). For example,  
952 the Alpine chain is a strong factor in modifying traveling synoptic and mesoscale systems and the  
953 Mediterranean Sea is an important source of moisture and precipitation in the region (Gimeno et al., 2010;  
954 Schicker et al., 2010) and of energy for storms (Lionello et al., 2006). The complex topography, coastline and  
955 vegetation cover of the region are well known to modulate the regional climate signal at small spatial scales  
956 (e.g. Millan et al., 1997; Gangoiti et al., 2001; Lionello et al., 2006).

957 So far, most global and regional climate simulations have investigated the impact of global warming on the  
958 Mediterranean climate without detailed considerations of the possible radiative influence and climatic

959 feedback from the different Mediterranean aerosols (anthropogenic, marine, biomass burning, secondary  
960 biogenic and mineral dust particles). The Mediterranean region is rich in a variety of particles (natural and  
961 anthropogenic) from both continental and marine sources (Lelieveld et al., 2002). In figure 1, we illustrate  
962 the significant differences in aerosol loading between the eastern, central, and western sub-basins and  
963 between the North and the South of the Mediterranean shown by long-term aerosol satellite products. The  
964 aerosol optical depth (AOD), which represents the integration of the extinction by particles along the whole  
965 atmospheric column displays annual mean values (Figure 1) from 0.2 to 0.5 (in the visible wavelengths),  
966 depending on the aerosol types observed over the Euro-Mediterranean region (Nabat et al., 2013).

967 Numerous studies have documented the AOD for polluted-anthropogenic Mediterranean aerosols at local  
968 scale over southeastern France (Mallet et al., 2006; Roger et al., 2006), Spain (Horvath et al., 2002, Alados-  
969 Arboledas et al., 2003, 2008), Western Mediterranean (Lyamani et al., 2015), Greece (Chazette and Liousse,  
970 2001; Gerasopoulos et al., 2003), the Crete Greece island (Fotiadi et al., 2006), and Italy (Tafuro et al., 2007,  
971 Ciardini et al., 2012). Under polluted conditions, they report low to moderate AOD values ranging between  
972 0.1 to 0.5 (at visible wavelengths). In parallel, multi-year TOMS and MODIS observations over the eastern  
973 Mediterranean (Hatzianastassiou et al., 2009) or the Po Valley (Royer et al., 2010) indicate the occurrence of  
974 high AOD values (up to more than 0.8 at 500 nm) over large urban areas surrounding megacities.

975 Numerous studies (Markowicz et al. (2002), Ravetta et al. (2007), Liu et al. (2009), Kaskaoutis et al. (2011),  
976 Barnaba et al. (2011), Amiridis et al. (2012), Baldassarre et al. (2015)) have been also dedicated to biomass  
977 burning aerosols over the Mediterranean, which are mainly observed in July and August (driest months of  
978 the year) when the development of forest fires is favoured (Pace et al., 2005). Long-term observations of  
979 absorbing aerosols have clearly shown the major role of long range transport of biomass (agriculture waste)  
980 burning in the eastern Mediterranean (Sciare et al., 2008). AOD data available for smoke particles show  
981 “intermediate” values between those observed for dust and anthropogenic particles. For example, AOD  
982 ranging between 0.3 and 0.8 (Pace et al., 2005) have been observed at Lampedusa from 5 to 22 August  
983 2003, in relation with intense fires developed in southern Europe and transported over the Mediterranean  
984 basin during a regional heat wave. In addition, the STAAARTE-MED experiment (August 1998 in the Eastern  
985 Mediterranean) has also documented a mean AOD of 0.39 (at 550 nm) for aged smoke plume from

986 Canadian fires (Formenti et al., 2002). This kind of long-range transport has been also observed over the  
987 Western Mediterranean (Ortiz-Amezcuca et al., 2014).

988 Concerning natural aerosols, different cases of Saharan mineral dust have been regularly documented with  
989 local optical measurements on the island of Lampedusa by Meloni et al. (2003, 2004), who indicate  
990 moderate AOD (at 415.6 nm) of about 0.23-0.26 and one significantly larger event with AOD values of 0.51.  
991 Meloni et al. (2008) also report AOD (at 500 nm) measurements ranging between 0.29 and 1.18 for the  
992 1999 to 2006 period. For some extreme cases, dust AOD peaks may be even larger reaching values up to 2  
993 as observed by di Sarra et al. (2011). In parallel to Lampedusa observations, Kubilay et al. (2003) have also  
994 documented three dust intrusion events at Erdemli (Turkish coast), occurring in spring from central Sahara,  
995 in summer from eastern Sahara, and in autumn from the Middle East/Arabian peninsula. In each case, the  
996 presence of dust particles significantly increased the AOD, up to 1.8. Over the western Mediterranean,  
997 different studies also reveal the impact of Saharan dust that occasionally can lead to extreme events with  
998 AOD (at 500 nm) above 1 (Guerrero-Rascado et al., 2009).

999 For [sea-spray](#) particles, which are the second main natural species observed over the Mediterranean, Nabat  
1000 et al. (2013) report a relatively low monthly mean AOD derived from satellites and modeling data, with  
1001 values lower than 0.05 (in the visible wavelengths). By using recent improvements in the [sea-spray](#) emission  
1002 scheme, Spada et al. (2013) show an averaged [sea-spray](#) AOD around 0.04 for the month of January (5 year  
1003 period, 2002-2006) which is the favourable period for generating primary [sea-spray](#) due to strong sea-  
1004 surface winds. Finally, and in the case of extreme wind episodes occurring over the western basin, Salameh  
1005 et al. (2007) show that the amount of aerosol loading, solely due to the Mistral, Tramontane and Ligurian  
1006 outflows, is as large as 3–4 times the background aerosol amount. They indicate that the contribution of  
1007 [sea-spray](#) particles to the total aerosol loading and optical depth ranges from 1 to 10%. Salameh et al.  
1008 (2007) report AOD around 0.15-0.20 (at 865 nm) within the [sea-spray](#) aerosol plume during such strong  
1009 wind events. In addition, Mulcahy et al. (2008) reported a high correlation between AOD and wind-speed  
1010 with AOD values of 0.3-0.4 at moderately-high wind speed.

1011 **In addition to AOD, the knowledge of SSA is essential to estimate the aerosol direct and semi-direct**  
1012 **radiative forcing. Concerning mineral dust particles observed over the Mediterranean, it should be noted**

1013 that significant variations in SSA are reported, with values near 1 for purely scattering aerosols, and quite  
1014 remarkable low values (0.74, 0.77 or 0.81) at Lampedusa (Pace et al., 2006; Meloni et al., 2003). At the high  
1015 altitude Alpine Jungfrauoch station, SSA values are generally higher than 0.9 in case of African dust but  
1016 occasional SSA as low as 0.75-0.80 are reported by Collaud-Coen et al. (2004). Intermediate values (0.85-  
1017 0.92) have been also reported over the Mediterranean basin (Kubilay et al., 2003; Meloni et al., 2004; Saha  
1018 et al., 2008). These estimates clearly indicate that significantly different SSA values are obtained following  
1019 the dust particle origins and/or possible mixing of mineral dust with other species. For example, Kubilay et  
1020 al. (2003) underlined the importance of mixing, showing SSA values clearly lower (0.85-0.90) in case of  
1021 mineral dust transport coincident with urban-industrial aerosols, as compared to pure dust (0.96-0.97).

1022 In addition, SSA observed in case of urban/industrial regimes has been also well documented over the  
1023 Mediterranean Sea and coastal regions. In most cases, moderate or low SSA (0.78-0.94) is observed due to  
1024 emissions containing absorbing black carbon aerosols. Over southeastern France, optical computations  
1025 performed by Saha et al. (2008) and Mallet et al. (2004) indicate SSA values of 0.83 and 0.85 (at 550 nm)  
1026 near the cities of Marseille and Toulon, respectively. Aircraft observations performed over the  
1027 Marseille/Etang de Berre area during the ESCOMPTE campaign show values ranging between 0.88 and 0.93  
1028 (at 550 nm) in the PBL (Mallet et al., 2005). These SSA values are close to those observed in South Spain  
1029 (0.86-0.90) by Horvarth et al. (2002). Over southeastern Italy, Tafuro et al. (2007) reported a value of 0.94  
1030 during summer time corresponding to anthropogenic particles. Finally, polluted particles transported over  
1031 the Mediterranean basin have also relatively low values as reported by Markowick et al. (2002) over Crete  
1032 Island (0.87) and by Di Iorio et al. (2003) (0.79-0.83) over the Lampedusa Island for two cases (25 and 27  
1033 May 1999) of “aged” anthropogenic aerosols originating from Europe.

1034 As opposed to dust and polluted aerosols, few studies have derived the biomass burning SSA over the  
1035 Mediterranean Sea. One estimate has been obtained during STAAARTE-MED by Formenti et al. (2002) who  
1036 reported a mean dry SSA of 0.89 (at 500 nm) for aged smoke from North America. Meloni et al. (2006)  
1037 report estimations at Lampedusa with values of  $0.82 \pm 0.04$  (at 415 nm) for smoke aerosols over the  
1038 Mediterranean region. The observed differences between SSA values could be due to the fact that the  
1039 smoke events described by Meloni et al. (2006) are more “local” and not (or somewhat less) mixed with

1040 other secondary species, as compared to biomass burning particles documented by Formenti et al. (2002),  
1041 which were issued from very distant Canadian fires. Finally, at Palencia (Spain), Cachorro et al. (2008)  
1042 reported a column-integrated SSA of 0.88 (at 440 nm) for a biomass burning event occurring in July 28,  
1043 2004. It should be remained that most estimations of SSA over the Mediterranean have been obtained from  
1044 surface in-situ or remote-sensing techniques. In that sense, the ChArMEx/ADRI-MED project provides  
1045 innovative observations of 3-D aerosol SSA, allowing investigating changes in its optical property during the  
1046 transport of aerosols over the Mediterranean.

1047 Concerning the aerosol vertical profiles and apart from a few airborne in-situ measurements (Formenti et  
1048 al., 2002), most of the available information in the Mediterranean region comes from lidar observations,  
1049 which provide highly resolved vertical profiles of aerosol backscattering at one or more wavelengths and,  
1050 depending on the complexity of the instrumental setup, particles depolarization and extinction. Several  
1051 sites are equipped with aerosol lidar systems and carry out regular observations in a coordinated way within  
1052 the European aerosol research lidar network EARLINET (European Aerosol Research Lidar Network;  
1053 Pappalardo et al., 2014; Wang et al., 2014). Numerous studies have been specifically dedicated to the  
1054 vertical distribution of Saharan dust during extended time periods and/or selected events from various  
1055 Mediterranean regions, mainly from ground-based systems: (i) the eastern basin in Thessaloniki (Hamonou  
1056 et al., 1999; Balis et al., 2004), Crete (Balis et al., 2006), the Aegean sea (Dulac et al., 2003), and Athens plus  
1057 Thessaloniki (Papayannis et al., 2005; Balis et al., 2006); (ii) the central basin in Lampedusa (Di Iorio et al.,  
1058 2003; Meloni et al., 2004), Lecce (Tafuro et al., 2006), and at Etna (Tafuro et al., 2006); and (iii) across the  
1059 western basin with the first spaceborne lidar (Berthier et al., 2006) and at Observatoire de Haute Provence  
1060 (Hamonou et al., 1999), and Barcelona (Pérez et al., 2006; Sicard et al., 2011). Finally, using data from 20  
1061 EARLINET lidar stations, Papayannis et al. (2008) indicate that African dust transport over the Mediterranean  
1062 basin is layered. Their analysis confirms early observations by Hamonou et al. (1999) that not only different  
1063 dust layers are superimposed at different altitudes, but that these layers have different source regions. The  
1064 dust layers were generally detected between 1.8 and 9 km altitude.

1065 Not only desert dust, however, can be transported above the marine atmospheric boundary layer. Balis et  
1066 al. (2004) report non-dust aerosols within elevated layers over Thessaloniki, and Formenti et al. (2002)



1067 report a forest fire haze layer from Canada observed from airborne measurements between approximately  
1068 1 and 3.5 km above the northeastern Mediterranean in August 1998. Pérez et al. (2004) describe the  
1069 complex interaction among orography, sea-breeze and pollution that cause the recirculation of pollutants  
1070 and produce a strong layering with pollution aerosol layers above the boundary layer in the region of  
1071 Barcelona. In addition, aerosol plumes are emitted sporadically in the Mediterranean free troposphere by  
1072 Etna volcano. Such plumes have been observed to travel at altitudes between 4 and 5 km (Pappalardo et al.,  
1073 2004) or above (Sellitto et al., 2015) at relatively short distance from Etna. To summarize, the lidar  
1074 observations clearly show that only part of the aerosol transport occurs in the MBL demonstrating the need  
1075 of using aircraft observations within the aerosol plume to determine the aerosol microphysical-chemical  
1076 and optical properties of particles transported in altitude and so not detectable at the surface. Indeed,  
1077 although lidar observations provide obviously crucial information on the aerosol vertical profiles, most of  
1078 lidar systems cannot derive information on the aerosol size distribution, optical properties and chemical  
1079 composition along the vertical. Such observations can only be obtained using in-situ aircraft vertical profiles  
1080 as proposed in this ChArMEx/ADRIMED experiment. As an example, this project provides interesting and  
1081 unique observations of 3-D aerosol size distribution during the transport over the Mediterranean basin,  
1082 allowing to investigate changes in size distribution between mixed and pure mineral dust.

1083 In terms of radiative effects, such atmospheric aerosol characteristics (loadings, absorbing properties,  
1084 vertical layering) are known (Nabat et al., 2012; Papadimas et al., 2012; Zanis et al., 2012) to significantly  
1085 change the radiative budget of the Mediterranean region by (1) decreasing the sea-surface incoming  
1086 shortwave radiations, (2) increasing/decreasing outgoing shortwave fluxes depending on the surface albedo  
1087 and (3) possibly heating turbid atmospheric layers when particles absorb solar light. This is the so-called  
1088 aerosol "Direct Radiative Forcing (DRF)". As for the AOD, many of the aerosol DRF calculations are now  
1089 referenced over the Mediterranean clearly showing that the DRF is significantly larger at daily time scales  
1090 than the one exerted by the additional anthropogenic greenhouse gases.

1091 Concerning polluted aerosols, shortwave DRF have been estimated by many authors (Horvath et al., 2002;  
1092 Markowicz et al., 2002; Meloni et al., 2003; Roger et al., 2006; Mallet et al., 2006; Saha et al., 2008; di Sarra  
1093 et al., 2008; Di Biagio et al., 2009, 2010). Studies show significant decreases of surface solar fluxes of about

1094 20-30 W m<sup>-2</sup> (daily mean) for different locations as Almeria (South Mediterranean coast of Spain), Finokalia  
1095 (Crete Island), Lampedusa, Marseilles and Toulon (southeastern France). In parallel, the combination of  
1096 surface and satellite remote-sensing observations performed at Lampedusa have been used to perform  
1097 calculations of the DRF, both in the shortwave (SW; Di Biagio et al., 2010) and longwave (LW; di Sarra et al.,  
1098 2011; Meloni et al., 2015) spectral regions for different cases of Saharan dust intrusions. These studies  
1099 emphasize that the radiative effect of desert dust in the LW spectral range is significant, and offsets a large  
1100 fraction of the SW forcing (di Sarra et al., 2011; Meloni et al., 2015). More recently, Sicard et al. (2014a,  
1101 2014b) have also produced estimations of the dust LW radiative effect, based on remote-sensing  
1102 observations in Barcelona and 1-D radiative transfer calculations.

1103 Concerning the smoke DRF, some calculations have been conducted over the Mediterranean region by  
1104 Markowicz et al. (2002), di Sarra et al. (2008), Kaskaoutis et al. (2011) or Formenti et al. (2002). One  
1105 estimate, proposed by Formenti et al. (2002) for an aged Canadian biomass-burning plume, reveals a  
1106 significant SW surface dimming of about  $\sim 60$  W m<sup>-2</sup>. In addition, the DRF induced by smoke aerosols at  
1107 Lampedusa between 3 and 23 August 2003, during the exceptionally hot and dry season, was derived by  
1108 Pace et al. (2005) for the 300-800 nm spectral range. The smoke atmospheric forcing was estimated to be  
1109 between +22 and +26 W m<sup>-2</sup>, with a corresponding SW heating rate possibly exceeding 2 K d<sup>-1</sup> at the smoke  
1110 plume altitude.

1111 At the regional scale, Papadimas et al. (2012) have proposed a recent estimation of the aerosol DRF using  
1112 MODIS data from 2000 to 2007 for both all-sky and clear-sky conditions. They derived a multi-year regional  
1113 mean surface of -19 W m<sup>-2</sup>, associated with a TOA DRF of -4.5 W m<sup>-2</sup>. Regional modelling studies have been  
1114 also recently proposed by Nabat et al. (2012, 2015) using the coupled-chemistry RegCM and the CNRM-  
1115 Regional Climate System Model (RCSM) models for multi-year simulations. These works reported a mean  
1116 regional surface (TOA) forcing of about -12 W m<sup>-2</sup> (-2.4 W m<sup>-2</sup>) and -16 W m<sup>-2</sup> (-5.7 W m<sup>-2</sup>) for the RegCM and  
1117 CNRM-RCSM models, respectively. RegCM has been also used to investigate direct and semi-direct radiative  
1118 effects of mineral dust over the Sahara and Europe in a test case of July 2003 (Santese et al., 2010). In this  
1119 work, Santese et al. (2010) computed a daily-mean SW DRF of -24 W m<sup>-2</sup> (resp. -3.4 W m<sup>-2</sup>) on 17 July and -  
1120 25 W m<sup>-2</sup> (-3.5 W m<sup>-2</sup>) on 24 July at the surface (TOA) on average over the simulation domain. Zanis et al.

1121 (2012) also proposed a regional estimate of the DRF of anthropogenic particles over the 1996-2007 period  
1122 using RegCM and showed a significant forcing of up to  $-23 \text{ W m}^{-2}$  at TOA over Eastern Europe. In addition,  
1123 Pere et al. (2011) have used the CTM-CHIMERE model coupled to the WRF model, for estimating the DRF of  
1124 anthropogenic particles during the heat wave of summer 2003 and showed significant effects with  
1125 implications on the planetary boundary layer height (decrease up to 30% in the presence of anthropogenic  
1126 aerosols) and local air-quality. In addition to their important effects on the surface and TOA DRF, most of  
1127 the Mediterranean aerosols are also able to absorb more or less effectively the solar radiations leading to a  
1128 significant atmospheric forcing and associated SW heating rate. Local studies previously mentioned (Roger  
1129 et al., 2006; Saha et al., 2008; Pace et al., 2005; Pere et al., 2011; Meloni et al., 2015) clearly report  
1130 significant SW heating rate due to absorbing particles with values reaching up to 2-3 K per day, depending  
1131 on the aerosol types. Finally, aerosols also have a significant effect on photolysis rates that may affect  
1132 tropospheric chemistry and ozone production over the basin (Casasanta et al., 2011, Mailler et al., 2015).

1133 In regards to such surface, TOA and atmospheric forcings, there is a need to investigate how the change in  
1134 the radiative budget due to natural/anthropogenic aerosols influence the surface temperature (both over  
1135 land and sea), relative humidity profiles, exchanges (latent heat fluxes) between ocean and atmosphere,  
1136 cloud-cover (semi-direct effect of absorbing particles), precipitation and finally the whole Mediterranean  
1137 hydrological cycle. The induced perturbations in the sea surface-atmosphere fluxes is expected to be  
1138 important despite the relatively small size of the Mediterranean Sea, since this basin plays an important role  
1139 at much larger scale by providing moisture for precipitation to its surroundings land region extending to  
1140 northern Europe and northern Africa (Gimeno et al., 2010 and Schicker et al., 2010). Indeed and as shown  
1141 by Ramanathan et al. (2001) for the Indian region or Foltz and McPhaden (2008) and Yue et al. (2011) for  
1142 the Atlantic Ocean, a modification of the sea-surface evaporative fluxes, due to the dimming radiative effect  
1143 of aerosols at the sea surface could significantly influence the lower troposphere moisture content and the  
1144 associated precipitation distribution around the Mediterranean. In parallel, the absorbing particles over the  
1145 Mediterranean (Mallet et al., 2013) could exert a semi-direct effect that could modify the vertical profiles of  
1146 relative humidity and cloud cover, which has to be quantified. To our knowledge, there is no regional  
1147 climate simulation over the Mediterranean basin at this time that includes an Ocean-Atmosphere (O-A)

1148 coupled system model for investigating this specific question.

1149 In that context of the referenced modelling and observations researchs over the Mediterranean basin, the  
1150 main objectives of the ChArMEx/ADRIMED project were the following:

- 1151 - to conduct an experimental campaign, based on surface and aircraft observations, for creating a huge 3-D
- 1152 database of physical, chemical and optical properties of the main Mediterranean aerosols, including (i)
- 1153 original in-situ aircraft observations of extinction coefficients, size distribution, black carbon concentrations
- 1154 as well as (SW and LW) radiative fluxes and associated heating rates, (ii) balloons observations of aerosol
- 1155 size distribution and (iii) surface measurements including original characterization of chemical properties
- 1156 - to investigate how the aerosol size distribution and optical (especially SSA) properties evolve along the
- 1157 vertical, between the MBL and elevated layers, and during the transport over the Mediterranean
- 1158 - to use experimental surface and aircraft observations to estimate the 1D-local DRF and forcing efficiency
- 1159 of different aerosols at the surface, TOA and within the atmospheric layer
- 1160 - to investigate how the modifications of the radiative budget due to aerosols affect the sea-surface
- 1161 evaporation fluxes, relative humidity profiles, cloud-cover, precipitation and more largely the
- 1162 Mediterranean hydrological cycle

1163 The present article describes the experimental setup of the campaign and the meteorological context and  
1164 illustrates important results detailed in a series of companion papers. The rest of this article is divided into  
1165 six different parts. In the first and second part (sections 2 & 3), we describe the in-situ and remote-sensing  
1166 instrumentation deployed at the two super sites (Ersa and Lampedusa) and secondary sites (Minorca, Capo  
1167 Granitola and the Barcelona and Granada EARLINET/ACTRIS stations), the additional AERONET/PHOTONS  
1168 (AErosol RObotic NETwork / PHOtométrie pour le Traitement Opérationnel de Normalisation Satellitaire,  
1169 <http://aeronet.gsfc.nasa.gov/>; Holben et al., 1998) and EARLINET/ACTRIS (European Aerosol Research Lidar  
1170 Network / Aerosols, Clouds, and Trace gases Research InfraStructure Network, <http://www.actris.net/>;  
1171 Pappalardo et al., 2014) network stations that we used, and the airborne observations obtained onboard  
1172 the two French research aircraft (ATR-42 and F-20) and with sounding and drifting balloons. The section 4 is  
1173 dedicated to present the main meteorological conditions, cloud cover and precipitation, which controlled  
1174 the aerosol emission and transport during the period of observations. The section 5 presents some

1175 examples of results concerning the in-situ and remote-sensing observations, in terms of aerosol physical,  
1176 chemical, optical properties, and vertical profiles, as well as 1-D DRF SW and LW calculations. In the last part  
1177 (section 6), the modelling effort is presented. Different models are involved in this project, from high  
1178 resolution meteorological and chemistry transport models to regional climate models. The modelling results  
1179 are used to describe the anthropogenic (carbonaceous, secondary inorganic and organic species) and  
1180 natural (dust and [sea-spray](#)) loading and the estimated DRF at the regional scale for the period of  
1181 experiment. [An example of results of longer \(inter-seasonal and inter-annual\) aerosol-climate simulations is  
1182 presented in the section 6, based on the work of Nabat et al. \(2015a\).](#)

## 1183 **2. Overview of the surface observation network**

1184 The regional experimental set-up deployed in the western and central Mediterranean during the campaign  
1185 ChArMEx SOP-1a is shown in Figure 2.

### 1186 **2.1 The Cape Corsica and Lampedusa surface super sites**

1187 Two super-sites were fully equipped for documenting the aerosol chemical, physical and optical properties  
1188 as well as their possible mixing and their vertical structure at local scale (Table 1). The main characteristics  
1189 of these two surface stations are presented here. The first station was located in Erba on Cape Corsica  
1190 ( $42^{\circ}58'10''\text{N}$ ,  $09^{\circ}22'49''\text{E}$ ), near the North tip of Corsica Island. This station was primarily instrumented for  
1191 investigating polluted air masses transported over the Mediterranean basin from the highly industrialized  
1192 regions of the Po Valley (Royer et al., 2010) and/or the Marseille-Fos-Berre (Cachier et al., 2005) zone and  
1193 Rhone Valley. This ground-based remote station is located at an altitude of about 530 m above mean sea  
1194 level (amsl) on a ridge equipped with wind mills and benefit from a direct view to the sea over a North  
1195 sector of  $\sim 270^{\circ}$  extending from the SW to SE. [The Cape Corsica peninsula is a remote site ensuring that the  
1196 in-situ measurements are not contaminated by local anthropogenic pollution.](#)

1197 The Lampedusa super-site ( $35^{\circ}31'5''\text{N}$ ,  $12^{\circ}37'51''\text{E}$ ) was established at the “Roberto Sarao” station  
1198 permanently operated by ENEA in the small island of Lampedusa ( $\sim 20 \text{ km}^2$ ), and it was augmented during  
1199 the field campaign by the observations of the Portable Gas and Aerosol Sampling UnitS (PEGASUS) mobile  
1200 station operated by LISA . This surface station was mainly used for documenting very aged air masses in  
1201 south westerly flow from Europe, southern air masses from northern Africa (Tunisia, Algeria and Libya)

1202 possibly laden with mineral dust, as well as marine aerosols. It is situated on a cliff at about 45 m amsl on  
1203 the NE tip of the island.

1204 The complete instrumentation deployed during the SOP-1a experiment for both super-sites is detailed in  
1205 Table 1. Briefly, it served to determine the complete aerosol physical, chemical and optical properties as  
1206 well as vertical profiles, and to measure radiative fluxes (broadband SW and LW, and spectral SW).

### 1207 **2.1.1 In situ measurements at super-sites**

1208 Both super-sites measured the mass concentration online using Tapered Element Oscillating Microbalance  
1209 (TEOM) analysers. The number size distribution of particles are also measured, including fine and coarse  
1210 fractions (radius ranges and corresponding instruments are reported in Table 1). The aerosol composition  
1211 was derived from chemical analyses of filters and cascade impactors (DEKATI and MOUDI) with time  
1212 resolution varying from 12 to 48h (depending on the aerosol load), but also from high-time resolution  
1213 online measurements by an ACSM (Aerosol Chemical Speciation Monitor) at Ersa, a C-TOF-AMS (Time of  
1214 Flight Aerosol Mass Spectrometer) at Lampedusa, and two PILS (Particle Into Liquid Sampler) systems at  
1215 both sites (Table 1). The original observations of aerosol chemical properties obtained from PM10-PILS  
1216 instrument at Ersa are detailed in Claeys et al. (2015). Concerning aerosol optical properties, scattering and  
1217 absorption coefficients (at wavelengths listed in table 1) have been estimated for both super-sites using a 3-  
1218  $\lambda$  nephelometer and a 7- $\lambda$  aethalometer, respectively. At Ersa station, the extinction coefficient (at 870 nm)  
1219 was also estimated using a Photoacoustic Extinctionmeter (PAX) instrument, while it has been estimated at 2-  
1220  $\lambda$  (450 and 630 nm) at Lampedusa using 2 Cavity Attenuated Phase Shift Spectroscopy (CAPS) systems.

1221 Additional in-situ measurements were performed at the Ersa station. The mixing state of fine particles (at  
1222 the two selected diameters of 50 and 110 nm in dry conditions) has also been estimated from their  
1223 hygroscopic behaviour using a VHTDMA (volatilization and humidification tandem differential mobility  
1224 analyser) system (Johnson et al., 2004). In parallel, a TSI (model 3800) aerosol time of flight mass  
1225 Spectrometer (ATOFMS) (Gard et al., 1997) was used to measure the size-resolved chemical composition of  
1226 single particles in the vacuum aerodynamic diameter ( $d_{va}$ ) size range 100–3000 nm.

### 1227 **2.1.2 Remote sensing and radiation measurements at super-sites**

1228 A Leosphere Raman lidar model RMAN510 was setup at low altitude (~11 m above sea level) in the small

1229 village of Macinaggio (42°57'44"N, 9°26'35"E) located on the eastern coast of Cape Corsica. The lidar was  
1230 operated at about 6 km East from the Ersa station and less than 700 m from the shoreline. The RMAN510  
1231 uses a laser emitting at 355 nm. It measures the total and polarized backscatter at 355 nm and the Raman  
1232 nitrogen signal at 387 nm at night-time. A second ALS300 510 lidar system has been deployed in Lampedusa  
1233 (Formenti et al., in prep.) as well as a more powerful University of Rome-ENEA homemade lidar measuring  
1234 backscatter at 532 and 1064 nm (Di Iorio et al., in prep.). The main characteristics of lidar systems are  
1235 provided and detailed in Table 1.

1236 At each station, a multi-wavelength sun-photometer from the AERONET/PHOTONS network was operated,  
1237 allowing the operational retrieval of column integrated AOD at 340, 380, 440, 500, 675, 870, 1020 nm (and  
1238 also at 1650 nm at Ersa) and aerosols optical and microphysical properties such as the single scattering  
1239 albedo, refractive index and particle size volume distribution (Dubovik and King, 2000; Dubovik et al., 2000,  
1240 2002, 2006). The Ersa sun-photometer is positioned since June 2008 near the navy semaphore on the  
1241 northwestern tip of Cape Corsica (43°00'13"N, 09°21'33"E, alt. ~75 m amsl) at about 4.2 km NNW of the  
1242 Ersa surface station.

1243 Both super-sites were complemented by a pyrgeometer and a pyranometer for monitoring longwave and  
1244 shortwave downward fluxes measurements, respectively. Additional radiation measurements were  
1245 performed at Lampedusa (Table 1). Spectral measurements of global, diffuse, and direct radiation were  
1246 carried out with other instruments deployed by ENEA and the Physikalisch-Meteorologisches  
1247 Observatorium Davos, World Radiation Center, (PMOD/WRC, Switzerland). Multi-filter rotating  
1248 shadowband radiometer observations were carried out jointly with AERONET sun-photometer (di Sarra et  
1249 al., 2015) and allowed the derivation of the AOD at several wavelengths. By combining these two  
1250 measurements, a long-term series of AOD, started in 2001, was obtained. Measurements of the spectral  
1251 actinic flux, allowing the determination of the photolysis rates (Mailler et al., 2015), were carried out with a  
1252 diode array spectrometer. Measurements of broadband irradiance included a CG3 pyrgeometer sensitive to  
1253 radiation in the atmospheric infrared window. Finally, the total ozone and spectral UV irradiance were  
1254 obtained with a Brewer spectrophotometer. Several radiosondes were also launched from Lampedusa  
1255 during the SOP-1a, and vertical profiles of temperature and humidity were continuously measured by a

1256 microwave radiometer.

## 1257 **2.2 The secondary sites**

### 1258 **2.2.1 Montesoro station**

1259 The Cape Corsica station was complemented by an additional remote-sensing setup at the peri-urban air  
1260 quality station of Montesoro, southward of Bastia at about 45 m amsl (Leon et al., 2015), including a  
1261 Leosphere model EZ lidar operating at 355 nm (42°40'17"N, 09°26'05"E) and a Cimel AERONET/PHOTONS  
1262 sun-photometer (42°40'19"N, 09°26'06"E). In addition, some air-quality parameters were monitored by  
1263 Qualitair Corse, including PM<sub>2.5</sub> and PM<sub>10</sub>. This station is less than 1 km far from the shore on the  
1264 northeastern coast of Corsica, about 32 km South of Macinaggio.

### 1265 **2.2.2 Barcelona station**

1266 The Barcelona station (41.39°N, 2.11°E, 115 m amsl) was equipped with the following fixed instruments  
1267 including an AERONET sun-photometer, an automated Sigma Space-NASA Micro Pulse Lidar (MPL) and a  
1268 Universitat Politècnica de Catalunya (UPC) home-made multi-wavelength lidar (Kumar et al., 2011). The MPL  
1269 lidar works at 532 nm and has a depolarization channel, while the UPC lidar works at 355, 532 and 1064 nm,  
1270 and also includes two N<sub>2</sub>- (at 387 and 607 nm) and one H<sub>2</sub>O-Raman (at 407 nm) channels. The MPL system  
1271 worked continuously. The UPC system was operated on alert in coordination with the two research aircraft  
1272 plans involved in the SOP-1a campaign. The UPC system is part of the EARLINET network.

### 1273 **2.2.3 Minorca station**

1274 An additional station was setup during the campaign, located at Cap d'en Font, on the southeastern coast of  
1275 the Balearic island of Minorca (Spain, 39°53'12"N and 4°15'31" E, ~10 m amsl), which is relatively central in  
1276 the western Mediterranean basin. The Mobile Aerosol Station (MAS) of the LSCE (Laboratoire des Sciences  
1277 du Climat et de l'Environnement) laboratory was equipped with the new Raman lidar WALI (Chazette et al.,  
1278 2014a, 2014b), an AERONET/PHOTONS sun-photometer, and a set of in-situ instruments. A 5-wavelength  
1279 Solar Light Microtops-II manual sun-photometer was also used. The WALI instrument, its calibration and the  
1280 associated errors are documented in Chazette et al. (2014a). During all the experiment, the acquisition was  
1281 performed continuously with a vertical resolution of 15 m. AOD at the lidar wavelength of 355 nm has been  
1282 extrapolated from that measured by sun-photometer at 380 nm and 440 nm using the Angström exponent



1283 (Chazette et al., 2015).

1284 The in-situ instruments installed on-board the MAS included a 3-wavelength TSI nephelometer, a Magee  
1285 Scientific Model AE31 7-wavelength aethalometer, a TEOM microbalance, and a Vaisala meteorological  
1286 probe type PTU300. The nephelometer was sampling through a PM<sub>10</sub> inlet to measure the aerosol scattering  
1287 coefficient at 3 wavelengths (450, 550 and 700 nm) with an integrating time step of 5-min. The  
1288 aethalometer was sampling through a PM<sub>2.5</sub> inlet to measure aerosol absorption (at 7 wavelengths) and  
1289 derive a 5-min average black carbon concentration. The TEOM measured dry PM<sub>10</sub> concentration every 30  
1290 min. In addition two optical particle counters (OPCs) were installed outdoors next to the sun-photometer on  
1291 a mobile platform. A MetOne HHPC-6 and a LOAC (Renard et al., 2015a, 2015b) respectively measured  
1292 aerosol particle number concentration in 6 channels above 0.3µm in diameter and in 19 channels above 0.2  
1293 µm. The LOAC instrument accuracy is discussed in detail by Renard et al. (2015a, 2015b).

#### 1294 **2.2.4 Granada station**

1295 The station of the Atmospheric Physics Group (GFAT) is located in the Andalusian Institute for Earth System  
1296 Research (IISTA-CEAMA), in Granada, Spain (37.16°N, 3.61°W, 680 m amsl). The station is at a relatively  
1297 short distance, about 200 km away, from the African continent and approximately 50 km away from the  
1298 western Mediterranean Sea. During the SOP-1a campaign, lidar measurements were performed  
1299 simultaneously with a multiwavelength Raman lidar and a scanning Raman lidar both from Raymetrics S.A.  
1300 The multi-wavelength Raman system is part of the EARLINET network. In addition, a ceilometer was  
1301 operated. Column integrated characterization of the atmospheric aerosol was performed following  
1302 AERONET protocols with two Cimel sun-photometers deployed at two different heights: Granada (680  
1303 m asl) and Cerro Poyos (37°6'32"N, 03°29'14"W, 1790 m asl) stations. In addition, in-situ instrumentation  
1304 was continuously operated providing measurements of aerosol light-absorption coefficient at multiple  
1305 wavelengths (multi-angle absorption photometer (MAAP) from Thermo ESM Andersen Instruments and  
1306 Aethalometer model AE31), size distribution and particle number concentration for diameters larger than  
1307 0.5 µm (TSI aerodynamic particle sizer APS model 3321) and light-scattering and backscattering coefficient  
1308 at dry and at relative humidity of 85% by means of a TSI tandem nephelometer humidograph system.  
1309 Furthermore, the chemical composition in the PM<sub>1</sub> and PM<sub>10</sub> size fractions was determined during 16 and

1310 17 June by collecting aerosol samples using two high-volume samplers (Alados-Arboledas et al., in prep.).

### 1311 **2.2.5 Capo Granitola station**

1312 Several instruments were also deployed at Capo Granitola (37°34'N, 12°40'E), a site along the Southern  
1313 coast of Sicily. The site, within a combined effort of ENEA, Univ. of Florence, and Univ. of Valencia, was  
1314 equipped with a PM<sub>10</sub> sampler, a MultiFilter Rotating Shadowband Radiometer (MFRSR) to derive spectral  
1315 AOD, and radiometers and spectrometers for the measurement of global, direct, and diffuse radiation  
1316 throughout the SW and LW spectral ranges.

## 1317 **2.3 Surface remote-sensing network**

1318 Two surface remote-sensing networks were operated during the ChArMEx SOP-1a experiment, namely the  
1319 AERONET/PHOTONS and EARLINET/ACTRIS (Pappalardo et al., 2014) networks. These networks were highly  
1320 useful as they allow estimating the column-integrated aerosol loading as well as the vertical structure of  
1321 particles.

### 1322 **2.3.1 The AERONET/PHOTONS Sun-Photometer Network**

1323 AERONET (Aerosol Robotic Network; <http://aeronet.gsfc.nasa.gov/>) is a federated network of ground-based  
1324 sun-photometers and the associated data inversion and archive system, that routinely performs direct sun  
1325 observations about every 15 min during daytime, and both almucantar and principal plane sky radiance  
1326 measurements, at selected solar angles (Holben et al., 1998). Along with AOD observations, the AERONET  
1327 aerosol retrieval algorithm (Dubovik and King, 2000) delivers the complete set of column-effective aerosol  
1328 microphysical parameters, including volume size distribution, refractive index at several wavelengths and  
1329 fraction of spherical particles (Dubovik et al., 2006). In addition, using these microphysical parameters, the  
1330 algorithm provides other column-effective aerosol optical properties such as wavelength dependent SSA,  
1331 phase function, and asymmetry parameter, as well as integral parameters of bi-modal particle size  
1332 distributions (concentration, mode radii and variances) (Dubovik et al., 2002). The accuracy of AERONET  
1333 retrievals is evaluated and discussed by Dubovik et al. (2000, 2002). In addition to microphysical and optical  
1334 aerosol properties, we also have used direct radiative forcing calculations operationally provided at any  
1335 AERONET location as an operational product of the network. The method of derivation is described in detail  
1336 by Garcia et al. (2012). Briefly, the broadband fluxes were calculated using the radiative transfer model

1337 GAME (Dubuisson et al., 2004; Roger et al., 2006) that has been integrated into operational AERONET  
1338 inversion code. Sun-photometer stations deployed during the SOP-1a campaign over the Western basin are  
1339 listed in the Table 2.

### 1340 **2.3.2 The EARLINET/ACTRIS network**

1341 Between 22 and 24 of June, four ACTRIS/EARLINET lidar stations, in addition to the EARLINET sites of  
1342 Barcelona and Granada, were operated in support of aircraft operations (Sicard et al., 2015a; Barragan et  
1343 al., in prep.):

- 1344 • Naples (40.84°N, 14.18°E); measurements of backscatter profiles at 355 and 532 nm, as well as  
1345 depolarization ratio profiles at 532 nm, on 22 June 2013.
- 1346 • Serra La Nave (Sicily, 37.68°N, 14.98°E); measurements of backscatter profiles at 355 nm, as well as  
1347 depolarization ratio profiles at 355 nm, on 22 June 2013.
- 1348 • Potenza (40.60°N, 15.72°E); measurements of extinction profiles at 355 and 532 nm, backscatter  
1349 profiles at 1064 nm, as well as depolarization ratio profiles at 532 nm, on 22 and 23 June 2013.
- 1350 • Lecce (40.30°N, 18.10°E); measurements of extinction profiles at 355 and 532 nm, backscatter  
1351 profiles at 1064 nm, water vapour profiles, as well as depolarization ratio profiles at 355 nm, on 22  
1352 and 24 June 2013.

## 1353 **3. Overview of the aircraft and balloon operations**

### 1354 **3.1 Overview of the ATR-42 and F-20 flights**

1355 Figure 3 summarizes ATR-42 and F-20 flights trajectories performed during the experiment and their main  
1356 characteristics. Most of the western Mediterranean basin has been investigated during the campaign by  
1357 both aircrafts, excluding areas under the control of African aviation authorities where authorizations for  
1358 scientific operations are very difficult to obtain. The first period of the campaign (16 to 20 June) was mainly  
1359 dedicated to ATR-42 flights over Spain and Minorca islands (16-17 June, flights 29-32) and Southern France-  
1360 Corsica Island (19-20 June, flights 33-34). During the second period (21-28<sup>th</sup> of June) of the SOP-1a, ATR-42  
1361 flights have been mostly conducted over the Sardinia-Sicily-Lampedusa region in the central Mediterranean  
1362 (flights 35-40). In July, two ATR-42 flights (41 and 42) were conducted over Lampedusa on 02-03 July and  
1363 two others (43 and 44) on 04 July over the Gulf of Genoa. It should be noted that most ATR-42 flights

1364 included some transects at fixed altitudes (generally ~30 min of duration) associated with vertical profiles  
1365 over surface super-sites and secondary stations. Details about each flight track are available on the  
1366 ChArMEx Operation Centre website (ChOC; <http://choc.seedoo.fr>). On Figure 3, F-20 flights trajectories are  
1367 also indicated with the day corresponding to each flight. Except for the 16 and 17 June when F-20 is not  
1368 flying, most of flights have been made jointly between the two aircraft. The longer flight range of the F-20  
1369 allowed us to document the Tyrrhenian Sea (not covered by the ATR-42) and to perform vertical profiles of  
1370 aerosols over Southern Italy in association with EARLINET/ACTRIS lidar observations. It should be finally  
1371 noted the additional F-20 flight between Sardinia and Spain on 27 June specifically dedicated to sample a  
1372 forest fire plume transported long-range from North America.

### 1373 **3.2 In-situ and remote sensing observations on board the ATR-42**

1374 The instrumentation deployed onboard the ATR-42, described in detail in Denjean et al. (2015) and Nicolas  
1375 et al. (in prep.) is summarized in Table 3. It is analogous to the one used for the two super-sites and was  
1376 devoted to the characterization of microphysical, chemical and optical properties of aerosols that have been  
1377 advected above the MBL and so not detectable at the surface. As indicated in Table 3, the number size  
1378 distribution of aerosols, including fine and coarse fractions, as well as the total concentration of particles  
1379 have been evaluated using SMPS, GRIMM, FSSP and UHSAS systems. The corresponding size ranges for all  
1380 instruments are indicated in Table 3. A  $3\text{-}\lambda$  nephelometer and  $1\text{-}\lambda$  Cavity Attenuated Phase Shift (CAPS  
1381 PMex) particle light extinction monitor system (Petzold et al., 2013) have been used conjointly for  
1382 estimating scattering and extinction properties of particles. The CAPS-PMex system, used for the first time  
1383 onboard the ATR-42, provides an additional constrain on the aerosol optical properties, useful to determine  
1384 the absorbing properties. Indeed, the aerosol absorbing characterization remains largely challenging using  
1385 filter techniques (Moosmüller et al., 2009). These optical inter-comparisons have been performed for  
1386 different aerosol plumes and are presented in Denjean et al. (2015).

1387 In addition, passive remote-sensing observations have been conducted during the SOP-1a experiment using  
1388 the PLASMA (Photomètre Léger Aéroporté pour la Surveillance des Masses d'Air) system, which is an  
1389 airborne sun-tracking photometer with two main characteristics: lightness and a wide spectral coverage (15  
1390 channels between  $0.34\text{--}2.25\ \mu\text{m}$ ; see Karol et al., 2013). The instrument contains also a microprocessor

1391 which derives the Sun position depending on time, latitude, longitude (provided by a GPS system) and the  
1392 rotation of the airborne (provided by a gyroscope). Spectral AOD is derived from these direct sun  
1393 measurements and the calibration coefficients. During the campaign, several AOD comparisons were done  
1394 between PLASMA and AERONET/PHOTONS sun-photometers (Cagliari, Lampedusa, Granada) showing  
1395 differences within 0.01 at all wavelengths. Moreover, as a consequence of performing AOD measurements  
1396 at different heights, the aerosol extinction vertical profiles have been also obtained during every  
1397 landing/taking off and during pre-scheduled vertical profiles (Torres et al., this special issue). Finally, upward  
1398 and downward radiative fluxes (SW & LW) have been measured onboard the ATR-42 by means of CMP22  
1399 and CGR4 radiometers calibrated before the campaign.

### 1400 **3.3 Remote-sensing observations on board the F-20**

#### 1401 **3.3.1 LNG observations**

1402 The LEANDRE Nouvelle Generation (LNG) was used in its backscatter configuration during the ChArMEx-  
1403 ADRIMED field operation onboard the SAFIRE F-20 aircraft. In the present campaign, the LNG system  
1404 involved three elastic channels at 1064, 532 and 355 nm. Depolarization was also measured in a fourth  
1405 channel operating at 355 nm. The profiles of atmospheric particulate extinction and backscatter coefficients  
1406 are then retrieved. Zenith pointing lidar measurements were taken before most of the flights from the  
1407 ground at the Cagliari airport (39.25 N, 9.06 E) in Italy. Lidar observations allow the detection of biomass  
1408 burning plumes (BBP) (see part 4.3) arriving at the Cagliari airport on 28 June as described by Ancellet et al.  
1409 ([submitted](#)).

#### 1410 **3.3.2 OSIRIS observations**

1411 OSIRIS (Observing System Including Polarisation in the Solar Infrared Spectrum) is an instrument devoted to  
1412 observation of the polarization and directionality of the solar radiation reflected by the surface-atmosphere  
1413 system. OSIRIS is based on the same imaging radiometer concept as the POLDER instrument (Deschamps et  
1414 al, 1994). It includes two optical systems: one for the visible and near infrared range (VIS-NIR, from 440 to  
1415 940 nm) and the other for the shortwave infrared (SWIR, from 940 to 2200 nm). OSIRIS has eight spectral  
1416 bands in the VIS-NIR and six in the SWIR. During the SOP-1a campaign, OSIRIS was flown aboard the French  
1417 F-20 aircraft and looked at nadir. The quantities used to derive the aerosol and cloud properties from OSIRIS

1418 are the normalized total and polarized (unitless) radiances. The aerosol algorithm used for OSIRIS over  
1419 ocean is an optimal estimation method (OEM), similar to the one described in Waquet et al. (2013). For  
1420 ocean targets, we use all the available angular and polarized information acquired in three spectral bands  
1421 (490, 670 and 865 nm) to derive the aerosol parameters and some properties of the surface. A combination  
1422 of two log normal size distribution functions is assumed (i.e. a fine mode and a coarse mode) as well as a  
1423 mixture of spherical and non-spherical particles (Dubovik et al., 2006). The main retrieved parameters are  
1424 the aerosol AOD, SSA, the fraction of spherical particles within the coarse mode and the complex refractive  
1425 index.

### 1426 **3.4 Balloons operations**

1427 Instrumented balloons were launched by the French Space Agency (CNES) from the airfield of Sant Lluís  
1428 (39°51'55"N, 04°15'15", 55 m asl) on Minorca Island, less than 6 km NE of the Cap d'en Font station  
1429 described above. Two types of balloons were launched to document dust transport events: (i) ascending  
1430 dilatable rubber balloons, and (ii) quasi-Lagrangian spherical pressurized drifting balloons, called BPCL  
1431 (Ballon Pressurisé de Couche Limite, or boundary-layer pressurized balloons).

1432 A total of 15 sounding balloons were launched during the campaign between 12 June and 02 July (Table 4)  
1433 and most balloons reached more than 30 km in altitude. Except for the first test balloon on June 12, the  
1434 payload of sounding balloons included a pair of meteorological sondes with temperature, humidity and GPS  
1435 sensors allowing the retrieval of the position ( $\pm 10$  m), derived pressure ( $\pm 1$  hPa) and wind ( $\pm 0.15$  m s<sup>-1</sup>),  
1436 respectively coupled, for certain flights (see Tables 4 and 5), to an ozone electrochemical sonde (Gheusi et  
1437 al., in prep.) and a LOAC OPC (Renard et al., 2015a, 2015b). Balloon trajectories were confined within the  
1438 area 39-41.2°N in latitude and 3-5°E in longitude.

1439 BPCLs are designed to drift and make observations with a payload of a few kg in the lower troposphere for  
1440 durations of up to several weeks (Vialard et al., 2009). Two versions were used, the standard one of 2.5 m in  
1441 diameter, launched pressurized, which is limited to a maximum float altitude of about 2.5 km (Ducrocq et  
1442 al., 2014), and one developed for ChArMEx of 2.6 m in diameter, launched unpressurized to reach a float  
1443 altitude of more than 3 km in altitude. The payload was composed of a GPS system, PTU instruments on the  
1444 upper pole of the balloon, a LOAC instrument on the lower pole of the balloon and two solar radiation

1445 sensors for upward and downward solar flux measurements. In addition a BPCL equipped with a modified  
1446 ozone electrochemical sonde (Gheusi et al., in prep.) instead of a LOAC was launched in parallel of a LOAC  
1447 balloon on 4 occasions on 16 and 17 June (BPCL B53 and B54, respectively), and on 02 July (BPCL B55 and  
1448 B57). 14 BPCL balloons were launched in total between 16 June and 02 July 2013 (Table 5). Trajectories are  
1449 plotted in Figure 4 with a visualization of daytime vs. night-time conditions. The longest flight in terms of  
1450 distance (1053 km) and time duration (32.6 h) was the ozone BPCL B57, which passed the Sicily strait and  
1451 reached the southern limit of the authorized flight domain south-south-west of Malta. Communication  
1452 failure occurred with the two balloons B53 and B70. Flights were automatically terminated by drilling the  
1453 envelope at a distance of 30 km from southeastern French coasts, western Sicily coast, or North Tunisian  
1454 coast. BPCL float altitudes ranged between about 1850 and 3350 m amsl (balloon B54 with an ozone sonde  
1455 and B71 with a LOAC, respectively). Pairs of balloons with LOAC measurements were launched at different  
1456 float altitudes to document Saharan dust transport on June 16 (2100 and ~3100 m amsl) and June 19 (2550  
1457 and ~3500 m amsl).

#### 1458 **4. Overview of Meteorological Conditions**

##### 1459 **4.1 Synoptic Situation**

1460 As mentioned below, the SOP-1a experiment was mostly characterized by moderate aerosol loading mainly  
1461 controlled by the contribution of mineral dust particles. This situation is well observed through the AOD  
1462 derived by MODIS (Tanré et al., 1997), MISR (Khan et al., 2010), PARASOL (Tanré et al., 2011) or SEVERI  
1463 (Thieuleux et al., 2005) sensors and averaged for the June-July 2013 period (Figure 5), which show an  
1464 average AOD ranging between 0.2 and 0.4 (at 550 nm) over the western and central Mediterranean basins.  
1465 During the SOP-1a, distinct meteorological conditions have led to the transport of mineral dust over the  
1466 basin as shown in the Figures 5 and 6. Figure 7 shows the dust mass concentration together with the  
1467 geopotential and wind at 700 hPa for the 16 June, 19 June, 22 June, 29 June and 02 July. In the following  
1468 sections, we discuss the meteorological conditions (surface wind, sea level pressure, 700 hPa geopotential  
1469 and wind direction) for these different days in order to understand the transport of mineral dust aerosols  
1470 over the Mediterranean.

1471 Wind direction and intensity vertical profiles as simulated by the ALADIN regional model (outputs every 3

1472 hours) as a function of time, for the 11 June to 06 July period and for the whole SOP-1a period at three  
1473 different sites: Ersa, Minorca and Lampedusa islands are shown in Figure 8. At the beginning of the SOP-1a,  
1474 the northwestern Mediterranean area was under the influence of a large pressure ridge at 700 hPa,  
1475 generating a westerly to south-westerly flow over Spain and southern France. Over Minorca, the near  
1476 surface (1000 - 850 hPa) winds were generally from the easterly to north-easterly direction (indicated by the  
1477 blue color in the Figure 8) while the wind direction estimated between 700 and 500 hPa was clearly from  
1478 the south, southwest direction (brown color), which is a favourable condition for the transport of mineral  
1479 dust above South-Spain and then Balearic islands (Figure 6). This point is well observed in figure 7, showing  
1480 the geopotential at 700 hPa for the 16<sup>th</sup> of June. The general circulation at 700 hPa during this dust event  
1481 indicates a reinforcement of the southwesterly winds in southern Spain advecting air masses with large  
1482 concentrations of dust aerosols as shown by SEVIRI AOD (AOD of 0.4-0.5) for that day (Figure 6). A low  
1483 pressure system moved from the British Isles towards the Gulf of Biscay and then the Iberian Peninsula  
1484 between the 17<sup>th</sup> and 20<sup>th</sup> June, leading to veering winds that became southerly over the northwestern  
1485 Mediterranean. Thus in Minorca, the direction of the wind changed from easterly to southerly direction  
1486 between 1000 and 850 hPa. A more pronounced southerly-southwesterly flow was also observed at 700  
1487 hPa in Minorca (19<sup>th</sup>-21<sup>st</sup> of June) as shown by the geopotential at 700 hPa. This circulation characterized by  
1488 the presence of the low geopotential over the Gulf of Biscay induced a strong southerly flow at 700 hPa  
1489 between the Balearic and Corsica islands associated with large dust optical depth concentrated in this zone  
1490 as shown by SEVIRI AOD (AOD of 0.3-0.4) for 19<sup>th</sup> June (Figure 6). This period of the SOP-1a corresponds to  
1491 the two ATR-42 flights 33 and 34 (Figure 3). After 20<sup>th</sup> June, this low pressure system moved eastward,  
1492 generating a trough located between France and Italy, and inducing a waving westerly flow over the north-  
1493 western Mediterranean. As a result, the aerosol loading over the western basin decreased between 21<sup>st</sup> and  
1494 24<sup>th</sup> June, but the westerly (resp. northerly) winds observed at 700 hPa in Minorca (resp. Ersa) (Figure 8)  
1495 reinforced the transport of dust aerosols over the central basin and the Lampedusa station (where winds  
1496 were from the north westerly direction at 3 km height). These meteorological conditions lead to an increase  
1497 of the dust optical depth over the central Mediterranean as shown by the SEVERI instrument and  
1498 AERONET/PHOTONS data. Between 25<sup>th</sup> and 29<sup>th</sup> June, a northwesterly flow set up between the Gulf of



1499 Lions and Sicily. The vertical profiles of the wind direction reveal a remarkable transition on 29<sup>th</sup> June with  
1500 significant changes in direction from westerlies to north, north-westerlies, notably over the Minorca and  
1501 Ersa stations above 850 hPa. The 700 hPa geopotential field on 29 June at 1200 UTC from the ALADIN  
1502 atmospheric model analysis shows a maximum over the Atlantic Ocean whereas a deep low pressure  
1503 system was located over southern Algeria. This strong geopotential gradient lead to intense northerly to  
1504 north-westerly winds at 700 hPa over the western basin leading to significant AOD over Libya (AOD of 0.4-  
1505 0.5) and the Alboran sea (AOD of 0.5-0.6) as shown in Figure 6. These meteorological conditions lead to low  
1506 dust optical thickness over the central Mediterranean as observed by AERONET/PHOTONS data. Finally,  
1507 during the last period of the SOP-1a experiment, (30 June - 05 July), weather conditions became more  
1508 anticyclonic over the region while low systems were confined to northern Europe. Figure 8 shows north-  
1509 westerly winds in the whole troposphere in Lampedusa and Minorca, limiting the presence of dust aerosols  
1510 to the southern part of the north-western Mediterranean.

#### 1511 **4.2 Surface temperature, cloud cover and precipitation**

1512 In terms of surface temperature, which is one of the most important meteorological variables that control  
1513 biogenic or biomass burning aerosol emissions over the Euro-Mediterranean region, the summer 2013 was  
1514 mostly characterized by moderate values as shown in Figure 9. Indeed, during the SOP-1a period, surface  
1515 temperatures (in °C and at 12:00 UTC) derived from NCEP reanalysis (Kalnay et al., 1996) for different days  
1516 reveal moderate values especially over the western Mediterranean region (South-West France and Spain).  
1517 One can observe temperatures of about 15-20°C (at 12:00 UTC) over Spain and Portugal, which are one of  
1518 the main regions of the Mediterranean where large fire events occur. In addition, part of France was also  
1519 characterized by moderate surface temperature but slightly higher than over Spain especially over  
1520 northeastern regions. A strong west to east gradient is observed over Europe with strongest values over the  
1521 eastern regions (around 30°C over Greece and the Balkans) compared to the western basin. A similar  
1522 conclusion is obtained over the Mediterranean Sea with differences of about 5°C between the eastern  
1523 (around 25°C for the SOP-1a period) and the western (around 20°C) basin. Among other factors (such as  
1524 cloud fraction and shortwave radiations), such moderate surface temperatures do not create favourable  
1525 meteorological conditions to produce intense Mediterranean biomass burning events and/or significant

1526 production of secondary organic and inorganic aerosols. Concerning smoke aerosols, GAFS-V1 emission  
1527 data, analysed for the SOP-1a period, do not reveal important primary BC and OC fluxes emissions (not  
1528 shown). This is consistent with the APIFLAME biomass burning emission estimates (Turquety et al., 2014)  
1529 data as reported by Menut et al. (2015).

1530 During the SOP-1a, the cloud cover retrieved over the Euro-Mediterranean region (excluding the  
1531 Mediterranean Sea) from CRU (Climate Research Unit) [data \(Harris et al., 2013\)](#) (Figure 10) indicates the  
1532 largest values (between 75 and 95%) over France, Benelux and Eastern Europe regions. In parallel, southern  
1533 France, as well as western Spain and the Balkans are characterized by moderate cloud cover with values  
1534 around 50-60 % for June 2013. Over the Mediterranean coast, the cloud cover strongly decreases for most  
1535 of countries, with values lower than 40 %. Such spatial cloud cover (observed during the SOP-1a) over the  
1536 Euro-Mediterranean could limit the photochemical processes over the main anthropogenic sources (such as  
1537 the Benelux and Po Valley) and the associated production of secondary aerosols. This could explain for a  
1538 part the low to moderate contribution of fine anthropogenic particles to the total atmospheric loading  
1539 during the SOP-1a. In parallel, the mean precipitation (averaged for June 2013), obtained from the TRMM  
1540 (Tropical Rainfall Measuring Mission) instrument over land and sea (CRU observations are only available  
1541 over land, see Figure 10), are found to be very heterogeneous over the Euro-Mediterranean continental  
1542 region, with some important values over the Balkans, Alps and eastern Europe (from 100 to 250 mm for the  
1543 month of June 2013) and moderate values over Italy, Croatia, western France and Benelux (80 to 100 mm,  
1544 as shown in the Figure 11). Over the Mediterranean Sea, southern Spain and northern Africa, the  
1545 precipitation was smaller, with most of values lower than 20 mm during the SOP-1a.

1546 To summarize, this global view of the synoptic situation, cloud cover and regional precipitation patterns  
1547 indicate that the meteorological conditions during the experimental campaign were favourable to moderate  
1548 mineral dust emissions, associated with a weak contribution of anthropogenic aerosols over the western  
1549 basin. This important characteristic of the SOP-1a is well observed in Figure 12, [which indicates the AOD](#)  
1550 [anomalies \(calculated for the period 2000-2013\)](#) of summer 2013 compared to all AOD summer derived  
1551 from MODIS and MISR data. Indeed, negative AOD anomalies of about -0.05 are found over the western  
1552 Mediterranean basin for the summer 2013, both from MODIS and MISR observations. To conclude, it

1553 appears that the period of observations during the SOP-1a was characterized by aerosol concentration  
1554 slightly lower but in the same range of magnitude that usually observed during summer over the western  
1555 Mediterranean. The level of aerosol concentration was found to be moderate but allows investigating  
1556 several dust and [sea-spray](#) events as well as an interesting intense biomass burning plume advected from  
1557 North America.

### 1558 **4.3 An aged smoke plume advected over Europe**

1559 During the SOP-1a, several large forest fires occurred in North America (Colorado, Alaska, Canada) from  
1560 June 17<sup>th</sup> to 24<sup>th</sup>, 2013, as identified by the MODIS instrument. Absorbing aerosol index produced from  
1561 GOME-2 by KNMI (<http://www.temis.nl/aviation/aai-pmd-gome2b.php?year=2013>) shows that a large  
1562 smoke plume crossed the north Atlantic and reached Western Europe coasts on June 25. Main fire areas,  
1563 with fire radiative power higher than 50 MW (Shroeder et al., 2010), have been detected over Canada  
1564 (Ancellet et al., [submitted](#)). Average MODIS AOD during the same period (23 to 28 June 2013) indicate  
1565 values as high as 1 over the Atlantic Ocean, suggesting that a significant fraction of the aerosol produced by  
1566 the fires was transported to Western Europe during the ChArMEx/ADRIMED field campaign. To investigate if  
1567 the western Mediterranean has been impacted by these fires, a forward simulation of the Lagrangian plume  
1568 dispersion model FLEXPART (Ancellet et al., [submitted](#)) has been conducted to quantify the spatial extent of  
1569 the fire plume transport for 11 days. Fires emissions areas were identified by MODIS observations over  
1570 several locations in Canada and Colorado. The aerosol mass is emitted in the transport model from June  
1571 17<sup>th</sup> to 28<sup>th</sup> in a 3 km layer as suggested by the CALIOP lidar observations over Canada. The biomass  
1572 burning plume reaches much lower latitudes over Europe, down to the Western Mediterranean 4-10 days  
1573 after the emission in Canada. During the SOP-1a, the plume was mainly present in the altitude range of 2.5 -  
1574 4.5 km and has been sampled by many remote sensing and in-situ instruments on June 27<sup>th</sup> and 28<sup>th</sup>; at  
1575 Minorca and Cagliari surface stations, and between Sardinia and Lampedusa onboard the ATR-42 aircraft.

## 1576 **5. Overview of aerosol physical-chemical-optical properties, vertical profiles and local direct** 1577 **radiative forcing**

### 1578 **5.1 Aerosol physical and chemical properties**

#### 1579 **5.1.1 Aerosol mass and number concentration at the two super-sites**

1580 First, PM concentrations between the two different stations are reported in the Figure 13, which reports the  
1581 daily time-series of PM1 and PM10 at Ersa, as well as PM10 and PM40 at Lampedusa. The results indicate a  
1582 significantly higher mass concentration at Lampedusa compared to Ersa. Indeed, the mass concentration  
1583 observed at Lampedusa is comprised between 10 and 30  $\mu\text{g m}^{-3}$ , with a mean of 21  $\mu\text{g m}^{-3}$ , which is two  
1584 times higher than the averaged PM10 ( $\sim 9 \mu\text{g m}^{-3}$ ) measured at Ersa. One can note the significant peak of  
1585 PM40 (maxima of 75  $\mu\text{g m}^{-3}$ ) at Lampedusa during the 24 to 26 June period that corresponds to a significant  
1586 production of primary marine aerosols. Finally, the PM1 concentration at Ersa is found to be almost  
1587 constant during the period of the campaign, with a mean value of 6  $\mu\text{g m}^{-3}$ . In order to take into account the  
1588 difference of altitudes between the two sites of Lampedusa and Ersa, we have applied a correction factor to  
1589 PM10 observed at Ersa (530 m) for estimating a new PM10 concentration corresponding to the altitude of  
1590 Lampedusa. In that sense, we have applied the logarithmic law reported by Piazzola et al. (2015) using a  
1591 value of 0.75 for the factor  $s$  to correct the mass concentration of sea spray aerosols only. The calculated  
1592 mean value of PM10 is about 12  $\mu\text{g m}^{-3}$  (Figure 13), closer to the mean value observed at Lampedusa (21  $\mu\text{g}$   
1593  $\text{m}^{-3}$ ). In addition, the background aerosol number concentrations (for  $D_p > 0.01 \mu\text{m}$ ) observed within the  
1594 boundary layer in Corsica averaged  $\sim 2000 \text{ cm}^{-3}$  (not shown). The lowest concentrations ( $\sim 200 \text{ cm}^{-3}$ ) resulted  
1595 from aerosol activation to cloud droplets, and scavenging from cloud droplets and rain drops, while high  
1596 concentrations as high as 10000  $\text{cm}^{-3}$  were observed during pollution events from continental European air  
1597 masses. The number concentrations showed a diurnal cycle suggesting that the site was situated within the  
1598 marine boundary layer during daytime and within the free troposphere during night-time. The analysis of  
1599 the diurnal variation of the particle number size distribution is further indicating that nucleation events also  
1600 increased the particle number concentration during daytime, about one third of the time (Sellegrì et al., in  
1601 prep.). The periods of high aerosol number concentrations detected between the 12<sup>th</sup> and 25<sup>nd</sup> of June were  
1602 also dominated by a single mode with diameters between 30 and 150 nm. The small Aitken mode ( $d_g < 50$   
1603 nm) associated with pollution events suggests a relatively fresh aerosol that has been formed during  
1604 transport from the European continent. The largest mode ( $d_g \sim 150 \text{ nm}$ ) occurred during the dust event on  
1605 18 June.

### 1606 5.1.2 Columnar particle volume size distribution

1607 We have used the column-integrated particle size volume distributions derived from AERONET/PHOTONS  
1608 sky radiance measurements (Dubovik et al., 2000). These size distributions allow investigating the changes  
1609 in aerosol size distribution between different stations during the SOP-1a and over the western basin. Four  
1610 different stations have been studied, which include the two super-sites of Lampedusa and Ersa, as well as  
1611 the aircraft and balloon base stations; Cagliari and Cap d'En Font, respectively. Daily volume size  
1612 distributions for both sites are represented in the Figure 14, as well as the averaged (red curve) size  
1613 distribution for the whole period (1 June to 5 July) and the number of observations. In addition, the mean  
1614 values of the volume radius, concentration of fine and coarse mode and the standard deviations of the  
1615 volume size distribution are reported in the Table 6. It should be noted that the scales of the y-axis are  
1616 different for each figure. One can note the bimodal size distribution for both stations with large spread of  
1617 radius values, especially for the coarse mode. The most important concentrations are obviously observed in  
1618 Lampedusa, near the mineral dust sources, with maxima of  $\sim 0.12 \mu\text{m}^3 \mu\text{m}^{-2}$  for the coarse mode. In parallel,  
1619 the lowest concentrations are observed at the Ersa station due to the absence of intense polluted-  
1620 photochemical or smoke aerosol events over southern France and Italy during the SOP-1a. In that sense, the  
1621 mean contribution (red curve) of the coarse mode to the aerosol volume size distribution appears to be  
1622 predominant at most sites, except at the Ersa station. However, the inclusion of the corrected factor  
1623 (Piazzola et al., 2015) for taking into account the altitude of the Ersa site reduces slightly the differences in  
1624 the concentration of the coarse mode with the Lampedusa station (see Table 6). This point is well noted for  
1625 the Cap d'En Font station, where the concentration of each modes appear as equivalent, due to the absence  
1626 of pollution from the Iberian Peninsula during the period of observations. For this site, it is interesting to  
1627 note the intense peak for the 27<sup>th</sup> June, with concentration near  $0.08 \mu\text{m}^3 \mu\text{m}^{-2}$ , which is due to the  
1628 transport of an important smoke plume over the Mediterranean (see Ancellet et al., [submitted](#); and  
1629 Chazette et al., [submitted](#)). Finally, the contribution of the coarse mode clearly increases for the two other,  
1630 more southern Italian sites of Cagliari and Lampedusa, which are more affected by the mineral dust  
1631 compared to Ersa and Cap d'En Font. The variability of AERONET products collected over a period of four  
1632 years at Ersa and Palma de Mallorca, near Cap d'En Font, is reported in Sicard et al. (2015b, this special  
1633 issue). It is interesting to note the variability ( $\pm 0.05$ ) in the derived size of the coarse mode at Lampedusa

1634 (see Table 6), which will be analysed in regards to dust sources in a future study. The derived volume  
1635 concentrations over these two stations highlight the moderate dust activity occurring during the SOP-1a  
1636 experiment, when compared to stations under high dust conditions. As an example of comparisons,  
1637 Dubovik et al. (2002) reported a large range of concentration for the coarse mode for dusty sites (such as  
1638 Cape Verde or Solar Village), which are characterized by larger concentrations, close to  $0.30 \mu\text{m}^3 \mu\text{m}^{-2}$ . In  
1639 parallel, the Bahrain (Persian Gulf) AERONET station is characterized by a concentration of  $0.14\text{-}0.15 \mu\text{m}^3$   
1640  $\mu\text{m}^{-2}$ .

### 1641 **5.1.3 Particle size distribution during transport**

1642 Figure 15 presents an example of the evolution of the aerosol particle number concentrations in the 19  
1643 particle size classes of the LOAC instrument as measured along the northward trajectory of the BPCL balloon  
1644 B74 from Minorca Island to the French coast (see Figure 4). The balloon was launched at 09:46 UTC on 16  
1645 June 2013 during a moderate desert dust event shown on top of Figure 6 (AERONET-derived AOD at 500 nm  
1646 of 0.15). It drifted at a constant altitude of  $\sim 2.1$  km at the bottom of the African dust layer observed with  
1647 the WALI lidar at Minorca (not shown; see Chazette et al., 2015), and was automatically forced to land on  
1648 the sea before reaching the coast South of Marseille, after a 12-h flight of 368 km. The dominant mineral  
1649 dust nature of the particles was confirmed by the LOAC particle typology measurements (Renard et al.,  
1650 2015b). The figure illustrates that LOAC has detected large particles of up to  $50 \mu\text{m}$  in diameter, although  
1651 the plume originated from North-Africa a few days before (Renard et al., 2015b). The concentrations of  
1652 particles remained relatively constant during the flight, suggesting either no significant sedimentation of the  
1653 largest particles during the flight or compensation by particles coming from above. The BPCL balloon B70  
1654 launched a few minutes later drifted at an upper altitude of  $\sim 3.1$  km and followed a different trajectory  
1655 towards East (Figure 4) but showed a quite similar extended particle size range with larger concentrations in  
1656 almost all channels except the extremes (not shown). The 4 other drifting balloons launched in the dust  
1657 layer during this event on June 17 and 19 (Table 5) did confirm the presence of very large particles ( $>20 \mu\text{m}$ ),  
1658 which cannot be reported by AERONET particle size distribution retrieval algorithm (Hashimoto et al., 2012).  
1659 In addition, observations of large particles ( $>15 \mu\text{m}$ ) was systematically found during all other LOAC balloon  
1660 flights drifting in African dust layers, which will need further analysis to better understand the process that

1661 can maintain such large particles in suspension during several days.

1662 Concerning the aerosol microphysical properties, aircraft observations have allowed to investigate the  
1663 vertical structure of aerosol size distribution showing particles characterized by large size ( $>10\ \mu\text{m}$  in  
1664 diameter) within dust plumes. In addition, in most of cases, a coarse mode of mineral dust particles,  
1665 characterized by an effective diameter  $D_{\text{eff},c}$  ranged between 5 and  $10\ \mu\text{m}$ , has been detected within the dust  
1666 layer located above the MBL. Such values are found to be larger than those referenced in dust source region  
1667 during FENNEC, SAMUM1 and AMMA, as well as measurements in the Atlantic Ocean at Cape-Verde region  
1668 during SAMUM-2 and at Puerto-Rico during PRIDE. The complete analysis of aerosol size distribution is  
1669 detailed in Denjean et al. (2015).

#### 1670 **5.1.4 Aerosol chemical composition**

1671 In terms of aerosol chemical properties, an example of averaged mass-size distributions for carbonaceous  
1672 (Elemental and Organic Carbon, EC and OC) species (mass size distribution of inorganic and mineral dust  
1673 aerosols are not shown) obtained at Ersa from a 12-stage cascade impactor (DEKATI system, see Table 1) is  
1674 reported in Figure 16. The aerosol chemical properties obtained from PILS instrument at Ersa are detailed in  
1675 Claeys et al. (2015). As mentioned in Table 1, the measurements were obtained by using a 2-day collection  
1676 period in order to obtain a sufficient aerosol mass on filters for chemical analyses. This system provides the  
1677 speciation of the mass size distribution, including fine and coarse fractions. Such information is very useful  
1678 to derive optical properties using Mie calculations (Mallet et al., 2011) for the main particle types (sulfates,  
1679 ammonium, nitrates, [sea-spray](#), dust, black and organic carbon). This provides crucial information's on key  
1680 radiative properties which are classically used in regional climate models (mass extinction efficiencies, SSA  
1681 and asymmetry parameter). Furthermore, it allows one to assess the spectral dependence of radiative  
1682 properties, which cannot always be estimated from in-situ instrumentation.

1683 Concerning OC (blue curves), observations clearly report a bi-modal mass size distribution with two  
1684 different peaks for the majority of cases. The first (almost constant) peak is found in the  $0.4\text{-}0.5\ \mu\text{m}$  size  
1685 range in diameter and more occasionally a second one occurs in the coarse fraction around  $3\ \mu\text{m}$ .  
1686 Compared to the few available data over the Western Mediterranean, these mass size distributions are  
1687 found to be different from those obtained over Southern France, especially for the accumulation mode.

1688 Indeed, during the ESCOMPTE experiment in southern France, Mallet et al. (2003) also observed a bi-modal  
1689 size distribution for OC aerosols but with a finer accumulation mode observed in the 0.1-0.2  $\mu\text{m}$  size range.  
1690 Differences between the two observations is likely due to the proximity of anthropogenic sources during the  
1691 ESCOMPTE experiment compared to the Ersa station, where the possible ageing of carbonaceous particles  
1692 could affect the size of aerosols. On the contrary, the coarse mode of OC appears in the same range of size,  
1693 around 3  $\mu\text{m}$ , for both experiments. Compared to data obtained in the eastern Mediterranean basin, the OC  
1694 mass size distributions are in good agreement with those estimated by Sciare et al. (2003) in Crete during  
1695 the MINOS campaign, with two modes around 0.4  $\mu\text{m}$  and 3  $\mu\text{m}$ . The BC (green curves in Figure 16) mass  
1696 size distribution is also characterized by a bi-modal size distribution, with two modes well correlated with  
1697 the mass size distribution of OC, except for the 16-19 June period (dust episode), where the size of EC fine  
1698 mode is higher ( $\sim 0.5\text{-}0.6 \mu\text{m}$ ) than OC aerosols, the EC coarse mode remaining similar at  $\sim 3 \mu\text{m}$ . This reveals  
1699 a possible external mixing of carbonaceous aerosols for this event.

1700 It should be also noted that the EC concentrations observed at the Ersa station are logically (due at least to  
1701 the altitude of the station and the absence of intense pollution during the SOP-1a, see section 4) lower  
1702 ( $0.39 \mu\text{g}\cdot\text{m}^{-3}$ ) than EC concentrations (PM<sub>2.1</sub>) reported by Eleftheriadis et al. (2006) from the eastern  
1703 Mediterranean during the summer season ( $0.6 \mu\text{g}\cdot\text{m}^{-3}$ ) in July 2000. The same ascertainment is obtained on  
1704 OC concentrations with higher values ( $4.2 \mu\text{g}\cdot\text{m}^{-3}$ ) reported by Eleftheriadis et al. (2006) compared to  
1705 observations at Ersa ( $1.5 \mu\text{g}\cdot\text{m}^{-3}$ ). Concerning the modes of the OC and EC particle mass size distributions,  
1706 the two identified modes detected in Ersa are consistent with those reported by Mallet et al. (2011) at the  
1707 Porquerolles coastal island (southeastern France), who also detected two (fine and coarse) different modes  
1708 of the mass size distributions for EC (0.3-0.4  $\mu\text{m}$  and 4-6  $\mu\text{m}$ ) and OC (0.3  $\mu\text{m}$  and 5-6  $\mu\text{m}$ ) aerosol particles.

1709 In most cases, we observed at Ersa lower concentrations of EC particles for both modes compared to OC  
1710 aerosols. The mass of OC and BC observed during the SOP-1a, for both modes, are found to be equivalent  
1711 with those observed by Sciare et al. (2003) in Crete in summer 2001. They report mean values of 0.30 and  
1712  $0.15 \mu\text{g m}^{-3}$  for fine OC and BC, respectively. During the MINOS experiment, the mean concentrations for OC  
1713 and BC coarse modes were about 0.1 and  $0.02\text{-}0.03 \mu\text{g m}^{-3}$ , what is also consistent with the observations at  
1714 Ersa. Finally, the mass concentrations obtained for each mode at Ersa are logically lower than those



1715 obtained during the ESCOMPTE experiment, located much closer to pollution sources. For example, EC and  
1716 OC fine mode concentrations were respectively between 0.8 and 2.8  $\mu\text{g m}^{-3}$  and between 3.1 and 6.9  $\mu\text{g m}^{-3}$   
1717 during ESCOMPTE (Mallet et al., 2003). In addition and as discussed in the parts 4.1 and 4.2, the  
1718 meteorological conditions (surface temperature, meteorological synoptic situations) observed during the  
1719 SOP-1a campaign were not favourable to produce large concentration of polluted or smoke aerosols,  
1720 compared to the ESCOMPTE campaign, where AOD as large as 0.3-0.5 (in the visible range) has been  
1721 observed due to important concentration of anthropogenic-polluted particles. It should be noted that, in  
1722 parallel to filter analyses, higher time resolved observations from the PILS systems have been deployed at  
1723 the two stations of Lampedusa and Erba (Claeys et al., in prep.) during the SOP-1a.

1724 In parallel to filters chemical analysis, over 700,000 single particle mass spectra were generated by the A-  
1725 TOFMS instrument during the sampling period (not shown). A K-means algorithm ( $K = 80$ ), as described in  
1726 detail by Healy et al. (2010) and Gross et al. (2010) was used to classify aerosol mass spectra into different  
1727 particle classes. More than 40 distinct ATOFMS particle classes were identified and subsequently grouped  
1728 into 8 general categories for clarity. Elemental carbon containing particles dominated the dataset (55% of  
1729 total spectra), followed by K-rich particles (30%) and sea-spray (7%). The remaining particle categories  
1730 include organic carbon (OC)-containing (3%), trimethylamine (TMA)-containing (3%), shipping (2%), Fe-  
1731 containing (0.5%) and Ca-containing (0.3%). EC particles dominated the first third of the sampling period,  
1732 decreased noticeably for approx. 6 days and then dominated the rest of the sampling period again. In  
1733 contrast, K-rich particle (associated with biomass burning and dust) numbers were high only for the latter  
1734 half of the campaign, with a peak on 27-28 June. The profiles of these two particle categories suggest  
1735 transport from regional sources. Sea-spray particle numbers were at their highest during the period where  
1736 EC particles were at their lowest, and were generally low when EC particle numbers were high. OC-  
1737 containing particles were present during the same period K-rich numbers peaked, suggesting an association  
1738 with the transport of biomass burning particles. TMA particles were present in low numbers throughout the  
1739 sampling period, suggesting a less regional source, independent of the air masses influencing EC and sea-  
1740 spray particle occurrence. The same can be said of Fe and Ca-containing particles, likely to be local dust,  
1741 while shipping particle numbers were slightly higher during the first half of the sampling period.

1742 Finally and concerning the aerosol chemical properties, an interesting aspect of the observations deployed  
1743 during the SOP-1a concerns the rBC concentrations obtained from the SP2 instrument onboard the ATR-42.  
1744 Despite its importance, studies on rBC were until now limited to surface-based measurements in the  
1745 Mediterranean region. Measurements of vertical distribution of rBC concentrations provide crucial  
1746 information for assessing the rBC radiative effects in the region. Figure 17 shows the vertical distributions of  
1747 rBC mass concentrations measured by the SP2 in the five areas (Granada, Minorca, Lampedusa, South-France  
1748 and Ersa). For the different vertical soundings, rBC mass concentrations ranged between 20 and 690 ng m<sup>-3</sup>  
1749 close to the surface. The surface rBC concentrations were generally less than 200 ng m<sup>-3</sup>, typical for  
1750 continental and regional background sites in the western Mediterranean basin (Ripoll et al., 2015). The  
1751 lowest surface concentration of rBC (~ 20 ng m<sup>-3</sup>) were found in south-France over the open sea with  
1752 almost no local contribution of anthropogenic aerosols. Maxima surface concentrations (~ 690 ng m<sup>-3</sup>)  
1753 were recorded over Granada where frequently heavy traffic emissions are occurring. These observations  
1754 were obtained between 07:15 and 07:45 UTC when the convection was not fully developed, which probably  
1755 did not favour the vertical transport of local emissions over Granada. A prominent feature in vertical profiles  
1756 is the presence of significant concentrations of rBC up to 5-6 km altitude. Therefore the regional transport  
1757 of rBC particles was not only limited to the MBL but occurred also at higher altitude. In most of the  
1758 observed cases, the rBC vertical distribution in the free troposphere reveals a strongly stratified structure  
1759 characterized by either single isolated plumes or more uniform layers. It is worth noting the presence of rBC  
1760 layers above the MBL in the open sea that could be attributed to convective transport from distant sources.  
1761 Only in few observed cases, rBC mass concentration decreased monotonically with increasing altitude, most  
1762 likely due to vertical transport of air masses from surface to higher heights.

## 1763 **5.2 Aerosol optical properties**

### 1764 **5.2.1 In-situ optical properties at the surface**

1765 Figure 17 reports the (daily mean) time-series of nephelometer observations obtained at the surface for the  
1766 Ersa and Lampedusa stations. Daily scattering coefficients (at the three nephelometer wavelengths of 450,  
1767 550 and 700 nm) are reported, as well as the scattering Angström exponent (AE) calculated between 450  
1768 and 700 nm. At 550 nm and at Ersa, the scattering coefficient presents a significant variability during the

1769 SOP-1a with peaks of about 35-40  $\text{Mm}^{-1}$  during the dust event (19-20<sup>th</sup> June) transported over the Corsica  
1770 island, associated to low values ( $15 \text{ Mm}^{-1}$ ) for certain periods of time, as for 21-22 June. The mean  
1771 scattering coefficient (at 550 nm) is  $24 \text{ Mm}^{-1}$ . Such scattering coefficient values are comparable to  
1772 observations reported by Vaishya et al. (2012) at the Mace Head station for Atlantic marine air, with  
1773 scattering coefficient (at 550 nm) ranged between 10 and  $25 \text{ Mm}^{-1}$  during the summer period. In terms of  
1774 scattering spectral dependence, the calculated scattering AE is found to be almost constant, with  $\text{AE} \sim 1.5-2$   
1775 and a mean value of 1.71 (indicating that scattering is mostly dominated by fine aerosols) during the SOP-  
1776 1a, except for the 23rd-24th of June. **The lowest values ( $\text{AE} \sim 0.3-0.5$ ) observed during this period are the**  
1777 **result of a large contribution of coarse sea-spray aerosols (Claeys et al., in prep.) due to moderate ( $5 \text{ m s}^{-1}$ )**  
1778 **westerly winds (see Figure 8) at the Ersa station,** which is also observed from the filter chemical size-  
1779 resolved analyses and detected on the A-TOFMS and VHTDMA data. In parallel, we observe that the dust  
1780 event occurring in Ersa on 18-20 June is not correlated to low scattering AE, revealing a possible  
1781 contribution of fine dust particles only to scattering, result of a possible deposition of the coarse dust  
1782 fraction during transport. The AERONET-derived AE between 440 and 870 nm shows values  $<1$  in the  
1783 afternoon of 19 June and early morning of June 20 suggesting that coarse dust is present in the column. At  
1784 Lampedusa, the daily scattering coefficient (at 550 nm and from PM40 inlet) is between 20 to  $90 \text{ Mm}^{-1}$   
1785 (mean value of  $50 \text{ Mm}^{-1}$ ), which is twice higher than at Ersa (Figure 17). The scattering AE was also highly  
1786 variable, with values ranging between 0.5 and 2.5 (mean value of 1.1). The range of variability of these  
1787 values is due to the observed switch from clean air masses strongly impacted by marine emissions to  
1788 polluted air masses of various ages, including very aged/processed air masses from Northern Europe. A  
1789 single intrusion of mineral dust at the site was recorded on June 9 as a result of a cyclone-type of transport  
1790 from Tunisia (Formenti et al., in prep.).

### 1791 **5.2.2 Remote-sensing observations from the surface**

1792 The optical properties obtained from sun-photometer observations for different AERONET/PHOTONS sites  
1793 are shown in Figure 18. **The AERONET/PHOTONS stations have been chosen as located in a domain**  
1794 **encompassing most of the SOP-1a in-situ and remote sensing observations (Figure 3) and they are**  
1795 **characterized by different aerosol regimes (see Table 2).** The total AOD, Absorbing Aerosol Optical Depth

1796 (AAOD), AOD for the fine (AOD<sub>f</sub>) and coarse (AOD<sub>c</sub>) modes of the volume size distribution, are indicated (at  
1797 440 nm) for 11 AERONET/PHOTONS stations (Table 2). As mentioned previously, the AOD time-series reveal  
1798 moderate values, never reaching values as large as reported during the summer 2012 ChArMEx/TRAQA  
1799 SOP-0 experiment (Rea et al., 2015). During summer 2013, the AOD was generally comprised between 0.1  
1800 and 0.7 (at 440 nm) for most of the AERONET/PHOTONS sites. Over the western basin, the Granada,  
1801 Minorca and Barcelona sites display the largest values during the transport of dust aerosols as detected by  
1802 satellite remote-sensing observations (Figure 6) for the 16 to 20<sup>th</sup> of June. During this dust event, the  
1803 contribution of fine and coarse modes to the total extinction AOD is equivalent. Over the central basin,  
1804 Lampedusa data reveal various peaks. The largest AOD was measured on June 6 (about 0.84 at 440 nm) and  
1805 8 (about 0.63 at 440 nm). Other peaks occurred around June 22 and July 01-02, with corresponding AOD of  
1806 about 0.30-0.40 (at 440 nm), with again an equivalent contribution of each mode of the volume size  
1807 distribution to the AOD. On June 27-28, an AOD peak was also observed over most of the sites and  
1808 corresponded to the transport of an aged smoke plume from the Canadian continent. In this specific case,  
1809 AOD was comprised between 0.25 and 0.50 (at 440 nm). Contrarily to the dust events, the contribution of  
1810 the different modes to AOD was significantly different during this episode. Indeed, as shown in Figure 18,  
1811 AOD was mostly controlled by the fine mode of the volume size distribution. This specific biomass burning  
1812 case is more deeply analysed by Ancellet et al. ([submitted](#)) and Chazette et al. ([submitted](#)).

1813 We have also used the SSA dataset for making comparisons of its optical parameters between different  
1814 stations. As for the size distributions, we have analysed dataset in four stations, which are Ersa, Lampedusa,  
1815 Cagliari and Cap d'En Font. All (daily) SSA retrievals, associated with the mean values (at the four  
1816 wavelengths), are included in the Figure 19. Due to the moderate AOD over the period, we used Level 1.5  
1817 AERONET/PHOTONS products. In that sense, it should be reminded that uncertainties associated to SSA  
1818 retrievals are important, about  $\pm 0.07$  as reported by Dubovik et al. (2000). The results indicate an important  
1819 variability of SSA and its spectral dependence over the different stations. At 440 nm, the mean SSA is  
1820 comprised between 0.91 and 0.98, with the lowest (resp. highest) value observed in Lampedusa (resp. Ersa).  
1821 Hence, aerosols appear as almost scattering at Ersa and moderately absorbing at Lampedusa. The  
1822 contribution of the coarse mode to the total size distribution could explain the lower values observed in

1823 Lampedusa at this wavelength. Indeed, the radiative effects and optical properties of dust are strongly  
1824 dependent on the coarse mode size distribution as the larger particles appreciably decrease the SSA  
1825 (McConnell et al., 2010; Otto et al., 2009). More recently and during the FENNEC experiment, Ryder et al.  
1826 (2013) have calculated SSA (at 550 nm) for dust aerosols using the full range of sizes measured, indicating  
1827 that dust SSA was highly sensitive to effective diameter: size distributions with the largest effective  
1828 diameters produced the lowest SSA values. [The presence of a coarse mode could also be due to the](#)  
1829 [presence of marine aerosols within the MBL in Lampedusa](#). Observations for the Cap d'En Font and Cagliari  
1830 stations reveal an intermediate value (0.93 at 440 nm) in Cagliari, which is also more affected by mineral  
1831 dust aerosols (Figure 14). We can also observe very low values in Cagliari (for the period of 14 to 17 June)  
1832 that could be due to local pollution. Anyway, it should be remained that those retrievals have been  
1833 performed under low AOD ( $\sim 0.10$  at 440 nm) conditions and are associated to large uncertainties. One  
1834 important point concerns the changes in the SSA spectral signature between Ersa (negative tendency  
1835 between 440 nm to 1020 nm) and Lampedusa (positive) stations. This observation is consistent with  
1836 AERONET/PHOTONS data analysed for a long-time period over the Mediterranean by Mallet et al. (2013),  
1837 who report different spectral variations in SSA, following the aerosol regime (dusty and/or polluted  
1838 particles). One of the main conclusions here is that aerosols are found to be moderately absorbing during  
1839 the SOP-1a period, what is consistent with in-situ observations performed onboard the ATR-42 aircraft and  
1840 summarized by Denjean et al. (2015).

### 1841 **5.2.3 ATR-42 and F-20 aircraft observations**

1842 In parallel to surface observations, an example of the vertical profiles of aerosol optical properties obtained  
1843 from ATR-42 measurements is shown Figure 20 that corresponds to the flight 35-36 over the station of  
1844 Lampedusa for the 22<sup>nd</sup> of June (see also Denjean et al., 2015 and Nicolas et al., in prep.). Scattering  
1845 coefficients (in  $Mm^{-1}$ ) are plotted at 450, 550 and 700 nm (left) versus altitude (in meter). Completely  
1846 different behaviours in the scattering spectral dependence as a function of altitude were observed. Two  
1847 different aerosol plumes characterized by a significant spectral dependence (typically of submicronic  
1848 polluted, smoke or fine marine aerosols) are observed around 1000 and 2000-2500 m. Above 3000 m, the  
1849 spectral dependence is clearly reduced, corresponding to air masses with high mineral dust concentrations.

1850 For this upper aerosol layer, the scattering coefficient increases up to  $60 \text{ Mm}^{-1}$ . The analysis of the extinction  
1851 (at 530 nm) vertical profiles obtained from the CAPS system (Table 3) reveals an excellent agreement with  
1852 nephelometer data showing the peaks of extinction at similar altitudes (see Denjean et al., 2015), with  
1853 maxima ( $\sim 90 \text{ Mm}^{-1}$ ) logically observed within the dust plumes (4000-5000 m). Number concentrations, as  
1854 well as volume size distributions, highlight the significant atmospheric loading by particles with diameter  
1855 higher than  $1 \mu\text{m}$  above 3000 m (maxima of  $5000 \# \text{ cm}^{-3}$ ). For this atmospheric layer, the volume size  
1856 distribution is characterized by a coarse mode, around 6-8  $\mu\text{m}$ . As previously mentioned, vertical profiles of  
1857 optical properties in terms of AE, SSA, asymmetry parameters as well as their spectral dependence are  
1858 presented and discussed in details by Denjean et al. (2015) and Nicolas et al. (in prep.). The airborne SW  
1859 and LW radiation measurements and the comparison with radiative transfer model simulations at  
1860 Lampedusa are presented by Meloni et al. (in prep.).

### 1861 **5.3 Aerosol vertical structure**

#### 1862 **5.3.1 Lidar surface observations**

1863 Although deeply analysed in other dedicated papers, some examples of the aerosol vertical profiles are  
1864 presented here. First and over the Minorca station, surface lidar observations in Figure 21a were obtained  
1865 during June 16 and 17, that corresponds to the first event of transported mineral dust over the western  
1866 basin. They show a dust aerosol layer located between 1.5 and 5 km, with a maximum of aerosol extinction  
1867 (at 355 nm) around  $0.10 \text{ km}^{-1}$  on 16<sup>th</sup> of June between 12:00 and 14:00 Local Time (LT). Comparisons of  
1868 retrieved AOD with the lidar system is shown to be very consistent with sun-photometer observations for  
1869 these two days (Figure 21a, top), with moderate AOD (at 355 nm) ranging between 0.2 and 0.4 at  
1870 maximum. During 17 June, the dust layer is less intense and the aerosol extinction above 1.5 km decreases.  
1871 After 14:00 LT, Figure 21a clearly shows that most of the contribution to AOD is due to the MBL over the  
1872 Minorca station. At Ersa (Figure 21b), the dust event reached the northern tip of Corsica on 19 June. A deep  
1873 depolarizing aerosol layer was observed at altitudes between 3 and 6 km. In the night of the 20<sup>th</sup>, the  
1874 particulate depolarization ratio is close to 18% and the lidar ratio within the dust layer was estimated at 46  
1875 sr. The extinction coefficient remains moderate within the dust layer  $\sim 0.05 \text{ km}^{-1}$  (Figure 21b) between 4 and  
1876 6 km. It should be noted that a complete analysis of lidar observations series obtained over the cape Corsica

1877 site is reported in Leon et al. (2015). The dust event vertical distribution is further analysed by means of the  
1878 EARLINET lidar stations in Sicard et al. (2015) and by means of the EARLINET and ChArMEx lidar stations in  
1879 Barragan et al. (in prep.).

1880 In addition to Minorca and Ersa, two lidars were also operated at Lampedusa during the SOP-1a and  
1881 provided vertical profiles of aerosol backscattering and depolarization. The ENEA/University of Rome lidar  
1882 measures the aerosol backscattering at 532 and 1064 nm, plus the depolarization at 532 nm. This system  
1883 was operated throughout the campaign, although not continuously. The lidar data retrieval is described by  
1884 Di Iorio et al. (2009), and uses sun-photometer AOD observations to constrain the determination of the  
1885 aerosol backscattering profile. Figure 22a shows the evolution of the vertical profile of the aerosol  
1886 backscattering coefficient at 1064 nm on 3 July 2013 at Lampedusa. At low altitudes the air masses reaching  
1887 Lampedusa originated from the North. Air masses above 2 km conversely came from a southwesterly  
1888 direction crossing North Algeria and Tunisia, and carried desert dust. Elevated backscattering attributed to  
1889 dust was observed up to 5 km altitude, and a steep transition in the backscattering coefficient occurred at  
1890 this altitude throughout the day. Figure 22b shows the backscattering coefficient profile at 532 and 1064  
1891 nm, and the depolarization ratio measured at 15:45 UT by the ENEA/University of Rome and the LISA lidars.  
1892 Evidently, the backscattering coefficient above 2 km shows very small wavelength dependence, and  
1893 elevated values of the depolarization ratio, as expected from large irregular desert dust particles (Sassen,  
1894 1999). The influence of large particles is smaller below 2 km, where the backscattering coefficient shows  
1895 some dependency on wavelength, and the depolarization ratio decreases. The significant role played by the  
1896 large particles on 3 July is also confirmed by the aerosol size distribution and optical properties (i.e., values  
1897 and spectral dependency of the refractive index and single scattering albedo) retrieved from the AERONET  
1898 observations at Lampedusa. The average AOD (at 500 nm) was 0.28, and the Angström exponent ([calculated  
1899 between 440 and 870 nm](#)) was 0.39, as expected for cases with a large contribution of desert dust. The  
1900 retrieved columnar volume size distributions on the two days show that the mode with a median radius  
1901 around 2  $\mu\text{m}$  is 2-3 times more intense on 3 July than on 17 June.

1902 Finally, nighttime measurements at Potenza (Italy) on 21 June starting at 23:40 UT, which coincides with the  
1903 arrival of the Saharan dust event over southern Italy, indicate a clear signature of Saharan dust in the

1904 tropospheric layer between 1.8 and 3.9 km, an extinction-related AE value of approximately 0 is measured  
1905 between roughly 2 and 3 km and a quite constant LR around 50 sr at both 355 and 532 nm (not shown, see  
1906 Sicard et al., 2015a; Barragan et al., in prep.).

### 1907 **5.3.2 LNG observations**

1908 An example of LNG (Lidar Nouvelle Génération) observations onboard the F-20 aircraft is presented in the  
1909 Figure 23 for the 19<sup>th</sup> of June that corresponds to a flight (12:46 to 13:26 TU) from Sardinia to the Gulf of  
1910 Genoa. The aerosol extinction (in  $\text{km}^{-1}$  and at 532 nm) is represented in function of latitude during this flight  
1911 as well as the associated AOD with a high temporal and spatial frequency. One can observe the significant  
1912 North-South gradient during this dust event with low-values of AOD (around 0.1 at 532 nm) for latitude of  
1913 44°N and moderate-high AOD (0.40 to 0.55) for latitudes lower than 42-43°N. In terms of vertical structure,  
1914 this increase of AOD is due to an upper dust layer (around 5 to 6 km) characterized by an aerosol extinction  
1915 of about  $0.1 \text{ km}^{-1}$ . This intense dust layer transported over most of the investigated region (40.5°N-43.5°N) is  
1916 associated with a second more diluted aerosol layer observed between 3 and 4 km with LNG. Another  
1917 interesting aspect is the variability of aerosol extinction detected in the marine boundary layer showing  
1918 large differences throughout the F-20 transect. [The aerosol extinction is found to be significant around 41°N  
1919 to 41.5°N that could be due to sea-spray particles generated in south Corsica Island due to the local  
1920 acceleration of the wind occurring between the Corsica and Sardinia islands \(not shown\). This increase of  
1921 the aerosol loading in the MBL associated with dust aerosol transported to higher altitudes results in an  
1922 increase of total AOD at these latitudes.](#) Such aircraft lidar data will be useful for testing the different  
1923 modeling systems used for the SOP-1a experiment and more specifically their ability to reproduce complex  
1924 vertical aerosol structures over the western Mediterranean. Additional observations of the aerosol  
1925 extinction vertical profile obtained over different surface-stations from the passive remote-sensing PLASMA  
1926 instrument onboard the ATR-42 aircraft are presented in Torres et al. (in prep.).

### 1927 **5.3.3 Sounding balloon observations**

1928 Figure 24 shows an example of the vertical profile of the aerosol particle size distribution obtained on June  
1929 19 near the end of the dust episode that started on 16 June over Minorca. The daytime average AOD  
1930 geographical distribution derived from MSG/SEVIRI is shown in Figure 6. The vertical profile clearly shows



1931 the presence of the dust layer between about 2.5 and 4.5 km in altitude, in agreement with coincident lidar  
1932 continuous observations at Minorca that show the more limited vertical extent of dust compared to  
1933 previous days and the end of the episode on June 19 in this area (Chazette et al., submitted). It should be  
1934 noted that sounding balloons appear to under-detect very large particles within dust layers compared to the  
1935 drifting balloons. This can be due isokinetic sampling differences between sounding systems that have a  
1936 vertical velocity of several  $\text{m s}^{-1}$  and systems drifting at a constant air density that are quasi-Lagrangian.  
1937 However coincident AERONET and LOAC vertically integrated particle size distribution in the range 0.1-  
1938  $30 \mu\text{m}$  in diameter performed on June 16 and 17 were found quite comparable. In the marine atmospheric  
1939 boundary layer, the LOAC speciation index (Renard et al., 2015a) indicates hydrated particles. In the free  
1940 troposphere above dust, the concentration of particles rapidly decreased by one order of magnitude and  
1941 particles were mainly of submicronic size with sometimes a significant number of particles in the 1.1-3  $\mu\text{m}$   
1942 channel.

## 1943 **5.4 Local Direct Radiative Forcing**

### 1944 **5.4.1 Estimates using in-situ aircraft data and radiative transfer codes over the two super-sites**

1945 Before investigating the possible climatic effect of aerosols on the Mediterranean climate, an important  
1946 preliminary step is the calculation of the direct radiative forcing (DRF) exerted by aerosols. This can be  
1947 addressed by using in-situ (physical-optical properties) and remote-sensing (vertical profiles) observations  
1948 of aerosols as input to radiative transfer models. Simulated SW and LW radiative fluxes can be evaluated  
1949 using observed radiative fluxes both at the surface and onboard the two aircraft. The combination of in-situ  
1950 and remote sensing measurements provide a complete and unique dataset for conducting such 1-D  
1951 radiative transfer simulations. To this end, vertical profiles from the ATR-42 were combined with surface  
1952 observations from the two (Ersa and Lampedusa) stations to calculate the SW DRF of different aerosol  
1953 events (Nicolas et al., in prep.; Meloni et al., in prep.). Over the western basin and for the first period of the  
1954 campaign (16 to 20 June), different calculations, with the GAME radiative transfer model (Dubuisson et al.,  
1955 2004), of the downward and upward SW cloud-free irradiances have been performed by Nicolas et al. (in  
1956 prep.) for 6 vertical profiles over Granada, Minorca and Corsica islands. Briefly, the methodology is based on  
1957 extinction, SSA and phase function vertical profiles (and their spectral dependence), obtained from

1958 observations and Mie calculations, and associated with atmospheric thermodynamic properties. They  
1959 clearly show a significant change in surface radiative fluxes with a well-known decrease (dimming effect) of  
1960 downward radiations due to scattering and absorption of solar radiation by dust aerosols. Inter-comparisons  
1961 between observed/simulated downward and upward clear-sky SW fluxes show a good agreement during  
1962 the ascent and descent profiles. At TOA, Nicolas et al. (in prep.) reported a direct (instantaneous at noon)  
1963 SW DRF ranged between  $-4$  and  $-33 \text{ W m}^{-2}$ , revealing a cooling effect due to dust particles. These  
1964 simulations also indicate that the decrease in surface radiation is not completely compensated by the TOA  
1965 cooling, meaning that aerosols exerted a positive atmospheric forcing due to their ability to absorb solar  
1966 radiations.

1967 Similar calculations (not shown) have been done over the Lampedusa reference-site by Meloni et al. (in  
1968 prep.) by using a similar method based on lidar, sun-photometer, in-situ surface, ATR-42 and F-20  
1969 observations and the MODTRAN 5.3 radiative transfer code. Meloni et al. (in prep.) estimate both the SW  
1970 and the LW aerosol radiative forcing profiles and the balance between the two spectral components (SW  
1971 and LW). During the descent towards Lampedusa airport on 22 June, the instantaneous ( $12.5^\circ$  solar zenith  
1972 angle and aerosol optical depth at 500 nm of 0.32) SW cooling at the surface ( $-44 \text{ W m}^{-2}$ ) is reduced by  
1973 about 10% due to infrared emission. The dust SW radiative forcing at TOA is  $-6 \text{ W m}^{-2}$ . These values are  
1974 obtained using the AERONET aerosol size distribution and different aerosol refractive indices in the SW and  
1975 in the LW spectral regions. The LW contribution at the surface is lower than the values reported in previous  
1976 studies (di Sarra et al., 2011; Meloni et al., 2015), partially due to the different solar zenith angle and to the  
1977 presence of mixed aerosol below the dust layer down to the surface.

#### 1978 **5.4.2 Estimates of instantaneous clear-sky SW DRF using AERONET/PHOTONS observations**

1979 As reported previously, AERONET/PHOTONS network provides, in addition to microphysical and optical  
1980 aerosol properties, an estimate of the local (instantaneous) clear-sky direct radiative forcing at any  
1981 AERONET/PHOTONS location as an operational product of the network. The method of derivation is  
1982 described in Garcia et al. (2012). As mentioned above, the extremely good regional coverage of  
1983 AERONET/PHOTONS sun-photometer instruments during the SOP-1a allow a complementary estimate of  
1984 the local radiative (clear-sky) forcing to those derived by Meloni et al. (in prep.) and Nicolas et al. (in prep.).

1985 The Figure 25 indicated the averaged of all instantaneous (clear-sky) DRF (in  $W m^{-2}$ ) estimated during a day  
1986 for both AERONET/PHOTONS station. Estimates are reported at the surface (bottom left), at TOA (bottom  
1987 right) and within the total atmosphere (down). Averaged values of the DRF are also indicated in the Figure  
1988 25. As mentioned above, sun-photometers retrievals demonstrate a significant DRF during the SOP-1a  
1989 experiment. As an example and at the surface, the mean forcing is comprised between  $-15 W m^{-2}$   
1990 (Barcelona, not affected by dust transport) and  $-35 W m^{-2}$  in Burjassot. Such values are consistent with  
1991 independent 1-D estimates reported by Nicolas et al. (in prep.) and Meloni et al. (in prep.).  
1992 AERONET/PHOTONS data also reveal a negative DRF at TOA over most of sites, meaning that aerosols exert  
1993 in majority a cooling effect at TOA, with values around  $\sim -6$  to  $-12 W m^{-2}$ . These negative values are also due  
1994 to the fact that most of AERONET/PHOTONS stations are located over islands, which are characterized by  
1995 low surface albedo. Logically and due to the moderate values of aerosol absorption observed during the  
1996 SOP-1a (Denjean et al., this special issue), a positive atmospheric forcing is observed with mean values from  
1997  $+7$  to  $+30 W m^{-2}$  (with maxima in Burjassot), that could affect the vertical profiles of temperature and  
1998 relative humidity as shown recently by Nabat et al. (2015a).

#### 1999 **5.4.3 Estimates using in-situ radiative flux observations**

2000 As shown by di Sarra et al. (2011), an estimate of the aerosol radiative forcing can be obtained by comparing  
2001 irradiance measurements made during days characterized by different aerosol loads. In particular, the  
2002 identification of a cloud-free day with low aerosol amounts is important to provide a reference for pristine  
2003 conditions. During the SOP-1a, 17 June at Lampedusa displayed a very low aerosol optical depth (daily  
2004 average of 0.064 at 500 nm) and cloud-free conditions throughout the day, and was identified as the  
2005 reference day for pristine conditions. July 3, conversely, was one of the days characterized by the presence  
2006 of desert dust, with moderate values of the AOD (0.28). As shown in figure 22a, dust was present above 2  
2007 km altitude and there were no major changes in the aerosol vertical distribution during the day, as it also  
2008 appears from the limited daily variability of the AOD (daily standard deviation of the AOD at 500 nm of  
2009 0.015). Cloud-free conditions were present throughout the day.

2010 Figure 27 displays the downward solar irradiance measured on 3 July, compared with the one measured on  
2011 the pristine reference day (17 June). The irradiance measurements were corrected for the radiometer

2012 thermal offset as discussed by Di Biagio et al. (2009). The sharp narrow peak occurring on 17 June around  
2013 6:30 was related to a small isolated cloud, and these data were discarded from the analysis. The differences  
2014 between the downward irradiances measured on these two days were calculated as a function of the solar  
2015 zenith angle; these differences are due to the effect of aerosol and, to a smaller extent, column water  
2016 vapour. The effect of water vapour was estimated by means of a radiative transfer model (see e.g., di Sarra  
2017 et al., 2011), and the remaining difference was integrated over 24 hours to obtain the daily average effect,  
2018  $\Delta I$ , on the downward solar irradiance. The daily aerosol radiative forcing RF can be derived as:

$$2019 \text{ RF} = \Delta I(1-A)$$

2020 where  $\Delta I$  is the difference between the two curves of Figure 27 integrated over 24 hours, and A is the  
2021 surface albedo. For a surface albedo of 0.07 (di Sarra et al., 2011), the estimated surface RF is  $-14.8 \text{ W m}^{-2}$ .  
2022 The radiative forcing efficiency (RFE), which is the radiative forcing produced by a unit AOD, was calculated  
2023 as:

$$2024 \text{ RFE} = \text{RF} / (\text{AOD}_2 - \text{AOD}_1)$$

2025 where  $\text{AOD}_1$  and  $\text{AOD}_2$  are the measured daily average aerosol optical depth on 17 June and 3 July,  
2026 respectively. The estimated RFE is  $-67.4 \text{ W m}^{-2}$ . Di Biagio et al. (2010), based on a multi-year dataset at  
2027 Lampedusa, derived a similar value for desert dust ( $-68.9 \text{ W m}^{-2}$ ) at the equinox; di Sarra et al. (2010), for an  
2028 intense desert dust event occurring in March 2010 found values between  $-70$  and  $-85 \text{ W m}^{-2}$ . For a desert  
2029 dust event associated with the propagation of a gravity wave, with values of AOD similar to those of 3 July,  
2030 di Sarra et al. (2013) derived an RFE equal to  $-79 \text{ W m}^{-2}$ . Valenzuela et al. (2012) determined REF for  
2031 Saharan dust episodes over the western Mediterranean with different origins, showing values in the range  
2032 from  $-74 \text{ W m}^{-2}$  (for air masses coming from North Morocco) to  $-65 \text{ W m}^{-2}$  (for air masses coming from  
2033 Algeria and Tunisia). Values of the dust RFE at the surface in the same range were obtained by Derimian et  
2034 al. (2006), although they were derived in different conditions for which the influence of surface albedo  
2035 should be taken into account.

2036 The downward LW irradiance measured on 3 July was higher than on 17 June by  $23 \text{ W m}^{-2}$ . Most of this  
2037 effect is due to differences in the water vapour column amount (about 1 cm difference between the two  
2038 days, with larger values on 3 July). Once the water vapour contribution was subtracted by means of

2039 radiative transfer calculations, we found a net positive effect induced by the aerosol of about  $+5.5 \text{ W m}^{-2}$ .  
2040 This is, on the daily timescale, about 35% of the SW effect. The resulting aerosol RFE in the LW spectral  
2041 range is  $+25.5 \text{ W m}^{-2}$ , in agreement with previous results by di Sarra et al. (2011) who found values between  
2042  $+25.9$  and  $+27.9 \text{ W m}^{-2}$ , or Anton et al. (2014) who reported RFE values around  $+20 \text{ W m}^{-2}$  (in reference to  
2043 AOD at 675 nm).

#### 2044 **5.4.4 Estimations of the SW and LW radiative heating rate along the vertical**

2045 One important original aspects of this study concerns the estimates of the vertical profiles of SW and LW  
2046 radiative heating rate. To our knowledge, all the referenced estimates of this important parameter, which  
2047 controls for a part the semi-direct radiative effect of aerosols, have been conducted using remote-sensing  
2048 techniques or in-situ observations of aerosol optical properties, coupled with radiative transfer modeling.  
2049 Here, we propose a first estimates of the SW and LW heating rate derived directly from upward and  
2050 downward (SW and LW) radiative fluxes obtained on-board the ATR-42 aircraft. Because of the nature  
2051 mainly diffuse of longwave upward and downward irradiances (irradiances in thermal infrared), and of the  
2052 upward shortwave irradiance (irradiance in solar domain), in first approximation, no correction due to the  
2053 altitude of the aircraft will be applied to these measurements. Only shortwave downward irradiances will  
2054 be corrected. Three kinds of corrections are applied:

- 2055 - Correction of the aircraft attitude (unavoidable movements due to the aircraft pitch and roll)
- 2056 - Correction of cosine response of the pyranometer
- 2057 - Correction due to the non-horizontal position of the sensor when a stabilized leg (ie. determination  
2058 of offsets on roll and pitch)

2059 Let  $\theta_m$  the angle between the sun direction and the normal to the pyranometer sensor (depending on pitch,  
2060 roll and aircraft heading given by the inertial navigation system), and  $\theta_s$  the solar zenith angle, the attitude  
2061 correction coefficient is:

$$2062 \quad X_d^n = \frac{\cos \theta_m}{\cos \theta_s}$$

2063 Finally, we obtain the global (direct plus diffuse) downward irradiance, for the solar zenith angle  $\theta_s$ :

$$E_{SW}^{\downarrow}(\theta_s) = \frac{E_{SW}^{m\downarrow}(\theta_m)}{(X_d^n [1 - c(\theta_s)] - D) f(\theta_s) + D}.$$

2065 In this equation,  $E_{SW}^{m\downarrow}(\theta_m)$  is the measured global irradiance,  $c(\theta_s)$  is the cosine response of the  
 2066 pyranometer and  $f(\theta_s)$  is the part of direct downward irradiance in the global (estimation obtained from  
 2067 radiative transfer code). Taking into account these corrections, Figure 28a shows downward ( $E_{SW}^{Dwn}$ ),  
 2068 upward ( $E_{SW}^{Up}$ ), and net ( $E_{SW}^{Net}$ ) shortwave irradiances obtained from measurements performed onboard  
 2069 ATR-42 aircraft on 22 June between 10.35 and 11.30 TU. Irradiances are reduced to the mean solar zenith  
 2070 angle  $\theta_s = 29.7^\circ$ . Similarly, Figure 28b shows corresponding measurements of downward ( $E_{LW}^{Dwn}$ ), upward  
 2071 ( $E_{LW}^{Up}$ ), and net ( $E_{LW}^{Net}$ ) longwave irradiances. Total net irradiances are then determined versus the aircraft  
 2072 altitude for the mean air mass factor of the considered studied flight phase. Radiative cooling/heating rate  
 2073 is finally derived and shown in the figure 28c, in which the longwave (LW) and shortwave (SW) parts are  
 2074 distinguished.

2075 Concerning the SW heating rate vertical profiles (Figure 28c), one can observe the significant increase of  
 2076 the calculated instantaneous SW heating rate in the two different aerosol layers detected for this case  
 2077 (Figure 21), especially above 4 km, that corresponds to the maximum of extinction coefficient (up to 100  
 2078  $Mm^{-1}$ ) due to the presence of mineral dust. For this specific layer, the values of SW heating rate peak at 4-5  
 2079  $^\circ K$  per day for a solar angle of  $29.7^\circ$ . We can also observe a similar tendency in the second aerosol layer,  
 2080 located between 1.5 and 3 km (see Figure 21). Concerning the LW heating rate, the figure 28c indicates  
 2081 instantaneous values ranging between -2 to -4  $^\circ K$  per day, which is also consistent with the well known  
 2082 cooling effect of mineral dust in the longwave spectrum (Mallet et al., 2006, Zhu et al., 2007). As shown in  
 2083 Figure 28c, the net heating rate is dominated by the SW heating (the maximum LW cooling is less than 60%  
 2084 of the SW heating), which leads to net SW radiative heating ranging between +0.5 and +2 K per day inside  
 2085 the dust layer above the MBL. Such unique and original database of SW and LW radiative heating obtained  
 2086 over the western Mediterranean should be now used to evaluate the ability of the different models  
 2087 involved in the ChArMEx/ADRIMED project (see the following section 6) to simulate this important radiative  
 2088 property for the different identified dust cases.

## 2089 **6. Overview of Modeling Activities**

2090 Several models are used to analyze the SOP-1a period: the meso-scale meteorological COSMO-MUSCAT  
2091 model, the chemistry transport model (CTM) CHIMERE model, and two regional climate (RegCM and CNRM-  
2092 RCSM) models. These models differ in terms of horizontal and vertical resolutions, physical  
2093 parameterizations, aerosol-chemical schemes and are able to deliver complementary information to  
2094 address key scientific questions of the ChArMEx/ADRIMED experiment. Their main characteristics are  
2095 summarized in the Table 8.

### 2096 **6.1 COSMO-MUSCAT model**

2097 The parallelized multi-scale regional model system COSMO-MUSCAT (Wolke et al., 2012) consists of the non-  
2098 hydrostatic atmosphere model COSMO (Consortium for Small-scale Modelling) that is on-line coupled to the  
2099 3-D chemistry tracer transport model MUSCAT (MULTIScale Chemistry Aerosol Transport Model). The  
2100 atmospheric dust cycle consisting of the emission, transport and deposition of dust particles is simulated  
2101 within MUSCAT using meteorological and hydrological fields from COSMO. Dust emission is calculated using  
2102 the emission scheme by Tegen et al. (2002) and depends on local surface wind friction velocities, surface  
2103 roughness length, soil texture and soil moisture. Calculated dust emission fluxes depend on particle  
2104 diameter for individual size classes that are assumed to be log-normally distributed. Following Marticorena  
2105 and Bergametti (1995), dust emission is considered as threshold function of local friction velocities and thus  
2106 initial dust emission is computed as a function of soil particle size distribution. Dust emission is limited to  
2107 regions where active dust sources have been identified during 2006-2009 from MSG SEVIRI observations  
2108 (Schepanski et al., 2007). The advection of dust particles is described by a third order upstream scheme;  
2109 dust particles are transported as passive tracer in five independent size classes with limiting radius at  
2110 0.1 $\mu\text{m}$ , 0.3 $\mu\text{m}$ , 0.9 $\mu\text{m}$ , 2.6 $\mu\text{m}$ , 8 $\mu\text{m}$ , and 24 $\mu\text{m}$ . The removal of dust particles from the atmosphere is  
2111 described by dry and wet deposition taking particle size, particle density, and atmospheric conditions into  
2112 account. Here, the simulations of the atmospheric dust cycle are performed at a 28 km horizontal grid and  
2113 40 vertical layers, covering North African dust sources, the eastern North Atlantic, the Mediterranean basin  
2114 and Europe.

### 2115 **6.2 The CHIMERE chemistry-transport model**

2116 CHIMERE is a chemistry-transport model able to simulate concentrations fields of gaseous and aerosols  
2117 species at a regional scale. The model is off-line and thus needs pre-calculated meteorological fields to run.  
2118 In this study, we used the version fully described in Menut et al. (2013), forced by the WRF meso-scale  
2119 model. The horizontal domain is the same as the one of WRF, and, for the vertical grid, the 28 vertical levels  
2120 of WRF are projected on the 20 levels of the CHIMERE mesh. The gaseous species are calculated using the  
2121 MELCHIOR 2 scheme and the aerosols using the scheme developed by Bessagnet et al. (2004). This module  
2122 takes into account species such as sulfate, nitrate, ammonium, primary organic (OC) and black carbon (BC),  
2123 secondary organic aerosols (SOA), [sea-spray](#), mineral dust, and water. These aerosols are represented using  
2124 ten bins, from 40 nm to 20  $\mu\text{m}$ , in diameter. The life cycle of these aerosols is completely represented with  
2125 nucleation of sulfuric acid, coagulation, adsorption/desorption, wet and dry deposition and scavenging. This  
2126 scavenging is both represented by coagulation with cloud droplets and precipitation. The formation of SOA  
2127 is also taken into account. The anthropogenic emissions are estimated using the same methodology as the  
2128 one described in Menut et al. (2013) but with the HTAP masses as input data. These masses were prepared  
2129 by the EDGAR Team, using inventories based on MICS-Asia, EPA-US/Canada and TNO databases  
2130 ([http://edgar.jrc.ec.europa.eu/htap\\_v2](http://edgar.jrc.ec.europa.eu/htap_v2)). Biogenic emissions are calculated using the MEGAN emissions  
2131 scheme (Guenther et al., 2006), which provides fluxes of isoprene, terpene and pinenes. In addition to this  
2132 2013 version, several processes were improved and added in the framework of this study. First, mineral dust  
2133 emissions are now calculated using new soil and surface databases, as described in Menut et al. (2013).  
2134 Second, chemical species emissions fluxes produced by vegetation fires are estimated using the new high  
2135 resolution fire model presented in Turquety et al. (2014). Finally, the photolysis rates are explicitly  
2136 calculated using the FastJ radiation module (Mailler et al., 2015).

### 2137 **6.3 The RegCM Regional Climate model**

2138 The RegCM system is a community model designed for use by a varied community composed of scientists in  
2139 industrialized countries as well as developing nations. It is supported through the Regional Climate Network,  
2140 or RegCNET, a widespread network of scientists coordinated by the Earth System Physics section of the  
2141 Abdus Salam International Centre for the Theoretical Physics (ICTP, Giorgi et al., 2012). RegCM is a  
2142 hydrostatic, compressible, sigma-p vertical coordinate model. As a limited area model, RegCM requires



2143 initial and boundary conditions that can be provided both by NCEP or ECMWF analyses. The horizontal  
2144 resolution used need to be higher than 10 km, due to the hydrostatic dynamic core of the model, associated  
2145 with 23 vertical levels. A simplified aerosol scheme specifically designed for application to long-term climate  
2146 simulations has been incrementally developed within the RegCM system. Solmon et al. (2006, 2008) first  
2147 implemented a first-generation aerosol model including sulfates, organic carbon, and black carbon. Zakey et  
2148 al. (2006) then added a 4-bin desert dust module, and Zakey et al. (2008) implemented a 2-bin [sea-spray](#)  
2149 scheme. In RegCM, the dust emission scheme accounts for sub-grid emissions by different types of soil. The  
2150 dust emission size distribution can now also be treated according to Kok (2011). When all aerosols are  
2151 simulated, 12 additional prognostic equations are solved in RegCM, including transport by resolvable scale  
2152 winds, turbulence and deep convection, sources, and wet and dry removal processes. In RegCM, the  
2153 natural/anthropogenic aerosols are radiatively interactive both in the solar and infrared regions and so are  
2154 able to feedback on the meteorological fields.

#### 2155 **6.4 The CNRM-RCSM Regional Climate model**

2156 The fully coupled RCSM (Regional Climate System Model), which is developed at CNRM has been also used  
2157 within the ChArMEx/ADRIMED project. This model includes the regional climate atmospheric model  
2158 ALADIN-Climate (Déqué and Somot 2008), the regional ocean model NEMOMED8 (Beuvier et al., 2010) and  
2159 the land-surface model ISBA (Noilhan and Mahfouf, 1996). We used here the version described in Nabat et  
2160 al. (2015b) with a 50 km horizontal resolution. ALADIN-Climate includes the Fouquart and Morcrette  
2161 radiation scheme based on the ECMWF model incorporating effects of greenhouse gases as well as direct  
2162 effects of aerosols. The ocean model NEMOMED8 is the regional eddy-permitting version of the NEMOV2.3  
2163 ocean model that covers the Mediterranean Sea. Concerning the aerosol phase, the model ALADIN-Climate  
2164 incorporates a radiative scheme to take into account the direct and semi-direct effects of five aerosol types  
2165 ([sea-spray](#), desert dust, sulfates, black and organic carbon aerosols) through either AOD climatologies or a  
2166 prognostic aerosol scheme (Nabat et al., 2013, 2015b). On the one hand, Nabat et al. (2013) have proposed  
2167 a new AOD monthly climatology over the period 2003-2009, based on a combination of satellite-derived  
2168 and model-simulated products. The objective is having the best estimation of the atmospheric aerosol  
2169 content for these five most relevant aerosol species. On the other hand, a prognostic aerosol scheme has

2170 been recently implemented in ALADIN-Climate, and has shown its ability to reproduce the main patterns of  
2171 the aerosol variability over the Mediterranean (Nabat et al., 2015b).

2172 Using CNRM-RCSM with the new AOD monthly climatology over the period 2003-2009 (Nabat et al., 2013),  
2173 Nabat et al. (2015a) have notably highlighted the response of the Mediterranean Sea Surface Temperature  
2174 (SST) to the aerosol direct and semi-direct radiative forcing. Figure 29a presents the annual average  
2175 difference in SST over the period 2003-2009 between a simulation ensemble including aerosols and a  
2176 second one without any aerosol. Aerosols are found to induce an average decrease in SST by 0.5°C, because  
2177 of the scattering and absorption of incident radiation. As a consequence, the latent heat loss is also reduced  
2178 by aerosols (Figure 29b), as well as precipitation (Figure 29c). This result also underlines the importance of  
2179 taking into account the ocean-atmosphere coupling in regional aerosol-climate studies over the  
2180 Mediterranean.

## 2181 **6.5 SOP-1a multi-model aerosol simulations**

### 2182 **6.5.1 Aerosol Optical Depth**

2183 Figure 30 reports the AOD (in the visible range) simulated for the SOP-1a period and for the COSMO-M (550  
2184 nm), RegCM (between 440 and 670 nm), CNRM-RCSM (550 nm) and CHIMERE (500 nm) models. Except the  
2185 CTM-CHIMERE model which includes all the secondary species (SOA and inorganic), the others have  
2186 different aerosols schemes and take into account both natural (COSMO-M) or natural plus a part of  
2187 anthropogenic aerosols as described in the Table 7. The configurations used for each models are listed in  
2188 the Table 7. One can observe the large variability of AOD simulated by models over the Mediterranean  
2189 region with highest values clearly simulated by the COSMO-M (AOD ~1-1.5 in the visible wavelengths) over  
2190 the Northern Africa region. The CHIMERE model indicates two different regions where AOD peaks around 1,  
2191 over Algeria-Tunisia and southern of Morocco. For COSMO-M and CHIMERE, no intense dust AOD are  
2192 simulated over the northeast Africa (Lybia and Egypt) and values are below 0.25, contrary to RegCM and  
2193 CNRM-RCSM that simulate moderate AOD over this region with more intense peaks (~0.7 for CNRM-RCSM  
2194 simulations). Some identified regions with important AOD over Tunisia, Algeria, and South Morocco are well  
2195 captured by all models except COSMO-M which show more intense AOD south of Algeria. It should be noted  
2196 that this regional pattern of AOD is found to be consistent with MODIS observations as shown by Menut et

2197 al. (2015) for the CHIMERE model. Averaged over the SOP-1a period, all models simulate low to moderate  
2198 AOD over the EURO-Mediterranean region which is consistent with AERONET/PHOTONS observations  
2199 (Figure 14). Once again and as noted by Menut et al. (2015), this modeling exercise clearly shows that the  
2200 summer 2013 was not characterized by intense dust plumes or intense anthropogenic or forest fire  
2201 emissions. However, modeling results indicate regular dust intrusions during the SOP-1a characterized by  
2202 moderate atmospheric loads. Over Europe, the CTM CHIMERE model obviously simulate anthropogenic  
2203 aerosol AOD (AOD ~ 0.3), especially over the Benelux and Pô Valley that are not simulated by the two other  
2204 regional models. Indeed, CNRM-RCSM simulations reveal a more diffuse AOD about 0.2 over Europe with  
2205 maximum over Western France certainly due to the advection of primary marine particles generated over  
2206 the Atlantic Ocean. RegCM simulations indicate a plume of anthropogenic aerosols over the Balkan region  
2207 mainly due to secondary inorganic species. As RegCM does not use the spectral nudging technique in this  
2208 simulation and are only forced at the boundaries during the period of simulation, some biases in  
2209 meteorological fields could appear (as for the precipitation location and intensity), which need to be  
2210 evaluated. Finally and in addition to analysis of the AOD regional pattern, a specific comparison with in-situ  
2211 observations and remote-sensing (AERONET/PHOTONS and satellite) data has been made for the CTM-  
2212 CHIMERE model (Menut et al., 2015) and is planned in accompanied studies for the COSMO-M, RegCM and  
2213 CNRM-RCSM models, associated with an inter-comparison exercise for evaluating the dust emissions,  
2214 vertical distribution, size distribution and dry/wet deposition using all data collected in the framework of  
2215 the SOP-1a.

2216 In parallel to time averaged AOD simulated at the regional scale, we report comparisons of simulated AOD  
2217 with AERONET/PHOTONS data for the two reference stations (Lampedusa and Ersa). As reported in Table 7,  
2218 it should be reminded here that all models did not take into account aerosol species in a similar way. As an  
2219 example, COSMO-MUSCAT includes mineral dust only in this simulation, while CNRM-RCSM and RegCM  
2220 model include natural ([sea-spray](#) and dust) and sulfates as well as secondary ammonium and nitrate  
2221 particles (treated as bulk aerosols) but for RegCM only. The most complete regional model (in terms of  
2222 aerosol phase) is CHIMERE, which takes into account natural and all anthropogenic particles (including  
2223 secondary organics and inorganic) resolved in size by using large number of bins (Menut et al., 2013)

2224 compared to RegCM, CNRM-RCSM or COSMO-MUSCAT (number of dust bins between 3 to 4 bins). Figure 31  
2225 reports the time evolution of simulated and observed AOD at 550 nm for the two sites (Ersa and  
2226 Lampedusa) during the SOP-1a. Time correlation, as well as bias, is calculated after removing  
2227 AERONET/PHOTONS data for the 27<sup>th</sup> of June, strongly affected by smoke aerosols transported from  
2228 Northern America biomass burning sources that are not included in the different domains. Figure 31  
2229 indicates that all models are able to simulate AOD in the range of magnitude of observations. For the dusty  
2230 Lampedusa site, CNRM-RCSM and CHIMERE reveal high temporal correlations (0.82, 0.85, respectively),  
2231 with standard deviations close to AERONET/PHOTONS data, especially for CHIMERE. For this station,  
2232 COSMO-M and RegCM display moderate temporal correlation (0.55 and 0.49, respectively) compared to  
2233 CNRM-RCSM and CHIMERE. As already mentioned, one reason of lowest time-correlation for these models  
2234 is related to the fact that they are only forced at the boundaries and the synoptic conditions inside the  
2235 domain can derive during the simulation. This effect is limited for CNRM-RCSM that used the spectral  
2236 nudging technique and for CHIMERE forced by WRF meteorological field (Menut et al., 2015). For each  
2237 models, biases are shown to be low, both positive (for CNRM-RCSM and CHIMERE) and negative (for  
2238 COSMO-M and RegCM).

2239 For the Ersa station, less influenced by long-range transport of mineral dust during this period, temporal  
2240 correlations are lowest and found to be moderate (0.40) for CHIMERE and COSMO-M and low for RegCM  
2241 and CNRM-RCSM. In terms of bias, values are positive and low (0.02 to 0.04) for all models, except for  
2242 COSMO-M (-0.07) that does not include anthropogenic aerosols nor [sea-spray](#) in the present simulation  
2243 (Table 7). For each model, calculated standard deviations are in the same range of magnitude but slightly  
2244 higher than observations, especially for RegCM (bias of 0.08) that simulated a large AOD for 19-20 of June  
2245 period. By comparison with the values obtained in Lampedusa, these low correlations at Ersa reveal the  
2246 limitations of these models in terms of horizontal resolution with respect to the representativeness of the  
2247 site. Lampedusa being isolated in the middle of the Mediterranean and under the main pathways of African  
2248 mineral dust, AOD is mostly related to long-ranged transport. On the other hand, the site of Ersa in Corsica  
2249 may be under several types of aerosols contributions (anthropogenic, biogenic) more intense and more  
2250 spatially variables than in Lampedusa. Ersa being closer to large industrial areas, the models with a

2251 horizontal resolution of tens of kilometers are probably not highly enough resolved to catch small scales  
2252 aerosols plumes from the continent.

### 2253 **6.5.2 Regional SW 3-D direct radiative forcing**

2254 The SW (clear-sky) DRF, averaged for the SOP-1a period, has been estimated from the RegCM and CNRM-  
2255 RCSM models, both at the surface and TOA, as shown in the Figure 32. For this discussion, we only consider  
2256 these two models as they estimate the clear-sky SW DRF by taking into account natural and anthropogenic  
2257 aerosols, contrary to the COSMO-MUSCAT model in this study. At the surface first, one can observe the  
2258 large regional dimming due to anthropogenic (especially over Europe) and natural (Northern Africa and  
2259 Mediterranean) particles over the Euro-Mediterranean. Concerning the North African region, both models  
2260 simulate large surface forcing  $\sim -20 \text{ W m}^{-2}$  (with local maxima of  $-50 \text{ W m}^{-2}$  associated with higher AOD).  
2261 CNRM-RCSM is shown to simulate higher surface radiative forcing for the whole domain, especially over  
2262 Algeria. Although such RCM climate models are not designed to simulate finely the size distribution and the  
2263 chemical composition of aerosols as an A-Q system (Menut et al., 2013), a first estimate of the radiative  
2264 effect of polluted particles over Europe is provided. Figure 32 displays a negative forcing, obviously lower  
2265 than for mineral dust, of about  $-10$  to  $-15 \text{ W m}^{-2}$  for RegCM, especially over Balkans and no significant  
2266 radiative effect over the Benelux region for this period. Over the continental region, CNRM-RCSM simulated  
2267 a more diffuse surface forcing with values around  $-10 \text{ W m}^{-2}$ , including a large part of Europe (France,  
2268 Benelux and Eastern Europe). As shown recently by Nabat et al. (2015a), this decrease in SW radiations due  
2269 to aerosols could perturb the surface continental temperature, SST and latent heat fluxes over the  
2270 Mediterranean Sea and more largely on meteorological fields.

2271 At TOA, the dipole of the direct forcing between the North and the South of the domain is well reproduced  
2272 by the two RCM systems with more intense values for CNRM-RCSM. One can clearly observe positive forcing  
2273 at TOA (heating) over Northern Africa and negative forcing (cooling) over the Mediterranean and Europe.  
2274 This represents one of the characteristics of the Euro-Mediterranean region with a large variability of  
2275 surface albedo from the South (with higher values) to the North (low to moderate albedo). [Due to this](#)  
2276 [gradient in the surface albedo, moderate absorbing dust aerosols emitted over Northern Africa](#)  
2277 [\(characterized by high surface albedo\) decrease the shortwave radiations reflected at TOA, compared to a](#)

2278 non-turbid atmosphere. When advected above low surface reflectance as marine or dense forest over  
2279 Europe, dust aerosols increase the upward SW radiations at TOA, leading to a cooling effect. One can see  
2280 the transition between positive to negative TOA forcing that occurs over Northern Algeria and Morocco as  
2281 soon as dust particles are transported over darker surfaces. This TOA radiative forcing gradient is well  
2282 captured by such RCM models which use a finer resolution than GCM. Over Europe and Mediterranean, the  
2283 TOA forcing is simulated to be negative for both RCM with lower values around  $-5$  to  $-10$   $\text{W m}^{-2}$ . Such results  
2284 are consistent with the study of Nicolas et al. (in prep.), who performed two different simulations using  
2285 different surface albedo (from marine to continental), based on the ATR-42 observations above the Balearic  
2286 Islands and the Granada station. The inclusion of high surface albedo (0.27 at 870 nm) in the 1-D radiative  
2287 transfer model compared to low sea-surface albedo (0.02 at 870 nm) contributes to decrease the TOA  
2288 radiative effect at Granada.

2289 The last important point to mention here concerns the fact that most of SW radiations losses at the surface  
2290 are not completely compensated by fluxes reflected back to space. Hence, this gain of solar energy within  
2291 dusty layers (due to moderate dust SW absorption, see Denjean et al., this special issue) has been shown to  
2292 result in significant feedbacks on the temperature and relative humidity profiles over the Mediterranean  
2293 region with some important implications on its climate (Nabat et al., 2015a).

## 2294 **7. Conclusions**

2295  
2296 The special observing period (SOP-1a) performed during the Mediterranean dry season (11 June to 05 July  
2297 2013) over the western and central Mediterranean basins has been described in detail, as well as the 1D to  
2298 3D modeling effort, involved in the ChArMEx/ADRIMED project focused on aerosol-radiation-climate  
2299 interactions. Details of the in-situ and remote-sensing instrumentation deployed at the different sites and  
2300 the main meteorological conditions that occurred during the campaign have been provided. Some results  
2301 from the in-situ and remote-sensing observations, vertical profiles, 1-D and 3-D aerosols direct radiative  
2302 forcing (DRF) computations have also been presented. Concerning the aerosol loading during the SOP-1a,  
2303 our results indicate that numerous but moderate mineral dust plumes were observed during the campaign  
2304 with main sources located in Morocco, Algeria and Tunisia, leading to AOD between 0.1 to 0.6 (at 440 nm)  
2305 over the western and central Mediterranean. Analysis of synoptic situations demonstrates unfavorable

2306 conditions to produce large concentrations of polluted-smoke particles during the SOP-1a but interesting  
2307 sea-spray events have been observed.

2308 Aerosol extinctions measured on-board the ATR-42 show local maxima reaching up to  $150 \text{ Mm}^{-1}$  within the  
2309 dust plume, associated to extinctions of about  $50 \text{ Mm}^{-1}$  within the Marine Boundary Layer (MBL) possibly  
2310 due to the presence of sea-spray aerosols. By combining ATR-42 extinction, absorption and scattering  
2311 measurements, complete optical closures have been made revealing an excellent agreement in estimated  
2312 optical properties. This additional information on extinction properties has allowed calculating the dust  
2313 single scattering albedo (SSA) with a high level of confidence over the Western Mediterranean. Our results  
2314 show a surprising moderate variability from 0.90 to 1.00 (at 530 nm) for all flights studied, corroborated by  
2315 AERONET/PHOTONS SSA retrievals. The SSA derived during the ChArMEx/ADRIMED project has been also  
2316 compared with referenced values obtained near dust sources, showing a relatively low difference in this  
2317 optical parameter at 530 nm.

2318 Concerning the aerosol vertical structure, active remote-sensing observations, at the surface and onboard  
2319 the F-20, indicate complex vertical profiles of particles with sea-spray and pollution located in the MBL, and  
2320 mineral dust and/or even aged North American smoke particles located above (up to 6-7 km in altitude).  
2321 Microphysical properties of aerosols measured onboard the ATR-42 and balloon-borne observations for  
2322 transported/aged mineral dust reveal particle volume size distributions with diameters greater than  $10 \mu\text{m}$ .  
2323 In most of cases, a coarse mode of mineral dust particles, characterized by an effective diameter  $D_{\text{eff},c}$   
2324 ranging between 5 and  $10 \mu\text{m}$ , has been detected within the dust layer located above the MBL. Such values  
2325 are found to be larger than those referenced in dust source regions during FENNEC, SAMUM1 and AMMA,  
2326 as well as measurements in the Atlantic Ocean at Cape-Verde region during SAMUM-2 and at Puerto-Rico  
2327 during PRIDE.

2328 In terms of shortwave (SW) and longwave (LW) DRF, in-situ surface and aircraft observations have been  
2329 merged and used as inputs in different radiative transfer codes for calculating the 1-D DRF. Modeling results  
2330 show significant surface (instantaneous) SW radiative forcing down to as much as  $-90 \text{ W m}^{-2}$  over super-  
2331 sites. In parallel, AOD together with surface radiative fluxes observations have also been used to directly  
2332 estimate the local daily surface forcing in SW (and LW) spectral regions, showing a significant effect with

2333 values of  $-15 \text{ W m}^{-2}$  ( $+5.5 \text{ W m}^{-2}$ ) over Lampedusa. In parallel, aircraft observations provide also original and  
2334 new estimates of SW and LW radiative heating vertical profiles with significant values of SW heating of  
2335 about  $5^\circ\text{K}$  per day within the dust layer (for a solar angle of  $30^\circ$ ).

2336 Associated 3-D modeling studies, using regional climate (RCM) and chemistry transport (CTM) models,  
2337 indicate a relatively good agreement between simulated AOD and that determined from  
2338 AERONET/PHOTONS data. Such models allow 3-D calculations of the daily SW DRF revealing a regional DRF  
2339 of  $-10$  to  $-20 \text{ W m}^{-2}$  (at the surface and in clear-sky conditions), when averaged over the SOP-1a period. At  
2340 TOA, a significant dipole in the DRF is estimated between the North and the South of the domain, with  
2341 positive (heating) over Northern Africa and negative (cooling) DRF over the Mediterranean basin and  
2342 Europe, reflecting changes in surface albedo associated to moderately absorbing aerosols. A first climatic  
2343 simulation (conducted for the 2003 to 2009 period) that takes into account the ocean-atmosphere coupling  
2344 has demonstrated that the significant aerosol radiative forcing is responsible for a decrease in sea surface  
2345 temperature (on average  $-0.5^\circ\text{C}$  for the Mediterranean). In addition, the latent heat loss is shown to be  
2346 weaker in the presence of aerosols, resulting in a decrease in specific humidity in the lower troposphere,  
2347 and a reduction in cloud cover and precipitation.

2348 This unprecedented dataset of aerosol microphysical, chemical, optical properties and vertical profiles  
2349 obtained over the western Mediterranean will now be used for evaluating regional models to reproduce  
2350 such properties. In addition to classical model evaluations based generally on the AOD, new comparisons  
2351 between models and in-situ observations on aerosol absorbing (SSA and AAOD) properties and SW and LW  
2352 heating rates, which control the semi-direct effect of aerosols, should be conducted. Comparisons will also  
2353 be performed on the aerosol size distribution for investigating the ability of regional models to simulate the  
2354 observed large dust particle size during the transport over the Mediterranean, which could be helpful for  
2355 improving the representation of deposition in such models. In parallel, in-situ observations of sea-spray  
2356 particles obtained at the surface and from ATR-42 measurements will also be used to evaluate the different  
2357 primary sea-spray generation schemes, in terms of concentration and size distribution. The objective is to  
2358 improve the representation of microphysical and optical properties of aerosols in regional climate models  
2359 which will be used in multi-year simulations to assess the impact of natural and anthropogenic aerosols on



2360 climate in this region.

2361

2362

2363

2364

2365

2366

2367

2368

2369

2370

2371

2372

2373

2374

2375

2376

2377

2378

2379

2380

2381

2382

2383

2384

2385

2386

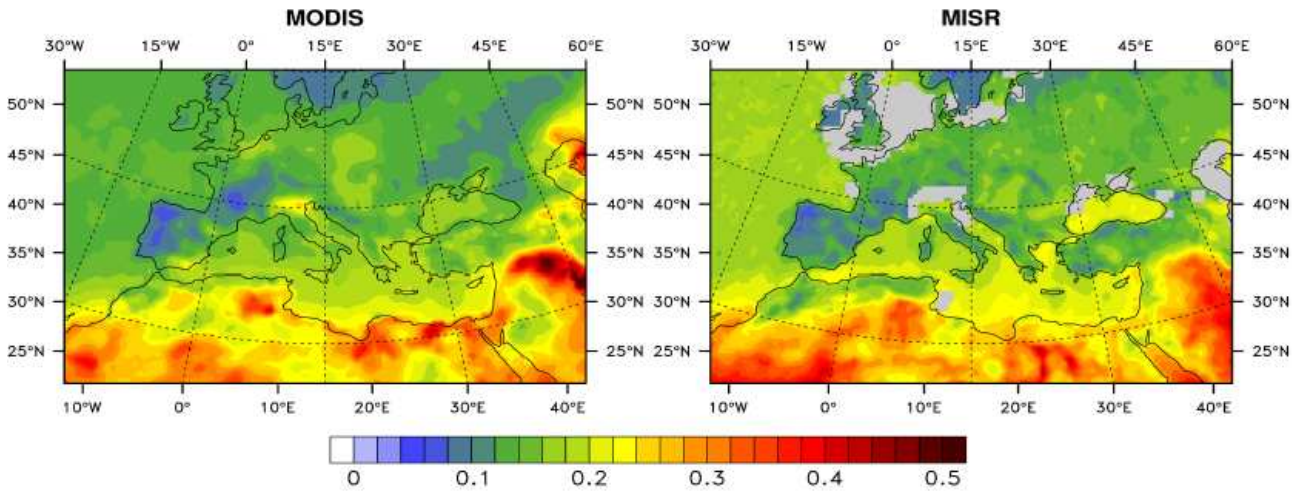
## 2387 Acknowledgments

2388 This research has received funding from the French National Research Agency (ANR) projects ADRIMED  
2389 (contract ANR-11-BS56-0006). This work is part of the ChArMEx project supported by ADEME, CEA, CNRS-  
2390 INSU and Météo-France through the multidisciplinary programme MISTRALS (Mediterranean Integrated  
2391 Studies at Regional And Local Scales). The station at Erba was partly supported by the CORSiCA project  
2392 funded by the Collectivité Territoriale de Corse through the Fonds Européen de Développement Régional of  
2393 the European Operational Program 2007-2013 and the Contrat de Plan Etat-Région. We acknowledge the  
2394 AERONET/PHOTONS sun-photometer networks and the PIs of the selected stations and their staff for their  
2395 work to produce the dataset used in this study. The financial support for EARLINET in the ACTRIS Research  
2396 Infrastructure Project by the European Union's Horizon 2020 research and innovation programme under  
2397 grant agreement n. 654169 and previously under grant agreement n. 262254 in the 7th Framework  
2398 Programme (FP7/2007-2013) is gratefully acknowledged. In particular, the authors are thankful to the  
2399 Italian EARLINET PIs (Maria Rita Perrone, Lecce; Nicola Spinelli, Naples; Gelsomina Pappalardo, Potenza;  
2400 Simona Scollo, Serra La Nave) and their staff. Measurements at Lampedusa by ENEA were partly supported  
2401 by the Italian Ministry for University and Research through the NextData and Ritmare Projects. This study,  
2402 especially the balloon campaign and part of the aircraft operations has also been supported by the French  
2403 space agency (CNES). The technical staff of SAFIRE, INSU Technical Division and the CNES Balloon sub-  
2404 directorate (with special mention to Aurélien Bourdon and Gilles Dupouy) are warmly acknowledged for  
2405 their contribution to the success of the experimental work. Contributions by Didier Bruneau (Latmos), Silvia  
2406 Becagli (Univ. of Florence, Italy), Marco Cacciani (Univ. of Rome, Italy), Julian Groebner and Natalia  
2407 Kouremeti (Physikalisch-Meteorologisches Observatorium Davos, World Radiation Center, Switzerland), and  
2408 José Antonio Martínez Lozano (University of Valencia, Spain) are gratefully acknowledged. Barcelona station  
2409 was partially supported by the Spanish Ministry of Economy and Competitiveness (project TEC2012-34575) and  
2410 of Science and Innovation (project UNPC10-4E-442) and FEDER funds, and by the Department of Economy  
2411 and Knowledge of the Catalan Autonomous Government (grant 2014 SGR 583). Granada station was  
2412 partially supported by the Andalusian Regional Government through project P12-RNM-2409 and by the  
2413 Spanish Ministry of Science and Technology through project CGL2013-45410-R. Sahar Hassazadeh,  
2414 Constantino Muñoz-Porcar, Santi Bertolín and Diego Lange are also acknowledged for their kind assistance  
2415 in operating the Menorca surface station, as well as François Gheusi, Brice Barret, Flore Tocquer, and Yves  
2416 Meyerfeld for their contribution to the balloon campaign preparation and/or deployment. Claude  
2417 Basdevant, Alexis Doerenbecher, and Fabien Bernard are acknowledged for their help and very useful tools  
2418 in support of our drifting balloon experiment. The Granada station was partially supported by the  
2419 Andalusian Regional Government through project P12-RNM-2409 and by the Spanish Ministry of Science  
2420 and Technology through project CGL2013-45410-R.

2421  
2422  
2423  
2424  
2425  
2426  
2427  
2428  
2429  
2430  
2431  
2432  
2433  
2434  
2435  
2436  
2437  
2438  
2439

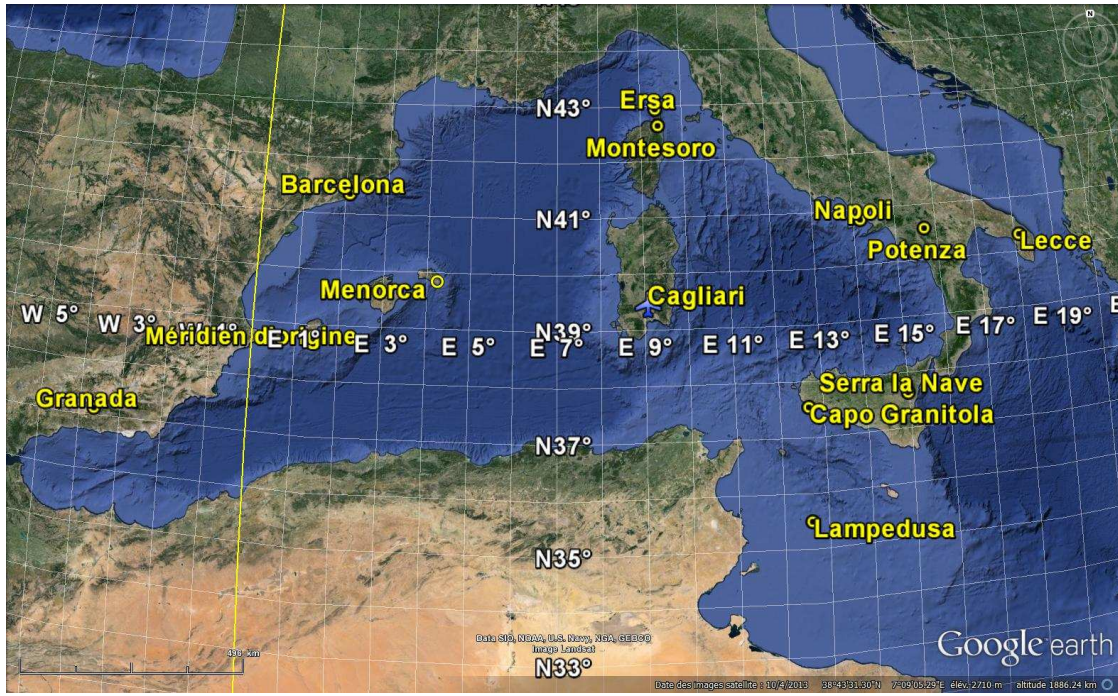
2440 **Figures References**  
2441

### AOD 2003-2012



2442  
2443  
2444  
2445  
2446  
2447  
2448  
2449  
2450  
2451  
2452  
2453  
2454  
2455  
2456  
2457  
2458  
2459  
2460  
2461  
2462  
2463  
2464  
2465  
2466  
2467  
2468  
2469  
2470  
2471  
2472  
2473  
2474  
2475  
2476  
2477  
2478  
2479  
2480

**Figure 1.** Aerosol Optical Depth (at 550 nm) derived from MODIS and MISR satellites for the 2003 to 2012 period.



2481  
 2482  
 2483  
 2484  
 2485  
 2486  
 2487  
 2488  
 2489  
 2490  
 2491  
 2492  
 2493  
 2494  
 2495  
 2496  
 2497  
 2498  
 2499  
 2500  
 2501  
 2502  
 2503  
 2504  
 2505  
 2506  
 2507  
 2508  
 2509  
 2510  
 2511  
 2512  
 2513  
 2514  
 2515  
 2516  
 2517  
 2518  
 2519

**Figure 2.** The regional experimental set-up deployed in the western and central Mediterranean during the campaign ChArMEx SOP-1a. The two aircraft were based at Cagliari.

ADRIDMED flights - ATR42 & Falcon20 - JUNE & JULY 2013

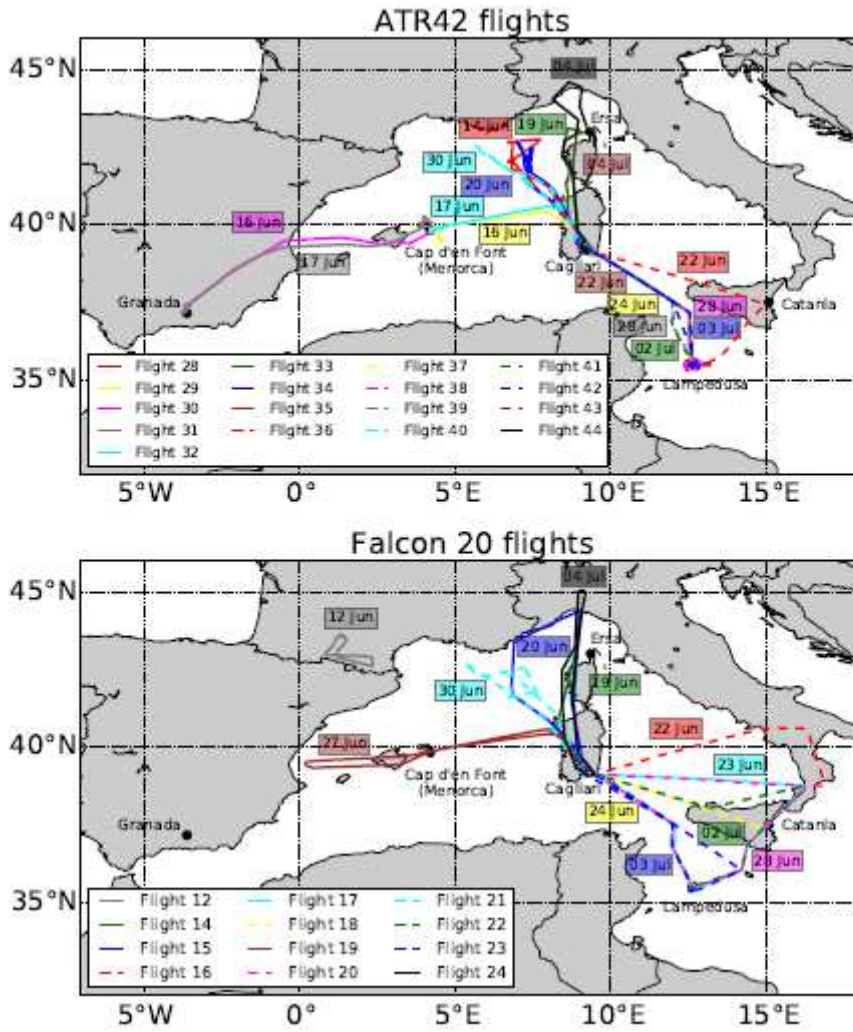
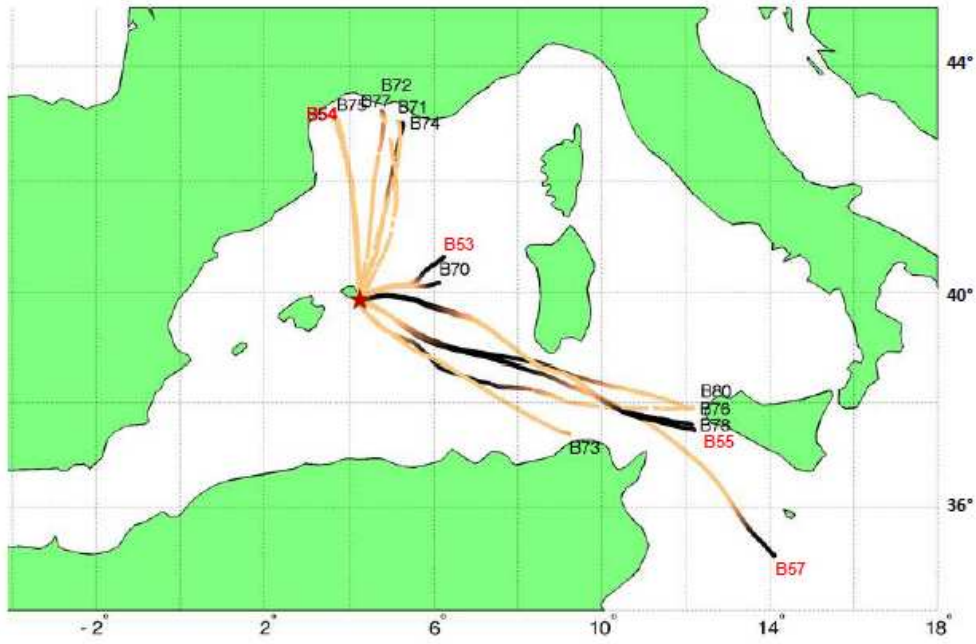


Figure 3. Overview of the different ATR-42 and F-20 flights trajectories performed during the SOP-1a experiment.

2520  
2521  
2522  
2523  
2524  
2525  
2526  
2527  
2528  
2529  
2530  
2531  
2532  
2533  
2534  
2535  
2536  
2537  
2538  
2539  
2540  
2541  
2542  
2543  
2544





**Figure 4.** Trajectories of the 14 BPCL drifting balloons launched from Minorca Island during the campaign. Dark portion along trajectories correspond to night-time conditions. The four red labels from B54 to B57 indicate balloons with an ozone sonde and the 10 others carried a LOAC instrument.

2545  
 2546  
 2547  
 2548  
 2549  
 2550  
 2551  
 2552  
 2553  
 2554  
 2555  
 2556  
 2557  
 2558  
 2559  
 2560  
 2561  
 2562  
 2563  
 2564  
 2565  
 2566  
 2567  
 2568  
 2569  
 2570  
 2571  
 2572  
 2573  
 2574  
 2575  
 2576  
 2577  
 2578  
 2579  
 2580  
 2581

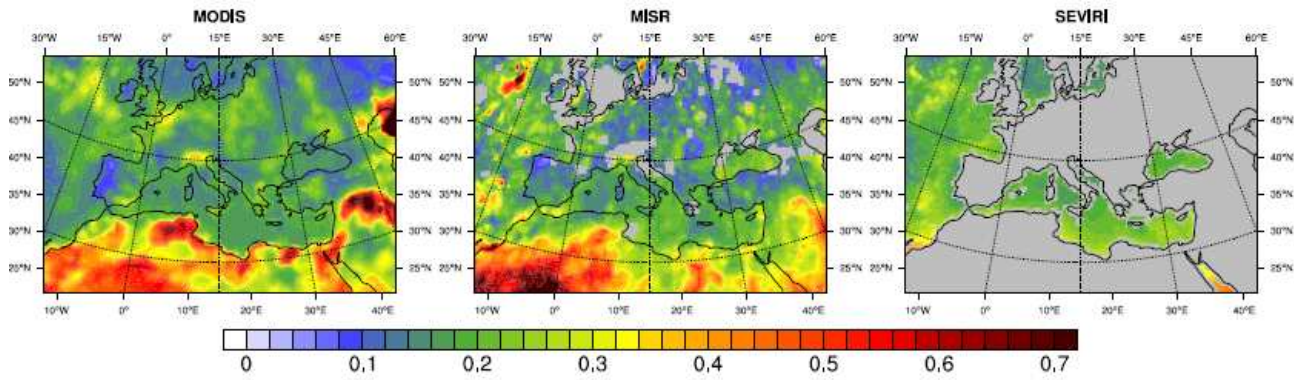
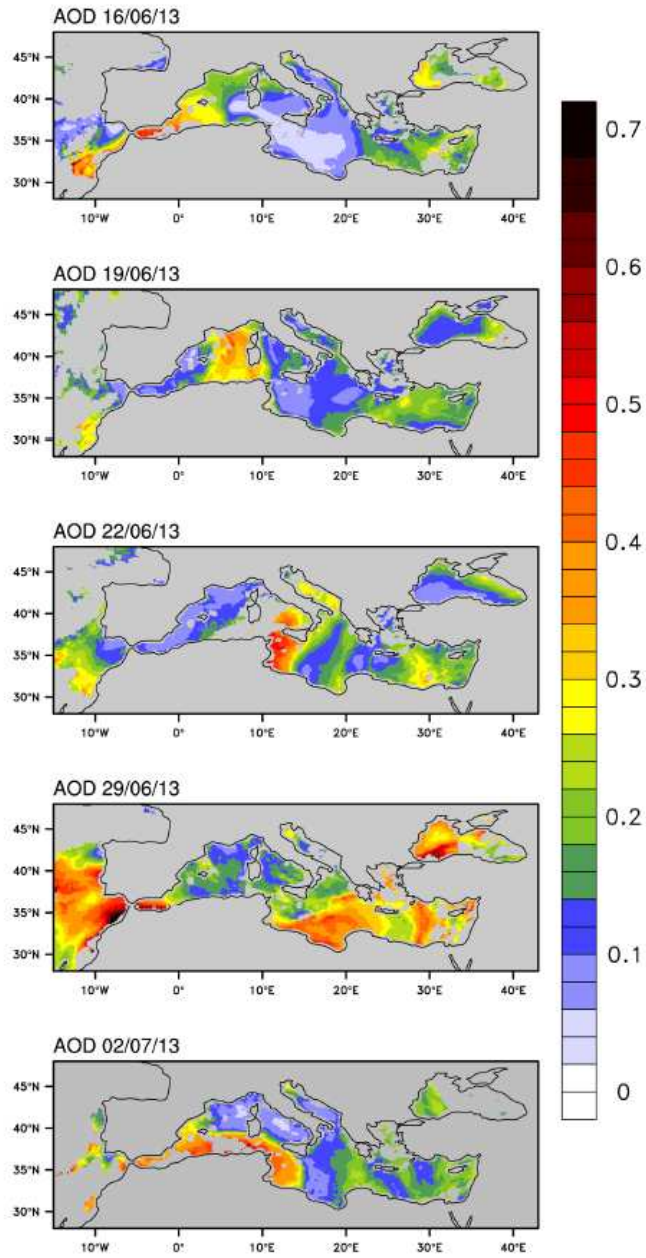


**Figure 5.** Total AOD (500 nm) obtained from the MODIS, MISR and SEVIRI (sea only) sensors for the June-July 2013 period.

2582  
 2583  
 2584  
 2585  
 2586  
 2587  
 2588  
 2589  
 2590  
 2591  
 2592  
 2593  
 2594  
 2595  
 2596  
 2597  
 2598  
 2599  
 2600  
 2601  
 2602  
 2603  
 2604  
 2605  
 2606  
 2607  
 2608  
 2609  
 2610  
 2611  
 2612  
 2613  
 2614  
 2615  
 2616  
 2617  
 2618  
 2619  
 2620  
 2621  
 2622  
 2623  
 2624  
 2625  
 2626  
 2627  
 2628



2629  
 2630  
 2631  
 2632  
 2633  
 2634  
 2635  
 2636  
 2637  
 2638  
 2639  
 2640  
 2641  
 2642  
 2643  
 2644  
 2645  
 2646  
 2647  
 2648

**Figure 6.** AOD MSG/SEVIRI observations for five different days during the SOP-1a experiment (16/06, 19/06, 22/06, 29/06 and 03/07).



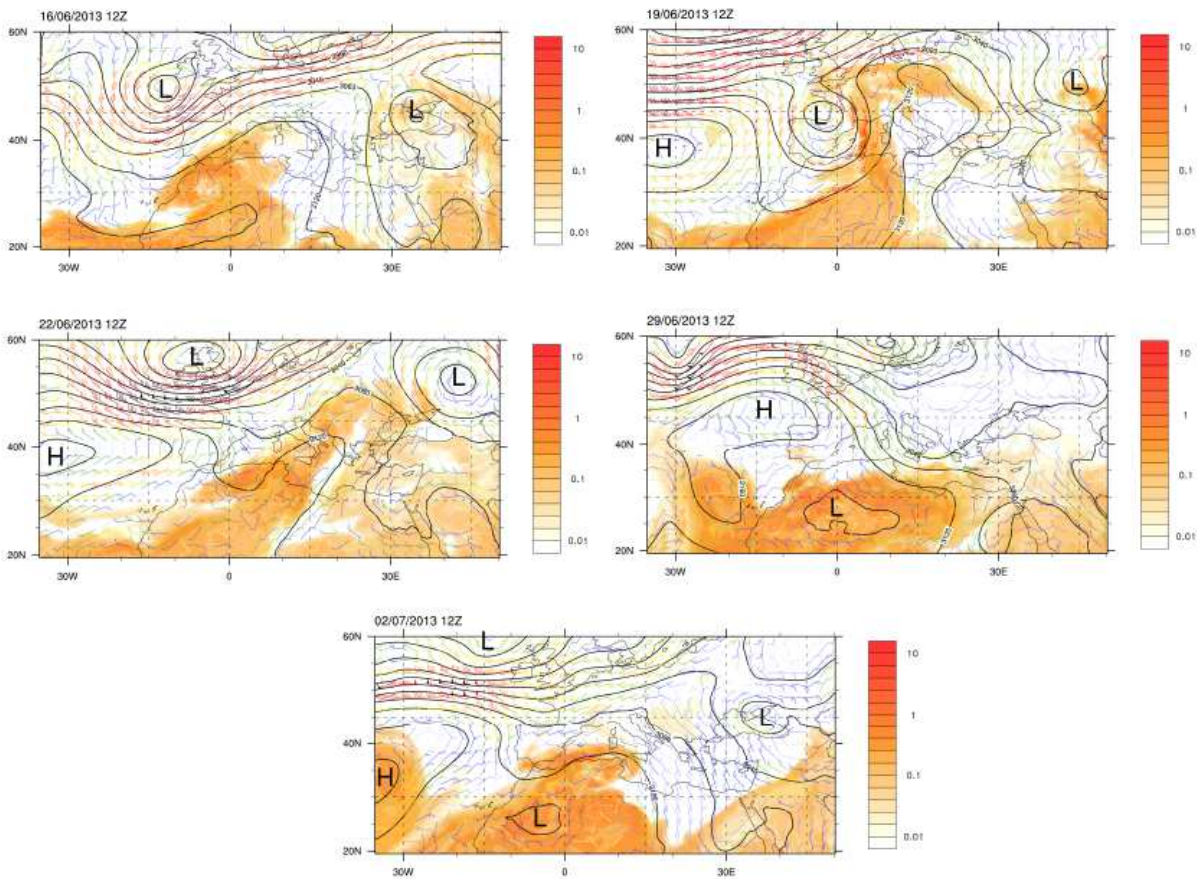
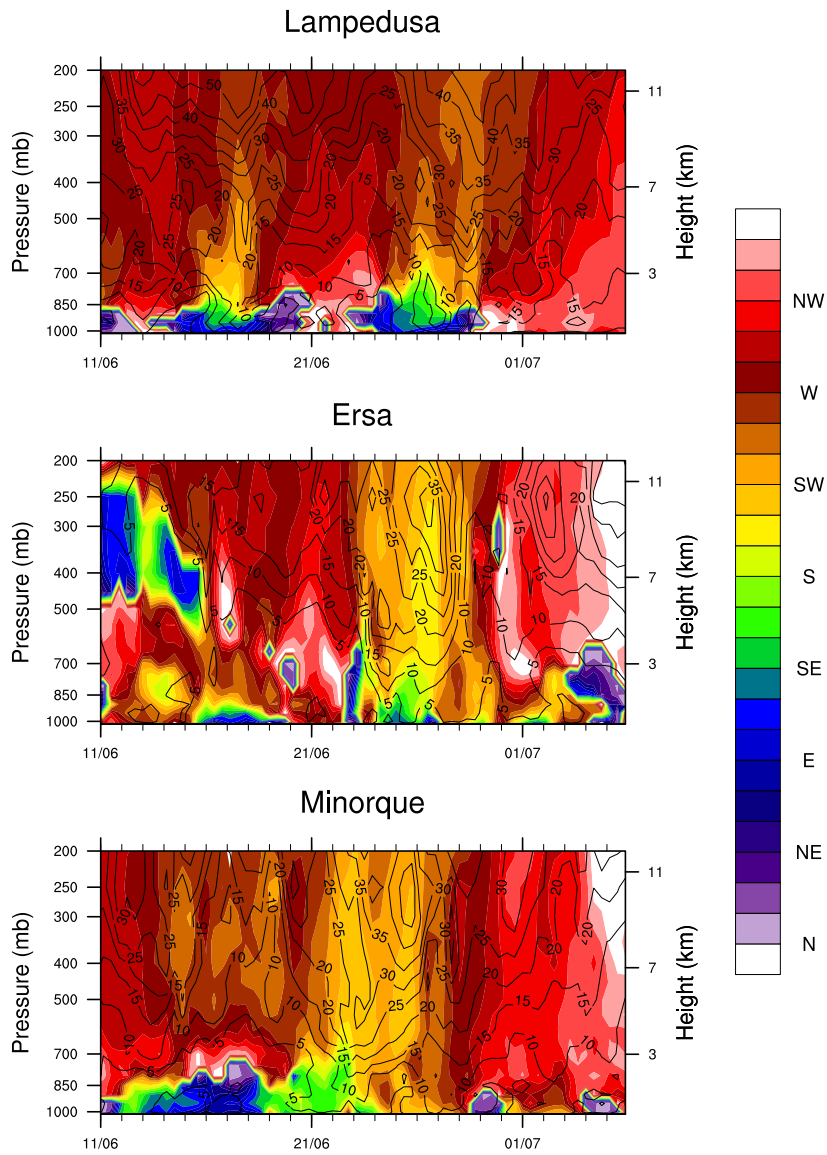


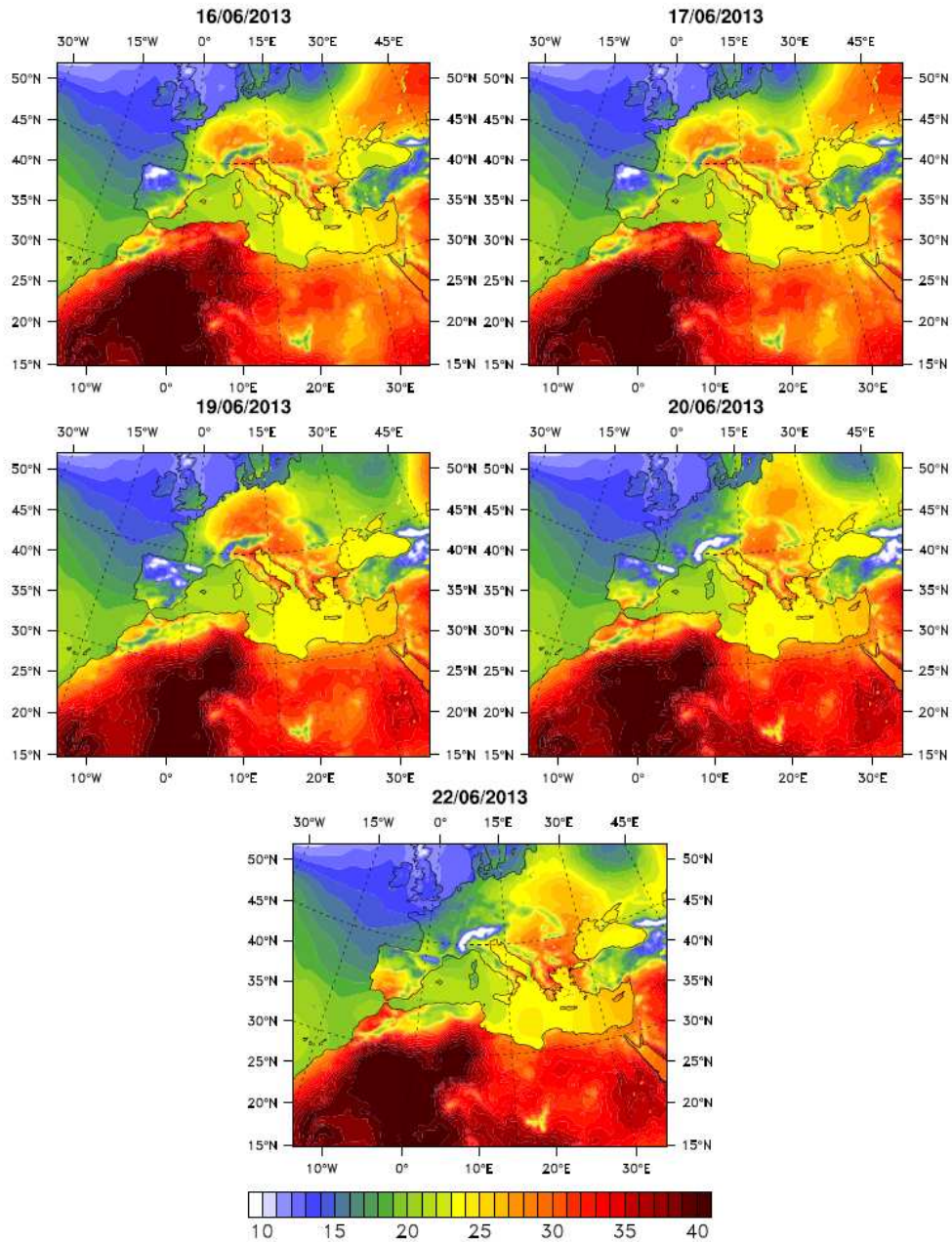
**Figure 7.** Geopotential at 700 hPa, mass dust concentration (in  $\text{mg}\cdot\text{m}^{-3}$ ), and wind intensity at 700 hPa for the 06, 19, 22, 29 of June and 02 of July at 12:00 UTC, simulated from the ALADIN model.

2649  
 2650  
 2651  
 2652  
 2653  
 2654  
 2655  
 2656  
 2657  
 2658  
 2659  
 2660  
 2661  
 2662  
 2663  
 2664  
 2665  
 2666  
 2667  
 2668  
 2669  
 2670  
 2671  
 2672  
 2673  
 2674  
 2675  
 2676  
 2677  
 2678  
 2679  
 2680  
 2681



2682  
 2683  
 2684  
 2685  
 2686  
 2687  
 2688  
 2689  
 2690  
 2691  
 2692  
 2693  
 2694  
 2695  
 2696  
 2697  
 2698  
 2699  
 2700  
 2701  
 2702  
 2703  
 2704  
 2705

**Figure 8.** Wind profiles between 1000 and 200 hPa during the SOP-1a experiment for three different sites (Ersa, Lampedusa and Minorca) simulated from the ALADIN model. The wind intensity (in  $m s^{-1}$ ) is also reported at the different stations.



2706  
 2707  
 2708  
 2709  
 2710  
 2711  
 2712  
 2713  
 2714  
 2715  
 2716  
 2717  
 2718  
 2719  
 2720  
 2721  
 2722  
 2723  
 2724  
 2725

**Figure 9.** Surface Temperature (at 12:00 UTC) obtained from NCEP re-analysis for the 16, 17, 19, 20 and 22 of June.

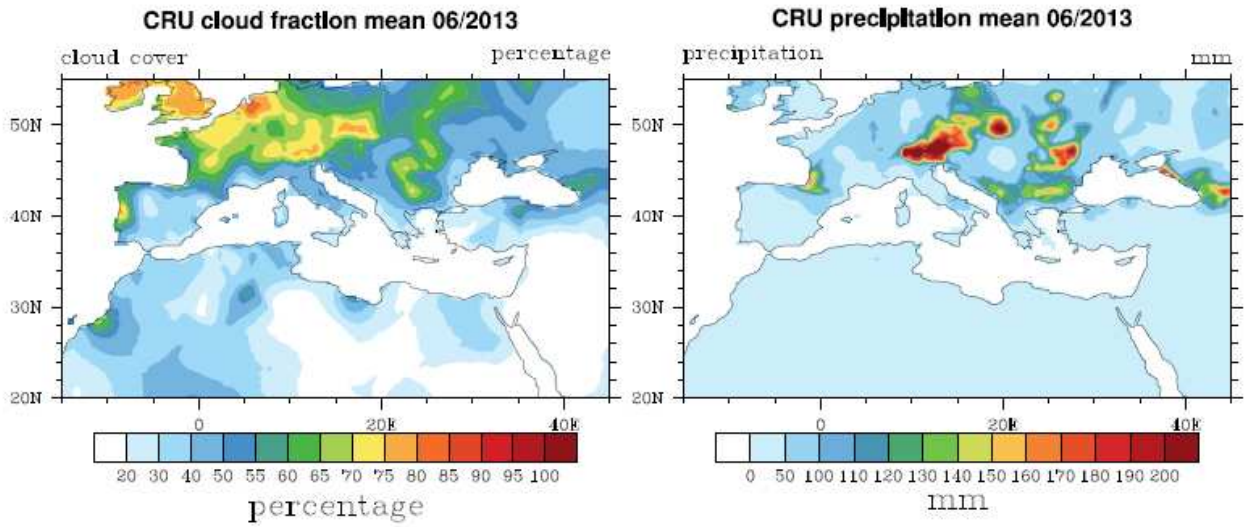
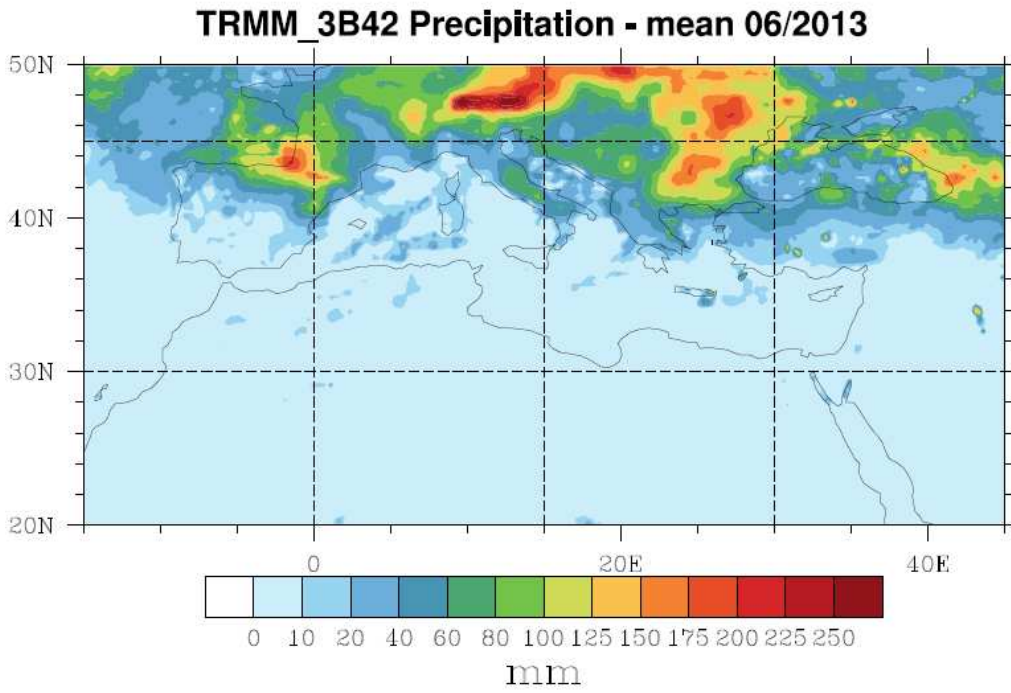


**Figure 10.** Monthly cloud cover and precipitation (over land only) derived from the Climate Research Unit (CRU) data for June 2013.

2726  
 2727  
 2728  
 2729  
 2730  
 2731  
 2732  
 2733  
 2734  
 2735  
 2736  
 2737  
 2738  
 2739  
 2740  
 2741  
 2742  
 2743  
 2744  
 2745  
 2746  
 2747  
 2748  
 2749  
 2750  
 2751  
 2752  
 2753  
 2754  
 2755  
 2756  
 2757  
 2758  
 2759  
 2760  
 2761  
 2762  
 2763  
 2764  
 2765  
 2766  
 2767





2768  
 2769  
 2770  
 2771  
 2772  
 2773  
 2774  
 2775  
 2776  
 2777  
 2778  
 2779  
 2780  
 2781  
 2782  
 2783  
 2784  
 2785  
 2786  
 2787  
 2788  
 2789  
 2790  
 2791  
 2792  
 2793  
 2794  
 2795  
 2796  
 2797  
 2798  
 2799  
 2800  
 2801  
 2802  
 2803  
 2804

**Figure 11.** Same figure as 10 but for the Tropical Rainfall Measuring Mission (TRMM) precipitation observations.

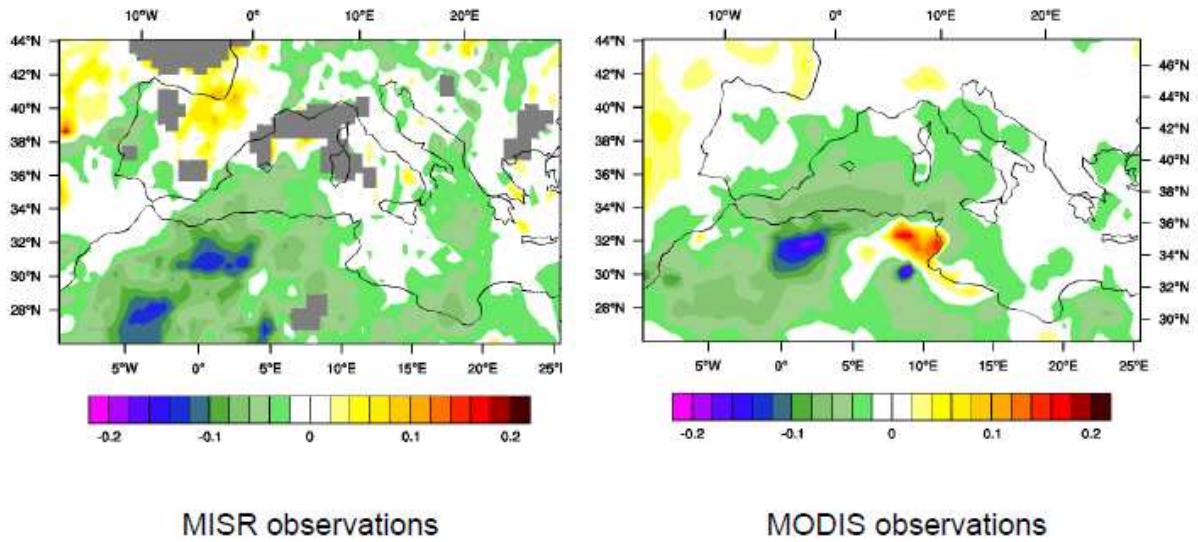
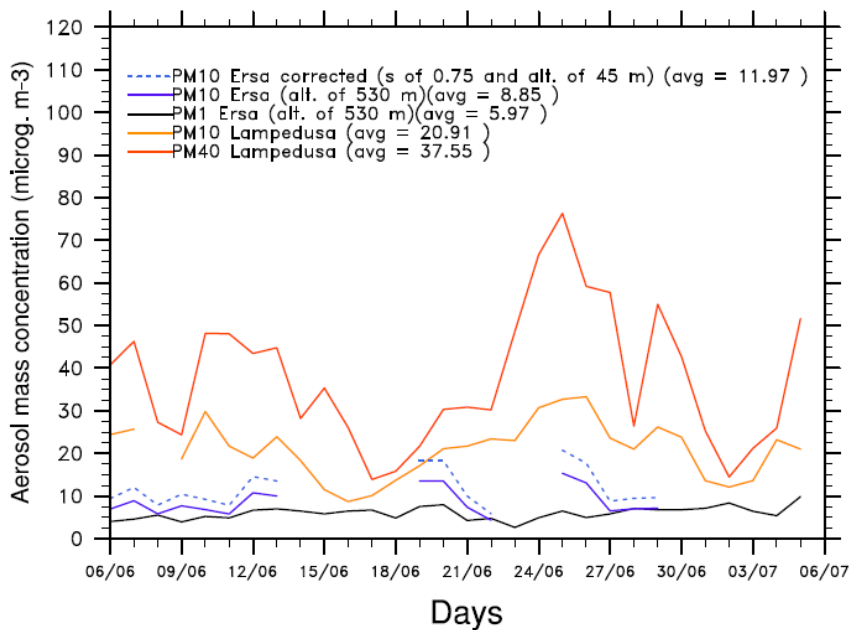


**Figure 12.** AOD anomaly for summer 2013 estimated from the MODIS and MISR sensor data.

2805  
 2806  
 2807  
 2808  
 2809  
 2810  
 2811  
 2812  
 2813  
 2814  
 2815  
 2816  
 2817  
 2818  
 2819  
 2820  
 2821  
 2822  
 2823  
 2824  
 2825  
 2826  
 2827  
 2828  
 2829  
 2830  
 2831  
 2832  
 2833  
 2834  
 2835  
 2836  
 2837  
 2838  
 2839  
 2840  
 2841  
 2842  
 2843  
 2844  
 2845



2846  
2847  
2848  
2849  
2850  
2851  
2852  
2853  
2854  
2855  
2856  
2857  
2858  
2859  
2860  
2861  
2862  
2863  
2864  
2865  
2866  
2867  
2868  
2869  
2870  
2871  
2872  
2873  
2874  
2875  
2876  
2877  
2878  
2879  
2880  
2881  
2882

**Figure 13.** Time-series of daily PM mass concentrations estimated at the Lampedusa (PM40 and PM10) and Ersal (PM1 and PM10) super-stations. Problems in PM10 data acquisition that occurred at Ersal explain the gaps. “PM10 Ersal corrected” curve correspond to PM10 estimated at an altitude of 45m to be comparable with Lampedusa results, following the logarithmic law provided by Piazzola et al. (2015), (see text in section 5.1.1 for details).

SOP-1a AERONET/PHOTONS Volume size distribution

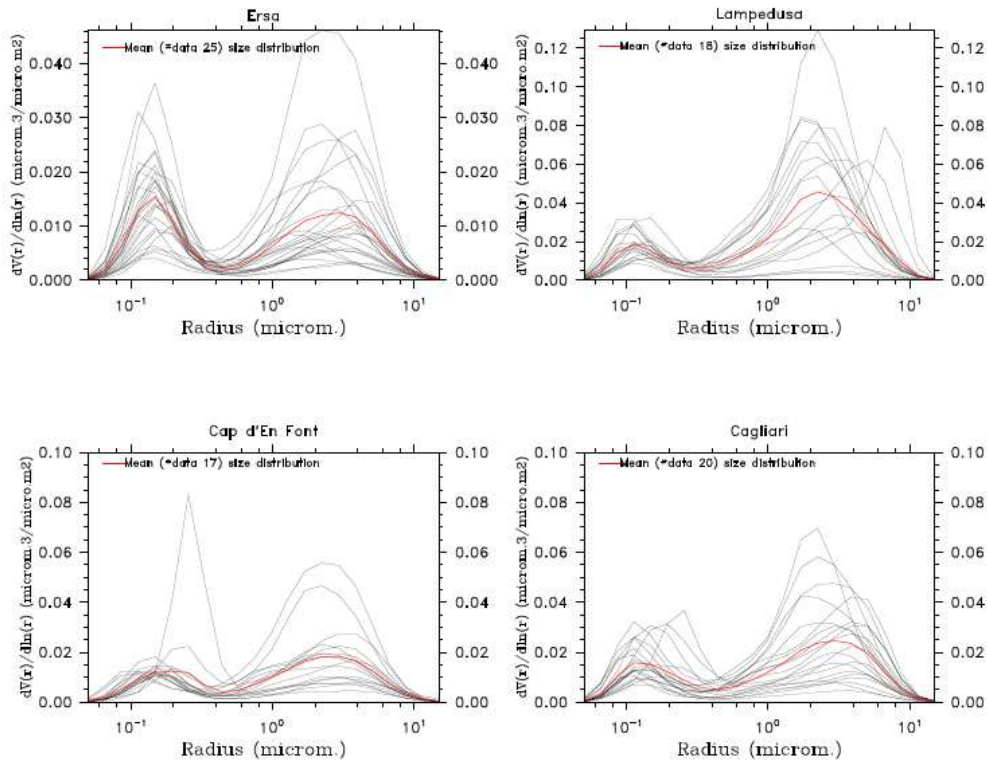
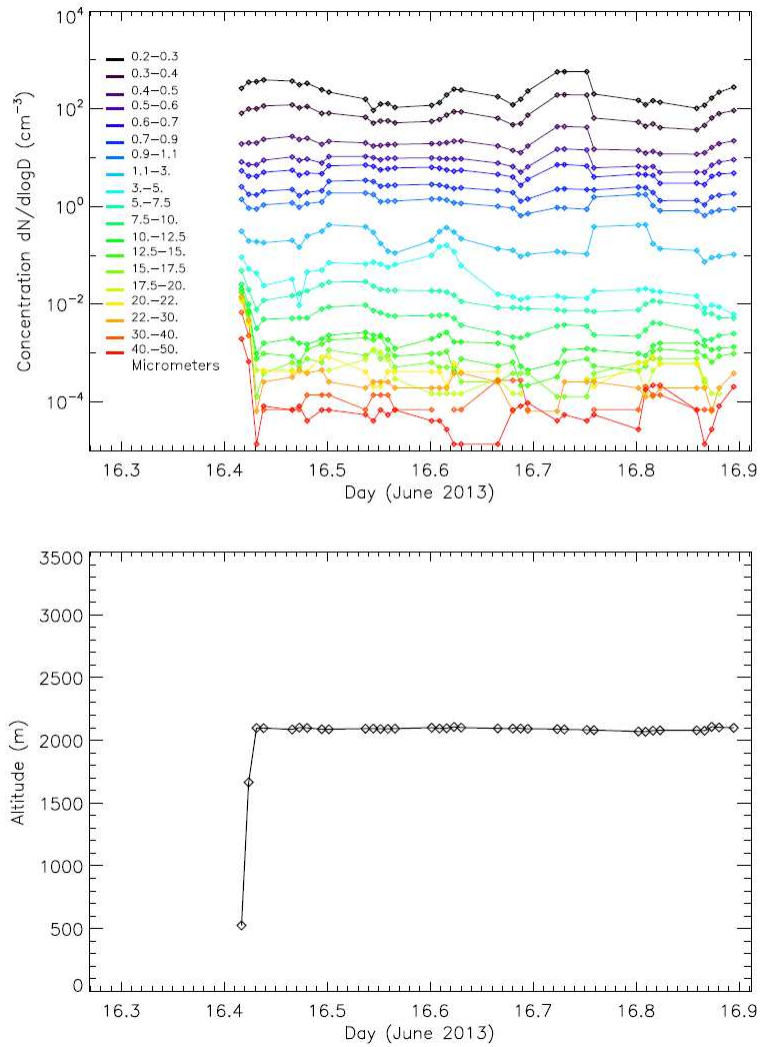


**Figure 14.** AERONET/PHOTONS volume size distribution derived at four different stations: Ersa, Lampedusa, Cagliari and Cap d'En Font (the red curve represents the mean of observations). The characteristics of the volume size distribution are provided in Table 6.

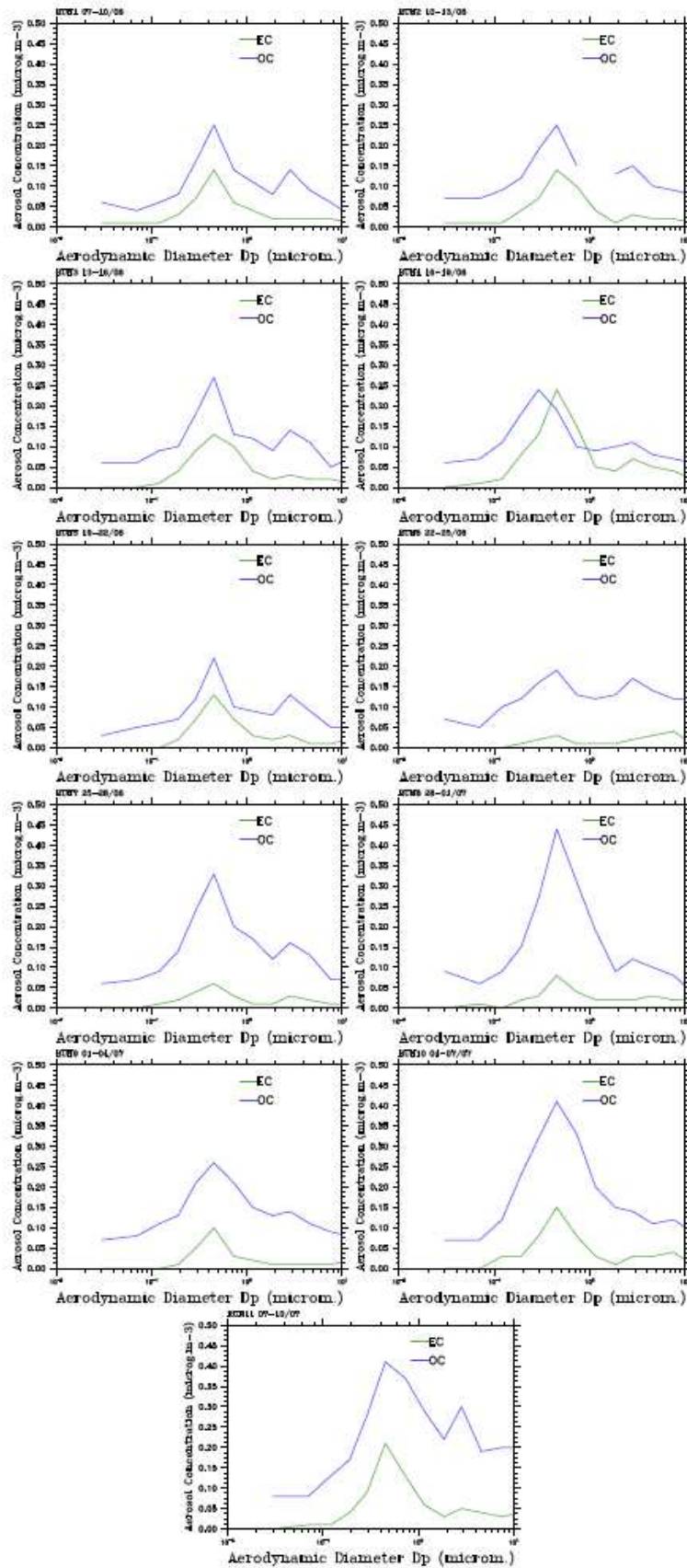
2883  
 2884  
 2885  
 2886  
 2887  
 2888  
 2889  
 2890  
 2891  
 2892  
 2893  
 2894  
 2895  
 2896  
 2897  
 2898  
 2899  
 2900  
 2901  
 2902  
 2903  
 2904  
 2905  
 2906  
 2907  
 2908  
 2909  
 2910





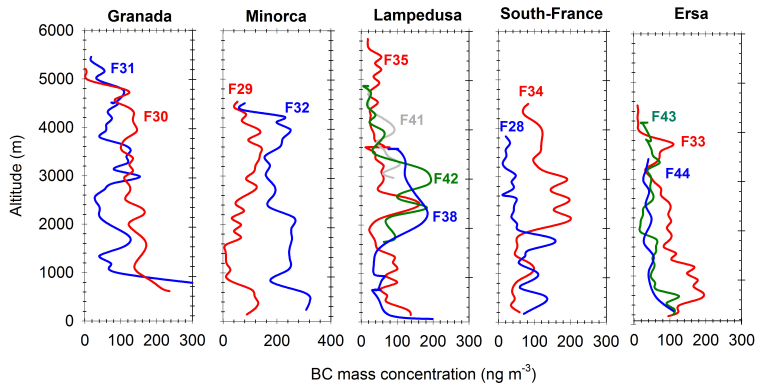
2911  
 2912  
 2913  
 2914  
 2915  
 2916  
 2917  
 2918  
 2919  
 2920  
 2921  
 2922  
 2923  
 2924  
 2925  
 2926  
 2927  
 2928  
 2929

**Figure 15.** Particle size distribution measured with a LOAC during the ~12-h flight of the BPCL balloon B74 drifting from Minorca Island towards Marseille (see trajectory in Figure 4). The first and last 20 min correspond to the ascending and descending phases of the quasi-Lagrangian flight which occurred at a constant altitude of 2091±10 m.



2930  
 2931  
 2932  
 2933  
 2934  
 2935

**Figure 16.** EC and OC (48h-mean) aerosol mass size distributions obtained at Ersa from the impactor DEKATI instrument for all the SOP-1a period.



2936  
2937  
2938

**Figure 17.** Vertical profiles of rBC concentrations estimated from SP2 instrument for 5 different zones (Granada, Minorca, Lampedusa, South-France and Ersa).

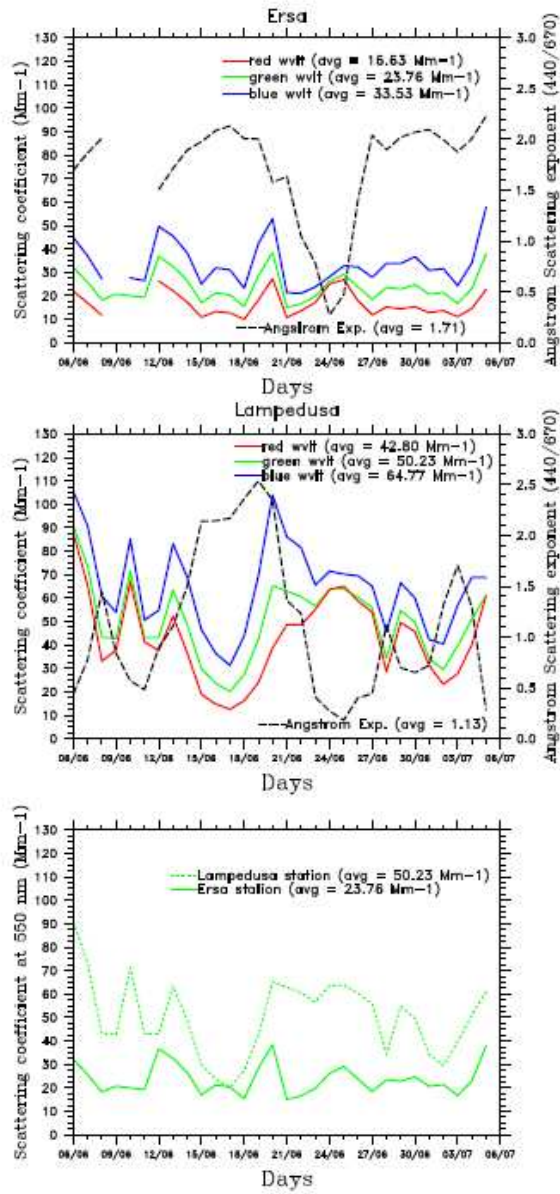


**Figure 18.** Time-series of daily scattering coefficient (in Mm<sup>-1</sup>) estimated in the Ersu and Lampedusa stations. The daily Angström Exponent (AE), calculated between 440 and 670 nm, is also reported.

2939  
 2940  
 2941  
 2942  
 2943  
 2944  
 2945  
 2946  
 2947  
 2948  
 2949  
 2950  
 2951  
 2952  
 2953  
 2954  
 2955  
 2956  
 2957  
 2958  
 2959

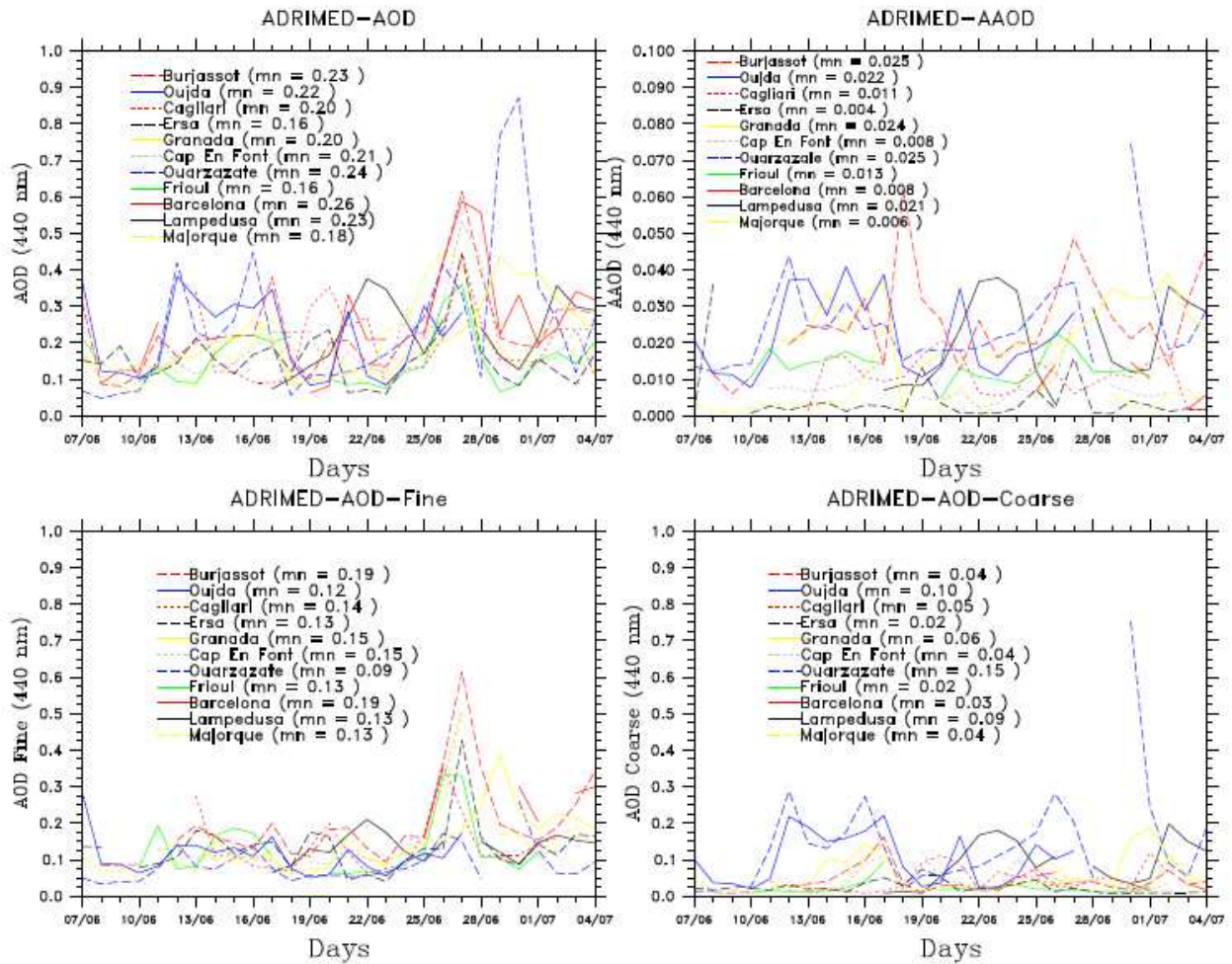
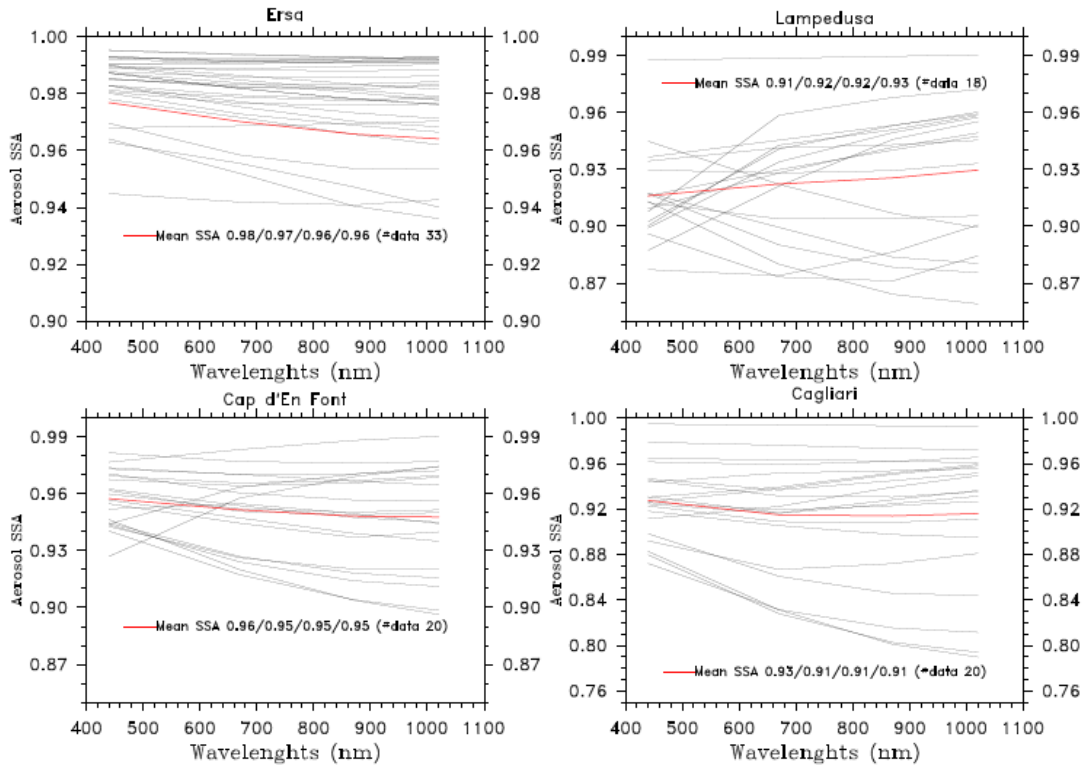


**Figure 19.** AERONET/PHOTONS observations of the total extinction AOD, AOD Fine (AODf), AOD Coarse (AODc) and Absorbing AOD (AAOD), at 440 nm obtained for the whole SOP-1a period.

2960  
2961  
2962  
2963  
2964  
2965  
2966  
2967  
2968  
2969  
2970  
2971  
2972  
2973  
2974  
2975  
2976  
2977  
2978  
2979  
2980  
2981  
2982  
2983  
2984  
2985  
2986  
2987

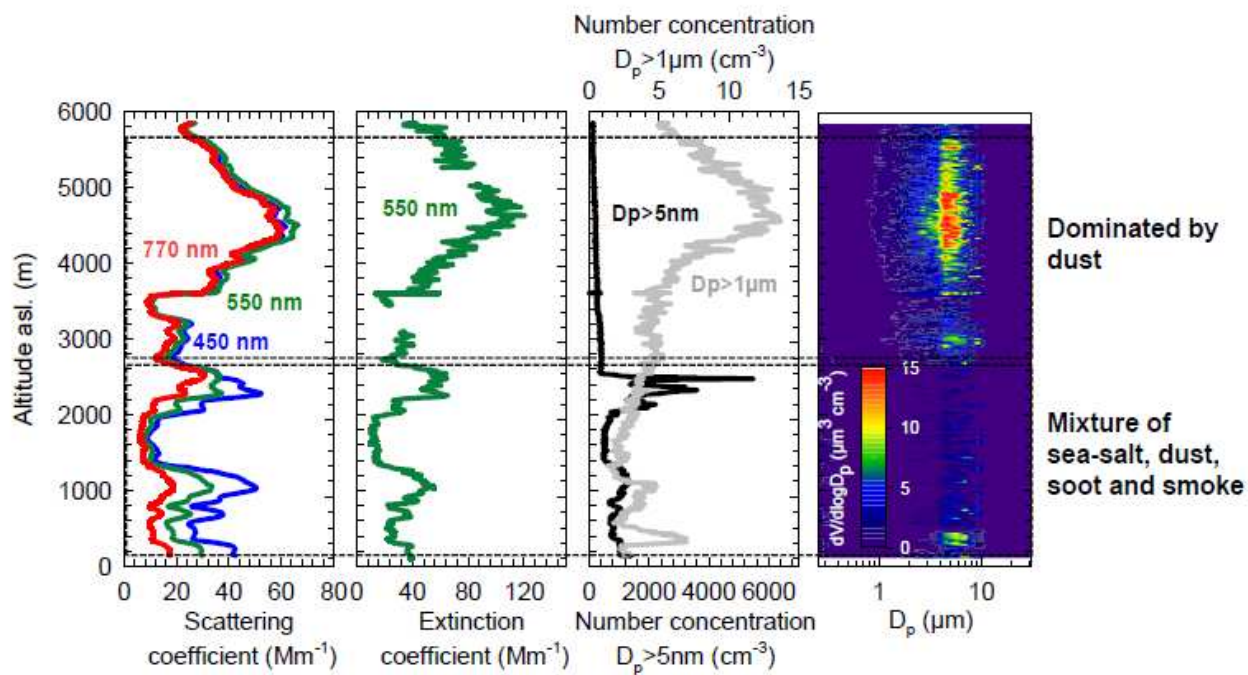
## SOP-1a AERONET/PHOTONS SSA



2988  
 2989  
 2990  
 2991  
 2992  
 2993  
 2994  
 2995  
 2996  
 2997  
 2998  
 2999  
 3000  
 3001  
 3002  
 3003  
 3004  
 3005  
 3006  
 3007  
 3008  
 3009  
 3010  
 3011  
 3012  
 3013  
 3014  
 3015  
 3016  
 3017  
 3018

**Figure 20.** AERONET/PHOTONS observations of the total single scattering albedo (SSA) at 440, 670, 880 and 1020 nm obtained for the whole SOP-1a period (the red curve represents the mean of observations).





3019  
 3020  
 3021  
 3022  
 3023  
 3024  
 3025  
 3026  
 3027  
 3028  
 3029  
 3030  
 3031  
 3032  
 3033  
 3034  
 3035  
 3036  
 3037  
 3038  
 3039  
 3040  
 3041  
 3042  
 3043  
 3044  
 3045  
 3046  
 3047  
 3048  
 3049  
 3050  
 3051  
 3052  
 3053  
 3054

**Figure 21.** Optical (scattering and extinction coefficients) and physical (number concentration and volume size distribution) aerosol properties estimated along the vertical onboard the ATR-42 aircraft for the flights 35-36 on 22 June over the Lampedusa station.

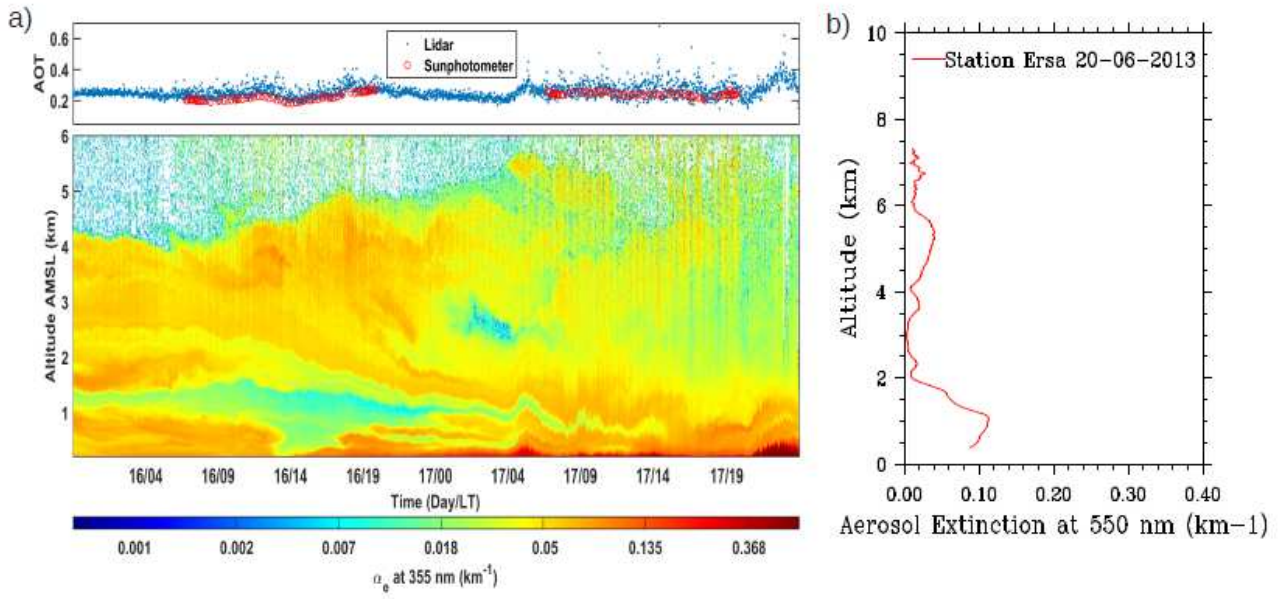


**Figure 22.** Minorca and Ersa lidar observations obtained during the dust plume of 16 to 17 June transported over the western Mediterranean basin.

3055  
 3056  
 3057  
 3058  
 3059  
 3060  
 3061  
 3062  
 3063  
 3064  
 3065  
 3066  
 3067  
 3068  
 3069  
 3070  
 3071  
 3072  
 3073  
 3074  
 3075  
 3076  
 3077  
 3078  
 3079  
 3080  
 3081  
 3082  
 3083  
 3084  
 3085  
 3086  
 3087  
 3088  
 3089  
 3090  
 3091  
 3092  
 3093  
 3094



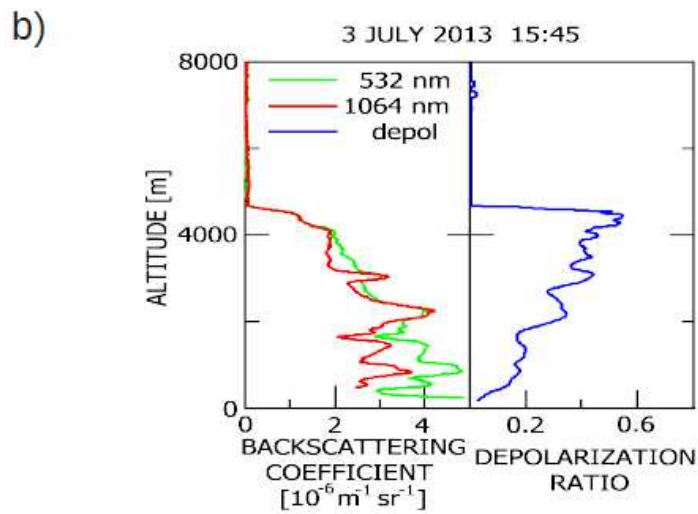
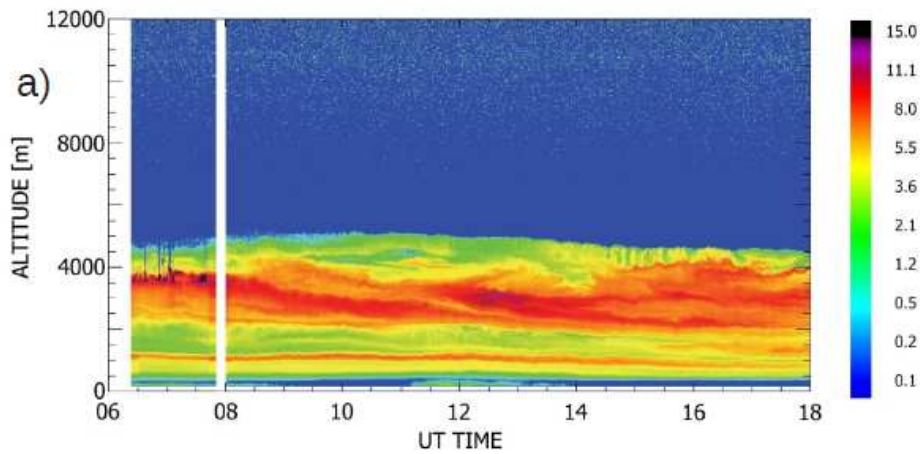
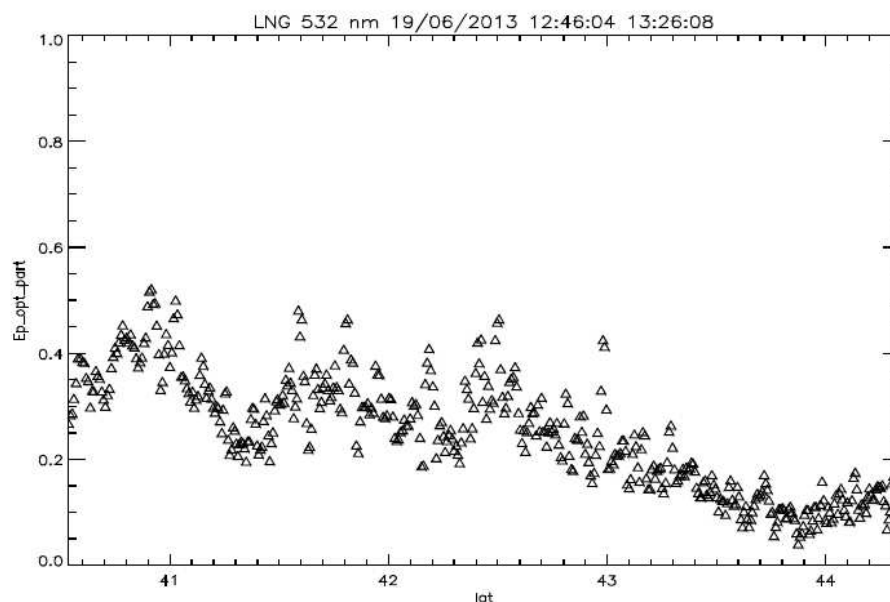
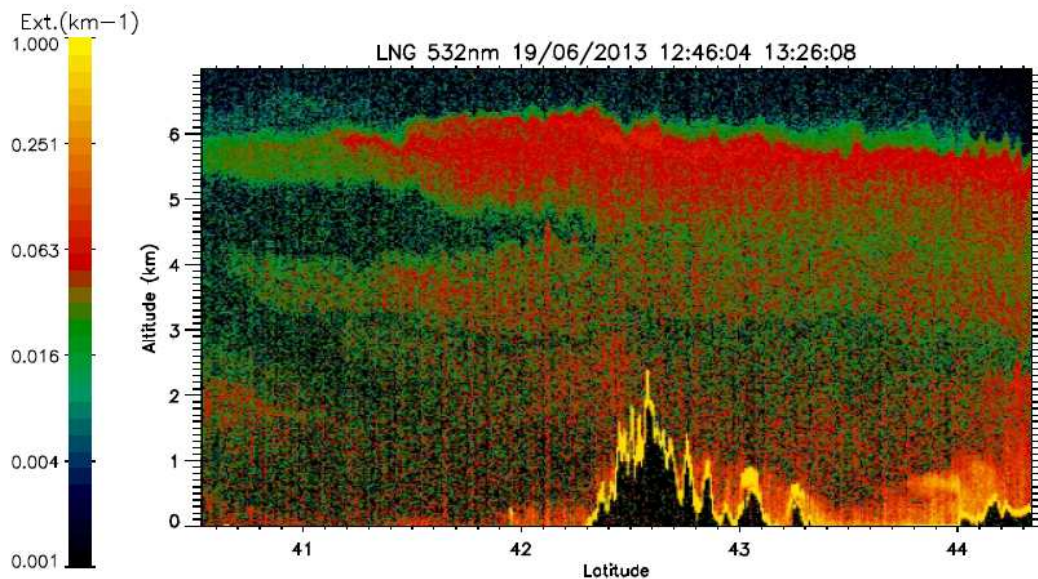


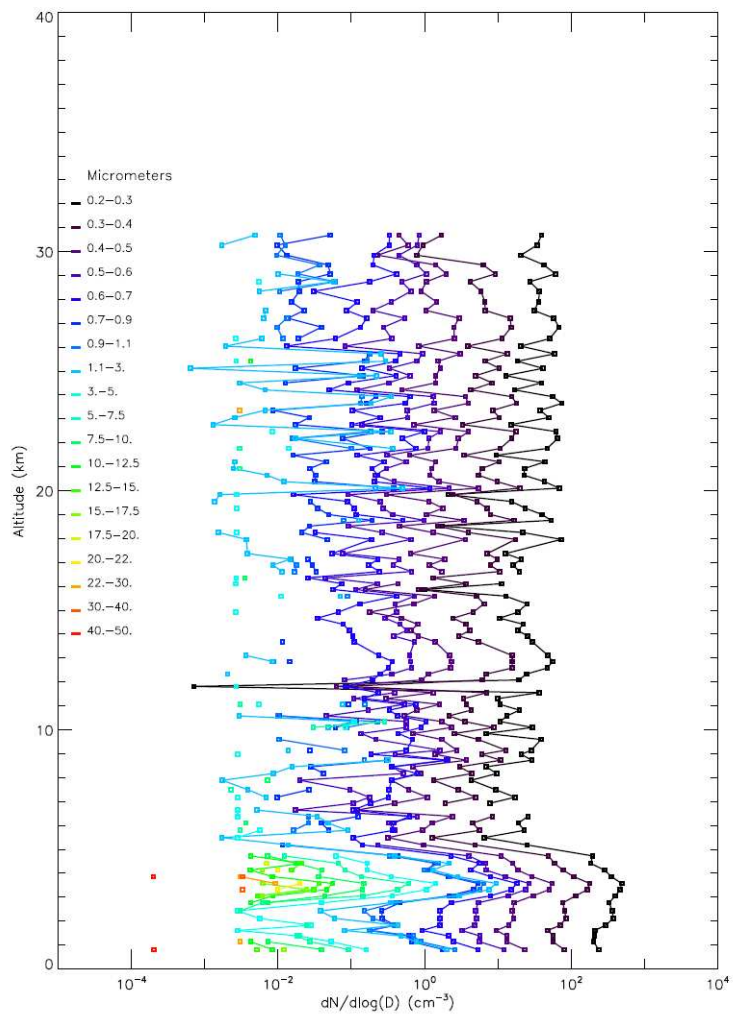
**Figure 23.** a) Time evolution of the vertical profile of the aerosol backscattering coefficient at 1064 nm at Lampedusa on 3 July 2013. The color scale is in units of  $10^{-7} \text{ m}^{-1} \text{ sr}^{-1}$ . b) Vertical profile of aerosol backscattering coefficient at two wavelengths and of aerosol depolarization ratio at 355 nm measured at Lampedusa on 3 July 2013 at 15:45 UT.

3095  
 3096  
 3097  
 3098  
 3099  
 3100  
 3101  
 3102  
 3103  
 3104  
 3105  
 3106  
 3107  
 3108  
 3109  
 3110  
 3111  
 3112  
 3113  
 3114  
 3115  
 3116  
 3117  
 3118  
 3119  
 3120



3121  
 3122  
 3123  
 3124  
 3125  
 3126  
 3127  
 3128  
 3129  
 3130  
 3131  
 3132  
 3133  
 3134  
 3135  
 3136  
 3137  
 3138  
 3139  
 3140  
 3141  
 3142

**Figure 24.** Observations of aerosol extinction coefficient (top, in  $\text{km}^{-1}$  at 532 nm) and aerosol optical depth (bottom) obtained from the lidar LNG system onboard the F-20 aircraft during the 19<sup>th</sup> of June that corresponds to the flight (12:46 to 13:26) from Cagliari to the Gulf of Genoa.



3143  
 3144  
 3145  
 3146  
 3147  
 3148  
 3149  
 3150  
 3151  
 3152  
 3153  
 3154  
 3155  
 3156  
 3157  
 3158  
 3159  
 3160  
 3161

**Figure 25:** Particle concentrations as a function of size and altitude in the troposphere and lower stratosphere from the LOAC flight under the meteorological balloon BLD9 launched from Minorca at the end of a dust event on 19 June 2013, 10:12 UT (Table 4; see the daytime averaged aerosol optical depth over the sea in Figure 6).

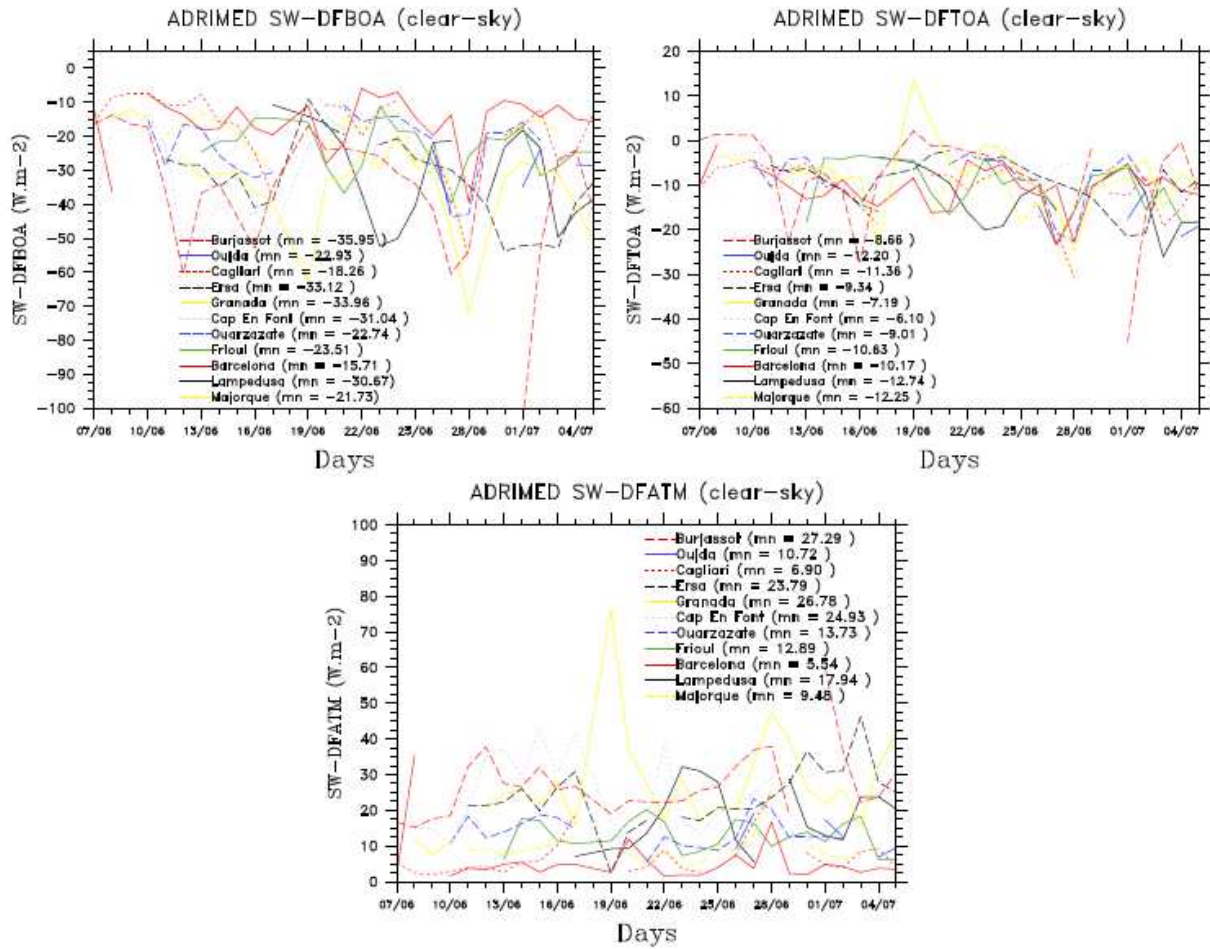


**Figure 26.** 1-D (clear-sky) instantaneous (shortwave only) DRF calculations (in W m<sup>-2</sup>) based on AERONET/PHOTONS dataset for the different stations listed in Table 2 (BOA, TOA and ATM refer to bottom of the atmosphere, top of atmosphere and atmospheric forcings).

3162  
3163  
3164  
3165  
3166  
3167  
3168  
3169  
3170  
3171  
3172  
3173  
3174  
3175  
3176  
3177  
3178  
3179  
3180  
3181  
3182  
3183  
3184  
3185  
3186  
3187

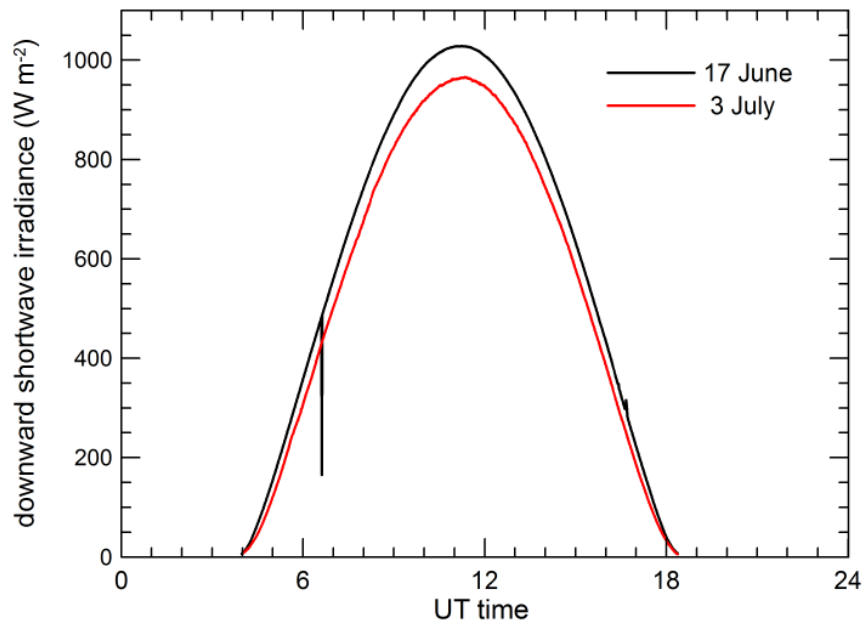


**Figure 27.** Time evolution of the downward solar irradiance observed at Lampedusa on 17 June and on 3 July, 2013.

3188  
 3189  
 3190  
 3191  
 3192  
 3193  
 3194  
 3195  
 3196  
 3197  
 3198  
 3199  
 3200  
 3201  
 3202  
 3203  
 3204  
 3205  
 3206  
 3207  
 3208  
 3209  
 3210  
 3211  
 3212  
 3213  
 3214  
 3215  
 3216  
 3217  
 3218  
 3219  
 3220  
 3221  
 3222  
 3223  
 3224  
 3225

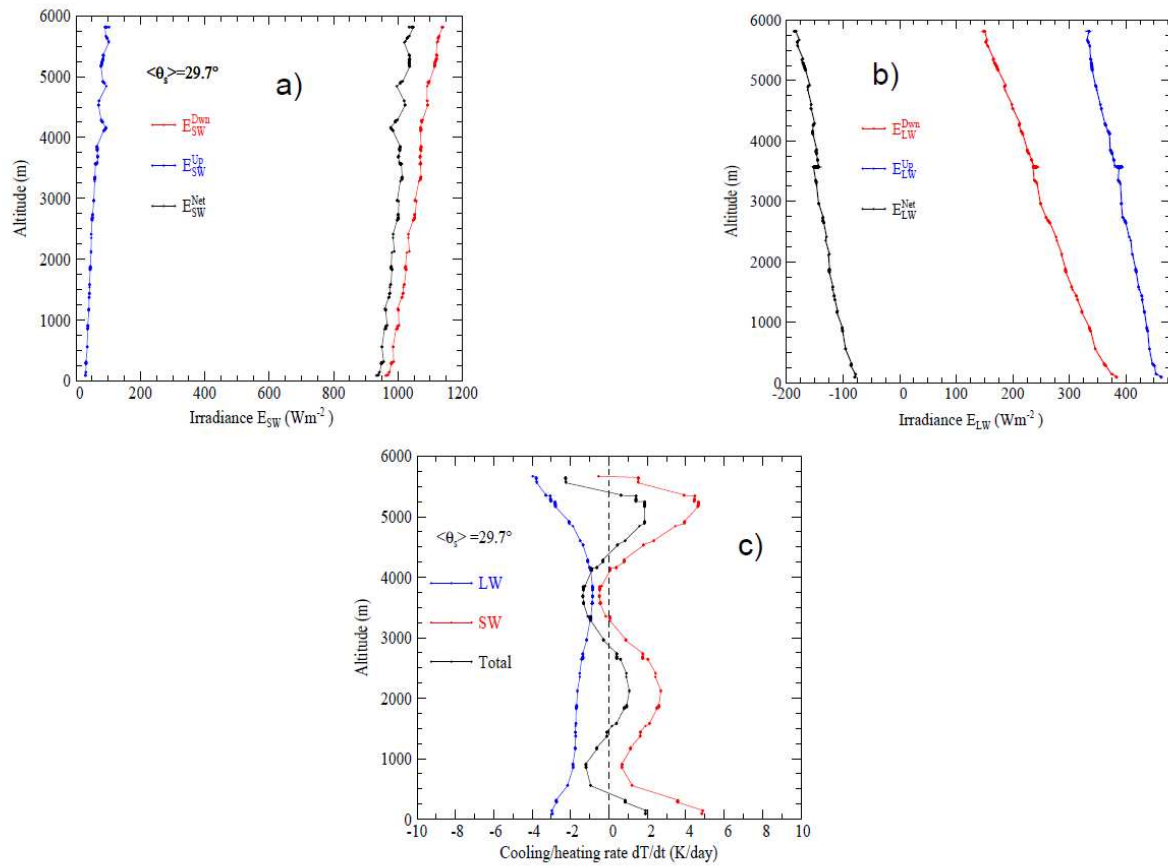
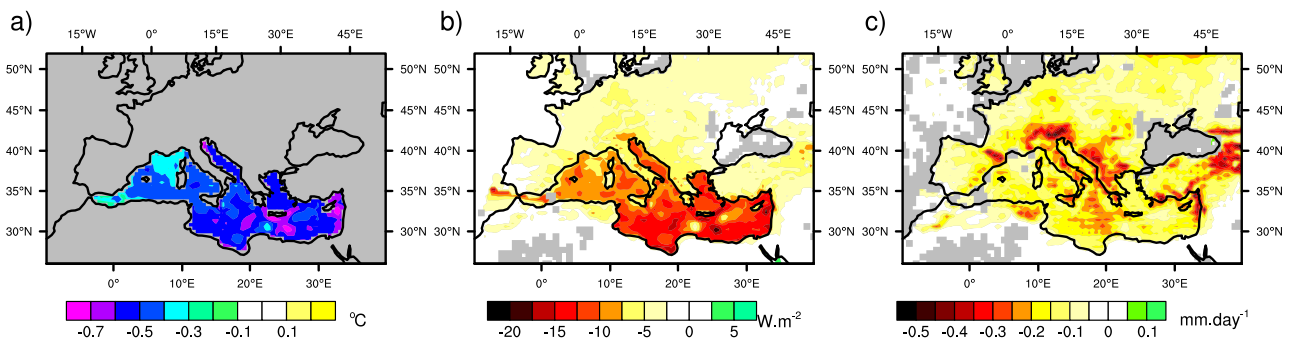


**Figure 28.** SW (a) and LW (b) upward and downward radiative fluxes observed over the Lampedusa station for the 22 June and estimated SW and LW heating rate (c) in the two spectral regions (see section 5.4.4 for details).

3226  
 3227  
 3228  
 3229  
 3230  
 3231  
 3232  
 3233  
 3234  
 3235  
 3236  
 3237  
 3238  
 3239  
 3240  
 3241  
 3242  
 3243  
 3244  
 3245  
 3246  
 3247  
 3248  
 3249  
 3250  
 3251  
 3252  
 3253  
 3254  
 3255





3256  
 3257  
 3258  
 3259  
 3260

**Figure 29.** Annual average difference in (a) Sea Surface Temperature (SST), latent heat loss (b) and precipitation (c) over the period 2003-2009 between a simulation ensemble including aerosols and a second one without any aerosol.

## Aerosol optical Depth (visible band)

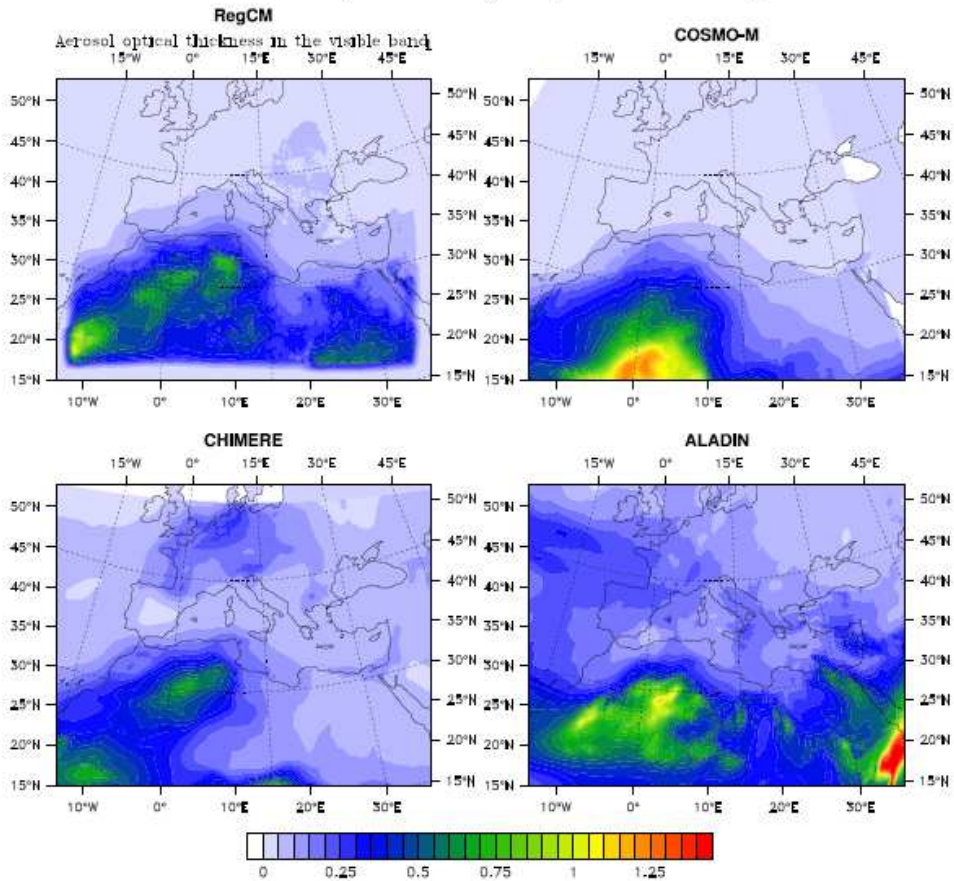


**Figure 30.** AOD averaged for the 15 to 25 June 2013 period from the meso-scale COSMO-MUSCAT (a), CTM-CHIMERE (b) models and the two regional climate models; CNRM-RCSM (c) and RegCM (d). Details about the model configurations are provided in Table 8.

3261  
 3262  
 3263  
 3264  
 3265  
 3266  
 3267  
 3268  
 3269  
 3270  
 3271  
 3272  
 3273  
 3274  
 3275  
 3276  
 3277  
 3278  
 3279  
 3280  
 3281  
 3282  
 3283  
 3284  
 3285  
 3286  
 3287  
 3288  
 3289



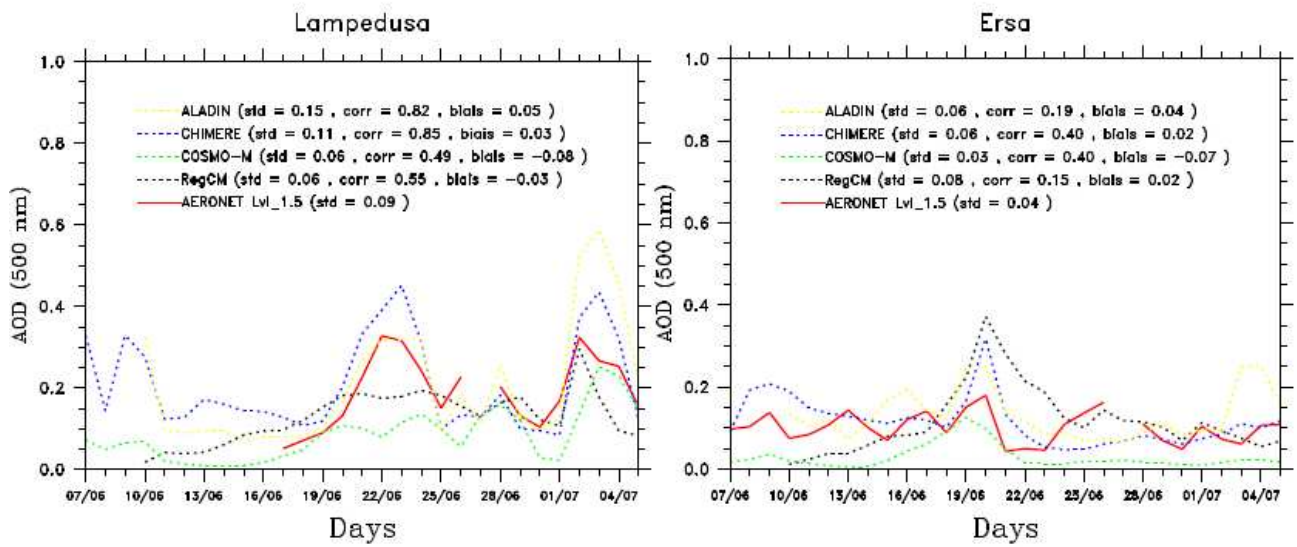
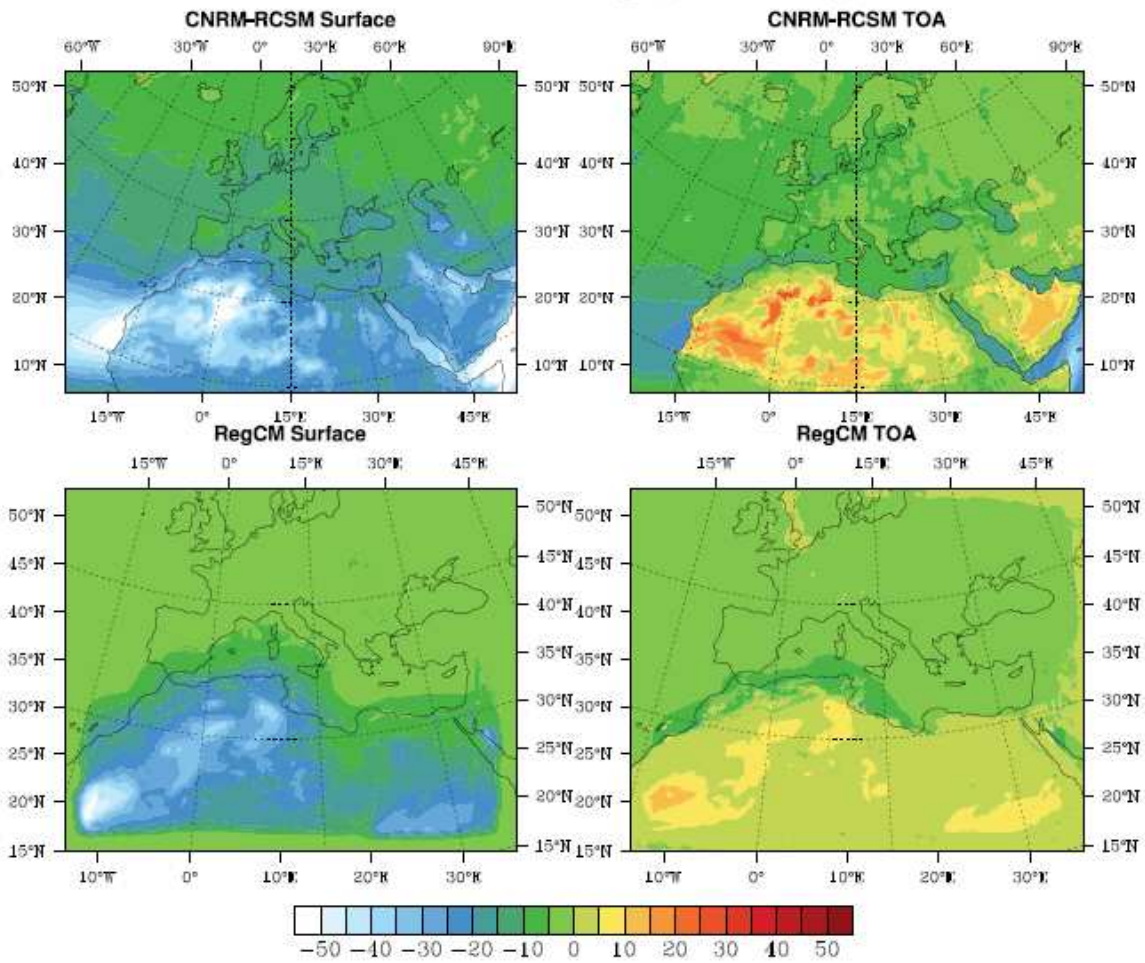


**Figure 31.** Times-series of AOD comparisons between AERONET/PHOTONS observations and COSMO-MUSCAT, CHIMERE, CNRM-RCSM and RegCM model outputs over the two stations of Ersa and Lampedusa.

3290  
 3291  
 3292  
 3293  
 3294  
 3295  
 3296  
 3297  
 3298  
 3299  
 3300  
 3301  
 3302  
 3303  
 3304  
 3305  
 3306  
 3307  
 3308  
 3309  
 3310  
 3311  
 3312  
 3313  
 3314  
 3315  
 3316  
 3317  
 3318  
 3319  
 3320  
 3321  
 3322  
 3323  
 3324  
 3325  
 3326  
 3327

## SW Direct Radiative Forcing (clear-sky) SOP-1a



3328  
 3329  
 3330  
 3331  
 3332  
 3333  
 3334  
 3335

**Figure 32.** Averaged surface and TOA SW DRF simulated in clear-sky conditions and over the SOP-1a period by the CNRM-RCSM and RegCM models.

	Ersa		Lampedusa	
	Instruments	Frequency	Instruments	Frequency
Number concentration	1 CPC (0.01 - 3 $\mu\text{m}$ )	continuous (1')	1 W-CPC (0.01 - 3 $\mu\text{m}$ )	continuous (2')
CCN concentration	1 CCN counter	continuous	1 CCN counter	continuous
Mass concentration	1 PM2.5	continuous	1 PM40 (TEOM)	continuous
	1 PM10	continuous		
Number size distribution	1 OPC (0.3 - 5 $\mu\text{m}$ )	continuous	2 GRIMM (0.25 - 32 $\mu\text{m}$ )	continuous
	1 APS (TSI)	continuous	1 APS (TSI) (0.5 - 20 $\mu\text{m}$ )	continuous
	1 SMPS (3 - 300 nm)	continuous	2 (dry/ambient) SMPS	continuous
Mass size distribution	2 Impactor DEKATI (13 stages)	48h	2 Impactor DEKATI (13 stages)	48h
			1 Impactor Nano-MOUDI	24 h
PM1 composition	1 PILS	continuous	AMS (Aerodyne)	continuous
			1 PILS	continuous
PM10 composition			1 FAI Hydra Sampler	12h
Mass BC concentration	1 (7- $\lambda$ ) aethalometer	continuous	1 PSAP	continuous (1h)
			1 MAAP	continuous
Vertical Profiles	1 (1- $\lambda$ 355 nm) Leosphere	continuous	1 (1- $\lambda$ ) Leosphere ALS 300	continuous (20')
			2 (3-l) ENEA/Univ. of Rome lidar	continuous (1')
			microwave radiometer (p, T, RH)	continuous (15')
			radiosondes	on event
Scattering coefficient	1 (3- $\lambda$ ) TSI nephelometer (450-550-700 nm)	continuous (1')	1 (3- $\lambda$ ) TSI nephelometer (450-550-700 nm)	continuous (1')
Absorbing coefficient	1 (7- $\lambda$ ) aethalometer (370-420-490-520-660-880-950 nm)	continuous	1 (7- $\lambda$ ) aethalometer (370-420-490-520-660-880-95 nm)	continuous
Extinction coefficient	1 (1- $\lambda$ ) (860 nm) PAX	continuous (1')		
Column optical properties	1 (9- $\lambda$ ) AERONET/PHOTONS	continuous (15' for AOD)	1 (9- $\lambda$ ) AERONET/PHOTONS	continuous (15' for AOD)
			2 (12-l) MFRSRs	continuous (15 s)
Mineral Aerosol Deposition	1 CARAGA	continuous (7-days)	1 CARAGA	continuous (7-days)
Downward shortwave irradiance	1 pyranometer	continuous (30 s)	1 (CMP 21) pyranometer	continuous (30 s)
Downward longwave irradiance	1 pyrgeometer	continuous (30 s)	1 (CGR4) pyrgeometer	continuous (30 s)
Downward window (8-14 $\mu\text{m}$ ) irradiance			1 modified CG3 pyrgeometer	continuous (60 s)
Direct Solar radiance			1 CHP1 Pyrheliometer	continuous (30 s)
Direct spectral solar radiation			1 PMOD Precision SpectroRad.	Continuous (30 s)
Spectral downward global solar irradiance			1 HyperOCR spectrometer	continuous (30 s)

Spectral downward diffuse solar irradiance	1 HyperOCR spectrometer	continuous (30 s)
Spectral direct solar irradiance	1 spectroradiometer	continuous (60 s)
Downward spectral actinic flux	1 Diode array spectrometer	continuous (60s)

**Table 1.** List of the Instrumentations deployed over the two super-sites (Ersa and Lampedusa) during the SOP-1a experiment for the characterization of physical, chemical and optical properties of aerosols, vertical profiles, columnar-averaged properties and radiation measurements. Meteorological parameters and gases concentrations are not included in this Table.

AERONET/PHOTONS Site Name	Latitude (°N)	Longitude (°E)	Altitude (m)	Site characteristics
Modena	44.63	10.94	56	Urban
Avignon	43.93	4.87	32	Rural
Villefranche-sur-Mer	43.68	7.33	130	Peri-urban coastal
Frioul	43.26	5.29	40	Peri-urban coastal
Toulon	43.13	6.00	50	Urban coastal
Ersa	43.00	9.35	80	Remote island
Rome Tor Vergata	41.84	12.65	130	Peri-urban
Barcelone	41.38	2.17	125	Urban coastal
IMAA-Potenza	40.60	15.72	820	Urban
Lecce University	40.33	18.11	30	Peri-urban coastal
Cap d'en Font	39.82	4.21	10	Remote Island
Oristano	39.91	8.5	10	Peri-urban coastal
Burjassot	39.50	-0.42	30	Urban coastal
Majorque	39.55	2.62	10	Peri-urban coastal
Cagliari	39.28	9.05	3	Urban coastal
Messina	38.20	15.57	15	Urban coastal
Granada	37.16	-3.6	680	Urban
Malaga	36.71	-4.47	40	Peri-urban
Blida	36.50	2.88	230	Rural coastal
Lampedusa	35.51	12.63	45	Remote Island
Oujda	34.65	1.90	620	Urban coastal
Ouarzazate	30.93	6.91	1136	Remote desert

**Table 2.** List of the long-term AERONET/PHOTONS sun-photometer stations operated in the western Mediterranean during the ChArMEx/ADRIMED (SOP-1a) experiment.

Parameter measured	Instrument	Abreviation	Location in the aircraft	Wavelength (nm)	Nominal size range ( $\mu\text{m}$ )
Size distribution	Forward Scattering Spectrometer Probe, Model 300, Particle Measuring Systems	FSSP-300	wing-mounted	632.8	0.28-20
	Ultra High Sensitivity Aerosol Spectrometer, Droplet Measurement Technologies	UHSAS	wing-mounted	1054	0.04-1
	Sky-Optical Particle Counter, Model 1.129, Grimm Technik	GRIMM1	AVIRAD inlet	655	0.25-32
	Optical Particle Counter, Model 1.109, Grimm Technik	GRIMM2	Communautory aerosol inlet	655	0.25-32
	Optical Particle Counter, Model 1.109, Grimm Technik	GRIMM3	Communautory aerosol inlet	655	0.25-32
	Scanning mobility particle sizer, custom-built (Villani et al., 2007)	SMPS	Communautory aerosol inlet	n/a	0.03-0.4
Integrated number concentration	Condensation Particle Counters, Model 3075, TSI	CPC	AVIRAD inlet	n/a	> 0.005
Scattering coefficient	$3\lambda$ Integrated Nephelometer, Model 3563, TSI	Nephelometer	AVIRAD inlet	450, 550, 700	n/a
Absorption coefficient	$3\lambda$ Particle Soot Absorption Photometer, Radiance Research	PSAP	Communautory aerosol inlet	467, 530, 660	n/a
Extinction coefficient	Cavity Attenuated Phase Shift, Aerodyne Research Inc.	CAPS	Communautory Aerosol inlet	530	n/a
	Photomètre Léger Aéroporté pour la Surveillance des Masses d'Air	PLASMA	roof-mounted	340-2250	n/a
Chemical composition	Filter sampling	n/a	AVIRAD inlet	n/a	n/a
	Single particle soot photometer, Droplet Measurement Technologies	SP2	Communautory aerosol inlet	1064	0.08-0.5

**Table 3.** In-situ instrumentation deployed onboard the ATR-42 during the SOP-1a experiment.



No.	Date (2013)	Start time (UTC)	Ceiling altitude (m)	Latitude at ceiling	Longitude at ceiling	Sensors
BLD1	12 June	21:13	21178	39.5156°N	04.3010°E	T, U
BLD2	15 June	21:40	32119	39.9903°N	04.1801°E	T, U, LOAC, O <sub>3</sub>
BLD3	16 June	10:29	31880	40.0527°N	04.1524°E	T, U, LOAC, O <sub>3</sub>
BLD4	16 June	21:13	33390	40.0999°N	04.0118°E	T, U, LOAC, O <sub>3</sub>
BLD5	17 June	10:01	32744	40.2109°N	03.9672°E	T, U, LOAC, O <sub>3</sub>
BLD6	17 June	18:25	33411	40.2502°N	03.9402°E	T, U, LOAC, O <sub>3</sub>
BLD7	18 June	16:34	35635	40.5832°N	04.0515°E	T, U, LOAC
BLD8	18 June	21:17	21507	40.6372°N	04.4889°E	T, U, LOAC, O <sub>3</sub>
BLD9	19 June	10:12	30902	40.6794°N	04.3691°E	T, U, LOAC, O <sub>3</sub>
BLD10	19 June	13:48	36129	40.6553°N	04.1970°E	T,U, LOAC
BLD11	27 June	09:43	35832	39.7546°N	04.4746°E	T,U, LOAC
BLD12	28 June	05:36	36293	39.4505°N	04.1709°E	T,U, LOAC
BLD13	29/30 June	23:31	36310	39.6168°N	03.7383°E	T,U, LOAC
BLD14	30 June	14:03	36319	39.8937°N	03.9568°E	T,U, LOAC
BLD15	02 July	10:27	32833	39.9942°N	04.2996°E	T, U, LOAC, O <sub>3</sub>

**Table 4.** Characteristics of the 15 sounding balloons flights from Sant Lluís, Minorca Island, during the ChArMEx SOP1a/ADRIMED campaign.



Date and time of launch (UT)	Balloon Nbr and type of sensor	Last data time (UT)	Last data location	Trajectory length (km)	Flight duration (h)	Approximate float altitude (m)
16 June, 09:46	B74, LOAC	16 June, 21:51	43.0265°N 05.2285°E	368	11:57	2100
16 June, 09:53	B53, O3	17 June, 00:26	40.6541°N 06.2398°E	203	14:28	3000-3050
16 June, 09:58	B70, LOAC	16 June, 23:01	40.1825°N 06.1293°E	174	13:17	3050-3150
17 June, 09:27	B54, O3	17 June, 16:49	43.1433°N 03.5293°E	371	07:22	1850-2000
17 June, 09:29	B75, LOAC	17 June, 16:51	43.0868°N 03.6866°E	365	07:23	1950-2050
17 June, 11:07	B72, LOAC	17 June, 19:07	43.2333°N 04.7403°E	382	08:03	2750
19 June, 10:34	B77, LOAC	19 June, 17:59	43.1576°N 04.7562°E	387	07:37	2550
19 June, 10:35	B71, LOAC	19 June, 15:03	43.0560°N 05.1336°E	369	04:39	3250-3350
27 June, 10:00	B80, LOAC	28 June, 12:07	37.9165°N 12.1605°E	759	26:19	2950-3050
28 June, 05:20	B73, LOAC	28 June, 17:24	37.4095°N 09.2346°E	523	12:16	2650-2750
02 July, 13:03	B76, LOAC	03 July,, 09:38	37.8897°N 12.1312°E	731	20:39	3150-3250
02 July, 13:11	B57, O3	03 July, 22:43	35.0900°N 14.1140°E	1053	33:44	3100-3200
02 July, 17:59	B55, O3	04 July, 02:20	37.3545°N 12.21980E	762	32.32	2400-2450
02 July, 17:50	B78, LOAC	04 July, 02:13	37.5639°N 12.1507°E	755	32.25	2350-2450

**Table 5.** Characteristics of the 14 BPCL drifting balloon flights.

	Ersa	Ersa corrected	Lampedusa	Cagliari	Cap d'En Font
Number of observations	25		18	20	17
$r_{vf}$ ( $\mu\text{m}$ )	$0.16 \pm 0.02$	#	$0.14 \pm 0.01$	$0.15 \pm 0.03$	$0.17 \pm 0.03$
$\sigma_f$	$0.43 \pm 0.03$	#	$0.50 \pm 0.06$	$0.46 \pm 0.04$	$0.45 \pm 0.04$
$r_{vc}$ ( $\mu\text{m}$ )	$2.49 \pm 0.43$	#	$2.36 \pm 0.48$	$2.52 \pm 0.28$	$2.48 \pm 0.30$
$\sigma_c$	$0.69 \pm 0.03$	#	$0.68 \pm 0.05$	$0.71 \pm 0.04$	$0.71 \pm 0.04$
$C_{vf}$ ( $\mu\text{m}^3/\mu\text{m}^2$ )	$0.02 \pm 0.01$	#	$0.02 \pm 0.01$	$0.02 \pm 0.01$	$0.02 \pm 0.01$
$C_{vc}$ ( $\mu\text{m}^3/\mu\text{m}^2$ )	$0.03 \pm 0.01$	0.04	$0.08 \pm 0.05$	$0.05 \pm 0.03$	$0.04 \pm 0.03$

**Table 6.** Main aerosol volume size distribution characteristics:  $r_{vf}$  ( $\mu\text{m}$ ),  $\sigma_f$ ,  $r_{vc}$  ( $\mu\text{m}$ ),  $\sigma_c$ ,  $C_{vf}$ ,  $C_{vc}$ , for the four different AERONET/PHOTONS stations: Ersa, Lampedusa, Cagliari and Cap d'En Font.  $C_{vi}$  denotes the particle volume concentration,  $r_{vi}$  is the median radius, and  $\sigma_i$  is the standard deviation. Each average value in the table is accompanied by its standard deviation (this is not an accuracy of the retrieval). As mentioned in the text, the concentration of the coarse mode at Ersa has been corrected to be comparable to results at other stations closer to the sea surface, using the logarithmic law proposed by Piazzola et al. (2015).

Models	Time of simulation	Horizontal resolution	Number of vertical layers	Aerosol species	Boundary Layer Forcing	Radiative transfer code
CHIMERE	01/06 - 31/07	50 km	20	Dust, Sea Salt, Secondary organic and inorganic, primary OC-BC	WRF	FastJX
CNRM-RCSM	01/06 - 31/07	50 km	31	Dust, Sea-Salt, Sulphates, primary OC-BC	ERA-Interim	SW: FMR (6 bands, Morcrette et al., 1989) LW: RRTM (Mlawer et al., 1997)
RegCM	13/06 - 05/07	25 km	23	Dust, Sea-Salt, Secondary inorganic, primary OC-BC	NCEP reanalysis	CCM3 or RRTM
COSMO-MUSCAT	15/05-31/07	28 km	40	Dust	GME	Ritter & Geleyn (1992)

**Table 7.** Main characteristics (period of simulations, horizontal resolution, number of vertical layers, main aerosol (primary and/or secondary) species, radiative transfer codes) of the four different 3-D models used during the SOP-1a experiment (see part. 6) (GME is for the global model of the German Weather Service).

## References

- Alados-Arboledas, L., Lyamani, H., Olmo, F.J. Aerosol size properties at Armilla, Granada (Spain), *Quarterly Journal of the Royal Meteorological Society*, 129 (590 PART A), pp. 1395-1413, 2003.
- Alados-Arboledas, L., Alcántara, A., Olmo, F.J., Martínez-Lozano, J.A., Estellés, V., Cachorro, V., Silva, A.M., Horvath, H., Gangl, M., Díaz, A., Pujadas, M., Lorente, J., Labajo, A., Sorribas, M., Pavese, G.: Aerosol columnar properties retrieved from CIMEL radiometers during VELETA 2002, *Atmos. Environ.*, 42, 2654-2667, 2008.
- Alados-Arboledas, L., et al.: Remote-sensing and in-situ characterization of atmospheric aerosol during ChArMEx/ADRIMED over Granada, in prep. for this special issue, 2015.
- Amiridis, V., Zerefos, C., Kazadzis, S., Gerasopoulos, E., Eleftheratos, K., Vrekoussis, M., Stohl, A., Mamouri, R.E., Kokkalis, P., Papayannis, A., Eleftheriadis, K., Diapouli, E., Keramitsoglou, I., Kontoes, C., Kotroni, V., Lagouvardos, K., Marinou, E., Giannakaki, E., Kostopoulou, E., Giannakopoulos, C., Richter, A., Burrows, J.P., Mihalopoulos, N.: Impact of the 2009 Attica wild fires on the air quality in urban Athens, *Atmos. Environ.* 46, 536–544, 2012.
- Ancellet, G., Pelon, J., Totems, J., Chazette, P., Bazureau, A., Sicard, M., Di Iorio, T., Dulac, F., and Mallet, M.: Mixing of aerosol sources during the North American biomass burning episode in summer 2013: analysis of lidar observations in the Mediterranean basin, *Atmos. Chem. Phys. Discuss.*, submitted to this special issue, 2015.
- Antón, M., Valenzuela, A., Mateos, D., Alados, I., Foyo-Moreno, I., Olmo, F. J., Alados-Arboledas, L.: Longwave aerosol radiative effects during an extreme desert dust event in southeastern Spain, *Atmos. Res.*, 148, 18-23, 2014.
- Baldassarre, G., Pozzoli, L., Schmidt, C. C., Unal, A., Kindap, T., Menzel, W. P., Whitburn, S., Coheur, P.-F., Kavgaci, A., and Kaiser, J. W.: Using SEVIRI fire observations to drive smoke plumes in the CMAQ air quality model: a case study over Antalya in 2008, *Atmos. Chem. Phys.*, 15, 8539-8558, doi:10.5194/acp-15-8539-2015, 2015.
- Balis, D.S., Amiridis, V., Nickovic, S., Papayannis, A., and Zerefos, C.: Optical properties of Saharan dust layers as detected by a Raman lidar at Thessaloniki, Greece, *Geophys. Res. Lett.*, 31, L13104, doi:10.1029/2004GL019881, 2004.
- Balis, D., Amiridis, V., Kazadzis, S., Papayannis, A., Tsaknakis, G., Tzortzakis, S., Kalivitis, N., Vrekoussis, M., Kanakidou, M., Mihalopoulos, N., Chourdakis, G., Nickovic, S., Pérez, C., Baldasano, J., and Drakakis, M.: Optical characteristics of desert dust over the East Mediterranean during summer: a case study, *Ann. Geophys.*, 24, 807-821, 2006.
- Barnaba, F., Angelini, F., Curci, G., and Gobbi, G. P.: An important fingerprint of wildfires on the European aerosol load, *Atmos. Chem. Phys.*, 11, 10487-10501, doi:10.5194/acp-11-10487-2011, 2011.
- Barragan, R., Sicard, M., Totems, J., Léon, J.-F., Renard, J.-B., Dulac, F., Mallet, M., Pelon, J., Alados-Arboledas, L., Amodeo, A., Augustin, P., Boselli, A., Bravo-Aranda, J. A., Burlizzi, P., Chazette, P., Comerón, A., D'Amico, G., Granados-Muñoz, M. J., Leto, G., Guerrero-Rascado, J. L., Madonna, F., Mona, L., Muñoz-Porcar, C., Pappalardo, G., Perrone, M. R., Pont, V., Rocadenbosch, F., Rodriguez, A., Scollo, S., Spinelli, N., Titos, G., Wang, X., and Zanmar Sanchez, R.: Characterization of aerosol transport and ageing during a multi-intrusion Saharan dust event over the western and central Mediterranean Basin in June 2013 in the framework of the ADRIMED/ChArMEx campaign, *Atmos. Chem. Phys.*, in prep. for this special issue, 2015.
- Berthier, S., Chazette, P., Couvert, P., Pelon, J., Dulac, F., Thieuleux, F., Moulin, C., and Pain, T.: Desert dust aerosol columnar properties over ocean and continental Africa from Lidar in-Space Technology Experiment (LITE) and Meteosat synergy, *J. Geophys. Res.*, 111, D21202, doi:10.1029/2005JD006999, 2006.
- Bessagnet, B., Hodzic, A., Vautard, R., Beekmann, M., Cheinet, S., Honoré, C., Liousse, C., and Rouil, L.: Aerosol modeling with CHIMERE: preliminary evaluation at the continental scale, *Atmos. Environ.*, 38, 2803–2817, 2004.
- Beuvier, J., Sevault, F., Herrmann, M., Kontoyiannis, H., Ludwig, W., Rixen, M., Stanev, E., Béranger, K., and Somot, S.: Modeling the Mediterranean Sea interannual variability during 1961–2000: Focus on the Eastern Mediterranean Transient, *J. Geophys. Res.*, 115, C08017, doi:10.1029/2009JC005950, 2010.
- Brauch, H.G.: Urbanization and natural disasters in the Mediterranean: Population growth and climate change in the 21<sup>st</sup> century, in *Building Safer Cities – The Future of Disaster Risk*, Edited by Kreimer, A., Arnold, M., and Carlin, A., The World Bank, Disaster Risk Management Series No.3, 149-164, 2003.
- Cachier, H., Aulagnier, F., Sarda, R., Gautier, F., Masplet, P., Besombes, J.L., Marchand, N., Despiiau, S., Croci, D., Mallet, M., Laj, P., Marinoni, A., Deveau, P.A., Roger, J.C., Putaud, J.P., Van Dingenen, R., Dell'Acqua, A., Viidanoja, J., Martins-Dos Santos, S., Liousse, C., Cousin, F., and Rosset, R.: Aerosol studies during the ESCOMPTE Experiment: an overview, *Atmos. Res.*, 74, 547-563, doi:10.1016/j.atmosres.2004.06.013, 2005.

- Cachorro, V. E., Toledano, C., Prats, N., Sorribas, M., Mogo, S., Berjon, A., Torres, B., Rodrigo, R., J. de la Rosa, and De Frutos, A.M.: The strongest desert dust intrusion mixed with smoke over the Iberian Peninsula registered with Sun photometry, *J. Geophys. Res.*, **113**, D14S04, doi:10.1029/2007JD009582, 2008.
- Casasanta, G., di Sarra, A., Meloni, D., Monteleone, F., Pace, G., Piacentino, S., and Sferlazzo, D.: Large aerosol effects on ozone photolysis in the Mediterranean, *Atmos. Environ.*, **45**, 3937-3943, doi:10.1016/j.atmosenv.2011.04.065, 2011.
- Chazette, P., and Lioussé, C.: A case study of optical and chemical ground apportionment for urban aerosols in Thessaloniki, *Atmos. Environ.*, **35**, 2497-2506, doi:10.1016/S1352-2310(00)00425-8, 2001.
- Chazette, P., Marnas, F., and Totems, J.: The mobile Water vapor Aerosol Raman Lidar and its implication in the framework of the HyMeX and ChArMEx programs: application to a dust transport process, *Atmos. Meas. Tech.*, **7**, 1629-1647, doi:10.5194/amt-7-1629-2014, doi:10.5194/amt-7-1629-2014, 2014a.
- Chazette, P., Marnas, F., Totems, J., and X. Shang, J.: Comparison of IASI water vapor retrieval with H<sub>2</sub>O-Raman lidar in the framework of the Mediterranean HyMeX and ChArMEx programs, *Atmos. Chem. Phys.*, **14**, 9583-9596, doi:10.5194/acp-14-9583-2014, doi:10.5194/acp-14-9583-2014, 2014b.
- Chazette, P., Totems, J., Ancellet, G., Pelon, J., and Sicard, M.: Temporal consistency of lidar observables during aerosol transport events in the framework of the ChArMEx/ADRIMED campaign at Menorca Island in June 2013, *Atmos. Chem. Phys. Discuss.*, submitted to this special issue, 2015.
- Chenoweth J., Hadjinicolaou, P., Bruggeman, A., Lelieveld, J., Levin, Z., Lange, M. A., Xoplaki, E., and Hadzikakou, M.: Impact of climate change on the water resources of the eastern Mediterranean and middle east region: modeled 21st century, *Water Resour. Res.*, **47**, W06506, doi:10.1029/2010WR010269, 2011.
- Ciardini, V., Di Iorio, T., Di Liberto, L., Tirelli, C., Casasanta, G., di Sarra, A., Fiocco, G., Fuà, D., and Cacciani, M.: Seasonal variability of tropospheric aerosols in Rome, *Atmos. Res.*, **118**, 205-214, doi:10.1016/j.atmosres.2012.06.026, 2012.
- Claeys, M., Roberts, G., Mallet, M., Sciare, J., Sellegri, K., Sauvage, B., Tulet, P., Arndt, J.: Characterisation of a sea salt episode during ADRIMED campaign: ageing, transport and size distribution study, in prep. for this special issue, 2015.
- Collaud Coen, M., Weingartner, E., Schaub, D., Hueglin, C., Corrigan, C., Henning, S., Schwikowski, M., and Baltensperger, U.: Saharan dust events at the Jungfraujoch: detection by wavelength dependence of the single scattering albedo and first climatology analysis, *Atmos. Chem. Phys.*, **4**, 2465-2480, 2004.
- Denjean, C., Chevaillier, S., Triquet, S., Grand, N., Cassola, F., Mazzino, A., Bourriane, T., Momboisse, G., Dupuy, R., Sellegri, K., Schwarzenbock, A., Mallet, M., and Formenti, P.: Size distribution and optical properties of mineral dust aerosols transported in the West Mediterranean, *Atmos. Chem. Phys. Discuss.*, **15**, 21607-21669, 2015.
- Déqué, M. and Somot, S.: Extreme precipitation and high resolution with Aladin, *Idöjaras Quaterly Journal of the Hungarian Meteorological Service*, **112**, 179-190, 2008.
- Derimian, Y., Karnieli, A., Kaufman, Y. J., Andreae, M. O., Andreae, T. W., Dubovik, O., Maenhaut, W., Koren, I., and Holben, B. N.: Dust and pollution aerosols over the Negev desert, Israel: Properties, transport, and radiative effect, *J. Geophys. Res.*, **111**, D05205, doi:10.1029/2005JD006549, 2006.
- Deschamps, P.-Y., Bréon, F.-M., Leroy, M., Podaire, A., Bricaud, A., Buriez, J.C., and Sèze, G.: The POLDER mission: Instrument characteristics and scientific objectives, *IEEE Trans. Geosci. Remote Sens.*, **32**, 598-615, 1994.
- Di Biagio, C., di Sarra, A., Meloni, D., Monteleone, F., Piacentino, S., and Sferlazzo, D.: Measurements of Mediterranean aerosol radiative forcing and influence of the single scattering albedo, *J. Geophys. Res.*, **114**, D06211, doi:10.1029/2008JD011037, 2009.
- Di Biagio, C., di Sarra, A., and D. Meloni, D.: Large atmospheric shortwave radiative forcing by Mediterranean aerosol derived from simultaneous ground-based and spaceborne observations, and dependence on the aerosol type and single scattering albedo, *J. Geophys. Res.*, **115**, D10209, doi:10.1029/2009JD012697, 2010.
- Di Iorio, T., Di Sarra, A., Junkermann, W., Cacciani, M., Fiocco, G., and Fuà, D.: Tropospheric aerosols in the Mediterranean: 1. Microphysical and optical properties, *J. Geophys. Res.*, **108**, 4316, doi:10.1029/2002JD002815, 2003.
- Di Iorio, T., di Sarra, A., Sferlazzo, D. M., Cacciani, M., Meloni, D., Monteleone, F., Fuà, D., and Fiocco, G.: Seasonal evolution of the tropospheric aerosol vertical profile in the central Mediterranean and role of desert dust, *J. Geophys. Res.*, **114**, D02201, doi:10.1029/2008JD010593, 2009.
- Di Iorio, T., Di Biagio, C., di Sarra, A., Formenti, P., Gomez Amo, J.-L., Meloni, D., and Pace, G.: Height resolved aerosol optical properties at Lampedusa during ADRIMED, in prep. for this special issue, 2015.
- di Sarra, A., Pace, G., Meloni, D., De Silvestri, L., Piacentino, S., and Monteleone, F.: Surface shortwave radiative forcing of different aerosol types in the central Mediterranean, *Geophys. Res. Lett.*, **35**, L02714,

- doi:10.1029/2007GL032395, 2008.
- di Sarra, A., Di Biagio, C., Meloni, D., Monteleone, F., Pace, G., Pugnaghi, S., and Sferlazzo, D.: Shortwave and longwave radiative effects of the intense Saharan dust event of 25-26 March 2010 at Lampedusa (Mediterranean Sea), *J. Geophys. Res.*, 116, D23209, doi:10.1029/2011JD016238, 2011.
- di Sarra, A., Sferlazzo, D., Meloni, D., Anello, F., Bommarito, C., Corradini, S., De Silvestri, L., Di Iorio, T., Monteleone, F., Pace, G., Piacentino, S., and Pugnaghi, S.: Empirical correction of multi filter rotating shadowband radiometer (MFRSR) aerosol optical depths for the aerosol forward scattering and development of a long-term integrated MFRSR-Cimel dataset at Lampedusa, *Appl. Opt.*, 54, 2725-2737, doi:10.1364/AO.54.002725, 2015.
- Dubovik, O., and King, M. D.: A flexible inversion algorithm for retrieval of aerosol optical properties from Sun and sky radiance measurements, *J. Geophys. Res.*, 105, 20673–20696, doi:10.1029/2000JD900282, 2000.
- Dubovik, O., Smirnov, A., Holben, B. N., King, M. D., Kaufman, Y. J., Eck, T. F., and Slutsker, I.: Accuracy assessment of aerosol optical properties retrieval from AERONET Sun and sky radiance measurements, *J. Geophys. Res.*, 105, 9791–9806, doi:10.1029/2000JD900040, 2000.
- Dubovik, O., Holben, B., Eck, T.F., Smirnov, A., Kaufman, Y.J., King, M.D., Tanré, D., and Slutsker, I.: Variability of absorption and optical properties of key aerosol types observed in worldwide locations, *J. Atmos. Sci.*, 59, 590–608, doi:http://dx.doi.org/10.1175/1520-0469(2002)059<0590:VOAAOP>2.0.CO;2, 2002.
- Dubovik, O., Sinyuk, A., Lapyonok, T., Holben, B. N., Mishchenko, M., Yang, P., Eck, T. F., Volten, H., Muñoz, O., Veihelmann, B., van der Zande, W. J., Léon, J.-F., Sorokin, M., and Slutsker, I.: Application of spheroid models to account for aerosol particle nonsphericity in remote sensing of desert dust, *J. Geophys. Res.*, 111, D11208, doi:10.1029/2005JD006619, 2006.
- Dubovik, O., Herman, M., Holdak, A., Lapyonok, T., Tanré, D., Deuzé, J. L., Ducos, F., Sinyuk, A., and Lopatin, A.: Statistically optimized inversion algorithm for enhanced retrieval of aerosol properties from spectral multi-angle polarimetric satellite observations, *Atmos. Meas. Tech.*, 4, 975-1018, doi:10.5194/amt-4-975-2011, 2011.
- Dubuisson, P., Dessailly, D., Vesperini, M., and Frouin, R.: Water vapor retrieval over ocean using near-infrared radiometry, *J. Geophys. Res.*, 109, D19106, doi:10.1029/2004JD004516, 2004.
- Ducrocq, V., Braud, I., Davolio, S., Ferretti, R., Flamant, C., Jansa, A., Kalthoff, N., Richard, E., Taupier-Letage, I., Ayrat, P.A., Belamari, S., Berne, A., Borga, M., Boudevillain, B., Bock, O., Boichard, J.L., Bouin, M.N., Bousquet, O., Bouvier, C., Chiggiato, J., Cimini, D., Corsmeier, U., Coppola, L., Cocquerez, P., Defer, E., Delanoë, J., Delrieu, G., Di Girolamo, P., Doerenbecher, A., Drobinski, P., Dufournet, Y., Fourrié, N., Gourley, J.J., Labatut, L., Lambert, D., Le Coz, J., Marzano, F.S., Montani, A., Nuret, M., Ramage, K., Rison, B., Rousset, O., Saïd, F., Schwarzenboeck, A., Testor, P., Van Baelen, J., Vincendon, B., Aran, M., and Tamayo J.: HyMeX-SOP1, the Field Campaign Dedicated to Heavy Precipitation and Flash-Flooding in Northwestern Mediterranean. *Bull. Amer. Meteorol. Soc.*, 95, 1083-1100, doi: 10.1175/BAMS-D-12-00244.1 and doi: 10.1175/BAMS-D-12-00244.2, 2014.
- Dulac, F., and Chazette, P.: Airborne study of a multi-layer aerosol structure in the eastern Mediterranean observed with the airborne polarized lidar ALEX during a STAAARTE campaign (7 June 1997), *Atmos. Chem. Phys.*, 3, 1817-1831, 2003.
- Eleftheriadis, K., Colbeck, I., Housiada, C., Lazaridis, M., Mihalopoulos, N., Mitsakou, C., Smolik, J., and Zdimas, V.: Size distribution, composition and origin of the submicron aerosol in the marine boundary layer during the eastern Mediterranean “SUB-AERO” experiment, *Atmos. Environ.*, 40, 6245–6260, 2006.
- Foltz, G.R., and McPhaden, M.J., Impact of Saharan dust on tropical North Atlantic SST, *J. Climate*, 21, 5048-5060, doi: http://dx.doi.org/10.1175/2008JCLI2232.1, 2008.
- Formenti, P., Boucher, O., Reiner, T., Sprung, D., Andreae, M. O., Wendisch, M., Wex, H., Kindred, D., Tzortziou, M., Vasaras, A., and Zerefos, C.: STAAARTE-MED 1998 summer airborne measurements over the Aegean Sea, 2. Aerosol scattering and absorption, and radiative calculations, *J. Geophys. Res.* 107, 4451, doi:10.1029/2001JD001536, 2002.
- Formenti, P., et al.: Characterisation of aerosols in a remote marine atmosphere in the West Mediterranean, *Atmos. Chem. Phys. Discuss.*, in prep. for this special issue, 2015.
- Fotiadi, A., Hatzianastassiou, N., Drakakis, E., Matsoukas, C., Pavlakis, K.G., Hatzidimitriou, D., Gerasopoulos, E., Mihalopoulos, N., and Vardavas, I.: Aerosol physical and optical properties in the Eastern Mediterranean Basin, Crete, from Aerosol Robotic Network data, *Atmos. Chem. Phys.*, 6, 5399–5413, doi:10.5194/acp-6-5399-2006, 2006.
- Gangoiti, G., Millán, M., Salvador, R., and Mantilla, E.: Long-range transport and re-circulation of pollutants in the western Mediterranean during the project Regional Cycles of Air Pollution in the West-Central Mediterranean Area, *Atmos. Environ.*, 35, 6267-6276, doi:10.1016/S1352-2310(01)00440-X, 2001.
- Garcia, O. E., Diaz, J. P., Exposito, F. J., Diaz, A. M., Dubovik, O., Derimian, Y., Dubuisson, P., and Roger, J.-C.:

- Shortwave Radiative Forcing and Efficiency of Key Aerosol Types using AERONET Data, *Atmos. Chem. Phys.*, 12, 5129-5145, doi:10.5194/acp-12-5129-2012, 2012.
- García-Ruiz, J. M., López-Moreno, J. I., Vicente-Serrano, S. M., Lasanta-Martínez, T., and Beguería, S.: Mediterranean water resources in a global change scenario, *Earth-Sci. Rev.*, 105, 121-139, doi:10.1016/j.earscirev.2011.01.006, 2011.
- Gard, E., Mayer, J. E., Morrical, B. D., Dienes, T., Fergenson, D. P., and Prather, K.A.: Real-time analysis of individual atmospheric aerosol particles: Design and performance of a portable ATOFMS, *Anal. Chem.*, 69, 4083-4091, doi:10.1021/ac970540n, 1997.
- Gerasopoulos, E., Andreae, M.O., Zerefos, C.S., Andreae, T.W., Balis, D., Formenti, P., Merlet, P., Amiridis, V., and Papastefanou, C.: Climatological aspects of aerosol optical properties in Northern Greece, *Atmos. Chem. Phys.*, 3, 2025-2041, doi:10.5194/acp-3-2025-2003/, 2003.
- Gheusi, F., Durand, P., Verdier, N., Dulac, F., Attié, J.-L., Commun, P., Barret, B., Basdevant, C., Clenet, A., Derrien, S., Doerenbecher, El Amraoui, L., Fontaine, A., Hache, E., Lambert C., Jaumouillé, E., Meyerfeld, Y., Roblou, L., and Tocquer, F.: Adapted ECC ozone sonde for long-duration flights aboard boundary-layer pressurized balloons, *Atmos. Meas. Tech.*, in prep. for this special issue, 2015.
- Gimeno, L., Drumond, A., Nieto, R., Trigo, R. M., and Stohl, A.: On the origin of continental precipitation, *Geophys. Res. Lett.*, 37, L13804, doi:10.1029/2010GL043712, 2010.
- Giorgi, F., and Lionello, P.: Climate change projections for the Mediterranean region, *Global Planet. Change*, 63, 90-104, doi:10.1016/j.gloplacha.2007.09.005, 2008.
- Giorgi, F., Coppola, E., Solmon, F., Mariotti, L., Sylla, M. B., Bi, X., Elguindi, N., Diro, G.T., Nair, V., Giuliani, G., Turuncoglu, U. U., Cozzini, S., Guttler, I., O'Brien, T. A., Tawfik, A. B., Shalaby, A., Zakey, A. S., Steiner, A. L., Stordal, F., Sloan, L. C., and Brankovic, C.: RegCM4: Model description and preliminary tests over multiple CORDEX domains, *Clim. Res.*, 52, 7-29, doi: 10.3354/cr01018, 2012.
- Gobbi, G.P., Barnaba, F., Giorgi, R., and Santacasa, A.: Altitude-resolved properties of a Saharan dust event over the Mediterranean, *Atmos. Environ.*, 34, 5119-5127, 2000.
- Gross, D. S., Atlas, R., Rzeszutarski, J., Turetsky, E., Christensen, J., Benzaid, S., Olson, J., Smith, T., Steinberg, L. and Sulman, J.: Environmental chemistry through intelligent atmospheric data analysis, *Environ. Model. Software*, 25, 760-769, doi: 10.1016/j.envsoft.2009.12.001, 2010.
- Guenther, A., Karl, T., Harley, P., Wiedinmyer, C., Palmer, P. I., and Geron, C.: Estimates of global terrestrial isoprene emissions using MEGAN (Model of Emissions of Gases and Aerosols from Nature), *Atmos. Chem. Phys.*, 6, 3181-3210, doi:10.5194/acp-6-3181-2006, 2006.
- Guerrero-Rascado, J. L., Olmo, F. J., Avilés-Rodríguez, I., Navas-Guzmán, F., Pérez-Ramírez, D., Lyamani, H., Arboledas, L.A.: Extreme saharan dust event over the southern iberian peninsula in september 2007: Active and passive remote sensing from surface and satellite, *Atmos. Chem. and Phys.*, 9 (21), 8453-8469, 2009.
- Hamonou, E., Chazette, P., Balis, D., Dulac, F., Schneider, X., Galani, E., Ancellet, G., and Papayannis, A.: Characterization of the vertical structure of Saharan dust export to the Mediterranean basin, *J. Geophys. Res.*, 104, 22257-22270, 1999.
- Hashimoto, M., Nakajima, T., Dubovik, O., Campanelli, M., Che, H., Khatri, P., Takamura, T., and Pandithurai, G.: Development of a new data-processing method for SKYNET sky radiometer observations, *Atmos. Meas. Tech.*, 5, 2723-2737, doi:10.5194/amt-5-2723-2012, 2012.
- Harris, I, Jones, P., Osborn, T., Lister, D.: Updated high-resolution grids of monthly climatic observations—the cru ts3.10 dataset. *Int J Climatol* 34:623-642. doi:10.1002/joc.3711, 2013.
- Hatzianastassiou, N., Gkikas, A., Mihalopoulos, N., Torres, O., and Katsoulis, B. D.: Natural versus anthropogenic aerosols in the eastern Mediterranean basin derived from multiyear TOMS and MODIS satellite data, *J. Geophys. Res.*, 114, D24202, doi:10.1029/2009JD011982, 2009.
- Healy, R. M., Hellebust, S., Kourtchev, I., Allanic, A., O'Connor, I. P., Bell, J. M., Sodeau, J. R., Wenger, J. C., Healy, D. A., Sodeau, J. R., and Wenger, J. C.: Source apportionment of PM<sub>2.5</sub> in Cork Harbour, Ireland using a combination of single particle mass spectrometry and quantitative semi-continuous measurements, *Atmos. Chem. Phys.*, 10, 9593-9613. doi:10.5194/acpd-10-1035-2010, 2010.
- Holben B.N., Eck, T.F., Slutsker, I., Tanré, D., Buis, J.P., Setzer, A., Vermote, E., Reagan, J.A., Kaufman, Y.J., Nakajima, T., Lavenu, F., Jankowiak, I., and Smirnov, A.: AERONET - A federated instrument network and data archive for aerosol characterization, *Rem. Sens. Environ.*, 66, 1-16, doi:10.1016/S0034-4257(98)00031-5, 1998.
- Horvath, H., Alados Arboledas, L., Olmo, F.J., Jovanovic, O., Gangl, M., Sanchez, C., Sauerzopf, H., and Seidl, S.: Optical characteristics of the aerosol in Spain and Austria and its effect on radiative forcing, *J. Geophys. Res.*, 107, 4386, doi:10.1029/2001JD001472, 2002.
- Johnson, G., Ristovski, Z., and Morawska, L.: Application of the VH-TDMA technique to coastal ambient aerosols, *Geophys. Res. Lett.*, 31, L16105, doi:10.1029/2004GL020126, 2004.



- Kahn, R. A., Gaitley, B. J., Garay, M. J., Diner, D. J., Eck, T. F., Smirnov, A., and Holben, B. N.: Multiangle Imaging SpectroRadiometer global aerosol product assessment by comparison with the Aerosol Robotic Network, *J. Geophys. Res.*, **115**, D23209, doi:10.1029/2010JD014601, 2010.
- Kalnay et al.: The NCEP/NCAR 40-year reanalysis project, *Bull. Amer. Meteor. Soc.*, **77**, 437-470, 1996.
- Karol, Y., Tanré, D., Goloub, P., Ververde, C., Balois, J. Y., Blarel, L., Podvin, T., Mortier, A., and Chaikovsky, A.: Airborne sun photometer PLASMA: concept, measurements, comparison of aerosol extinction vertical profile with lidar, *Atmos. Meas. Tech.*, **6**, 2383-2389, 2013.
- Kaskaoutis, D. G., Kharol, S. K., Sifakis, N., Nastos, P. T., Sharma, A. R., Badarinath, K. V. S., and Kambezidis, H. D.: Satellite monitoring of the biomass-burning aerosols during the wildfires of August 2007 in Greece: Climate implications, *Atmos. Environ.*, **45**, 716–726, doi:10.1016/j.atmosenv.2010.09.043, 2011.
- Kok, J. F.: A scaling theory for the size distribution of emitted dust aerosols suggests climate models underestimate the size of the global dust cycle, *P. Natl. Acad. Sci. USA*, **108**, 1016–1021, doi:10.1073/pnas.1014798108, 2011.
- Kubilay, N., Cokacar, T., and Oguz, T.: Optical properties of mineral dust outbreaks over the northeastern Mediterranean, *J. Geophys. Res.*, **108**, 4666, doi:10.1029/2003JD003798, 2003.
- Kumar, D., Rocadenbosch, F., Sicard, M., Comeron, A., Muñoz, C., Lange, D., Tomás, S., and Gregorio, E.: Six-channel polychromator design and implementation for the UPC elastic/Raman LIDAR, in: SPIE Remote Sens., Int. Soc. Opt. Photon., Prague, Czech Republic, 81820W–81820W, 2011.
- Lelieveld, J., Berresheim, H., Borrmann, S., Crutzen, P. J., Dentener, F. J., Fischer, H., Feichter, J., Flatau, P. J., Heland, J., Holzinger, R., Kormann, R., Lawrence, M. G., Levin, Z., Markowicz, K. M., Mihalopoulos, N., Minikin, A., Ramanathan, V., de Reus, M., Roelofs, G. J., Scheeren, H. A., Sciare, J., Schlager, H., Schultz, M., Siegmund, P., Steil, B., Stephanou, E. G., Stier, P., Traub, M., Warneke, C., Williams, J., Ziereis, H.: Global air pollution crossroads over the Mediterranean, *Science*, **298**, 794–799, doi:10.1126/science.1075457, 2002.
- Léon, J.F., Augustin, P., Mallet, M., Bourriane, T., Pont, V., Dulac, F., Fourmentin, M., and Lambert, D.: Aerosol vertical distribution, optical properties, and transport over Corsica (western Mediterranean), *Atmos. Chem. Phys. Discuss.*, **15**, 9507-9540, 2015.
- Lionello, P., Malanotte-Rizzoli, P., Boscolo, R., Alpert, P., Artale, V., Li, L., Luterbacher, J., May, W., Trigo, R., Tsimplis, M., Ulbrich, U., and Xoplaki, E.: The Mediterranean climate: An overview of the main characteristics and issues, in *The Mediterranean Climate Variability*, P. Lionello, P. Malanotte-Rizzoli and R. Boscolo Eds., *Developments in Earth and Environmental Sciences*, **4**, Elsevier, 1-26, 2006.
- Liu, Y., Kahn, R. A., Chaloulakou, A., and Koutrakis, P.: Analysis of the impact of the forest fires in August 2007 on air quality of Athens using multi-sensor aerosol remote sensing data, meteorology and surface observations, *Atmospheric Environment*, **43**, 3310–3318, 2009.
- Lyamani, H., Valenzuela, A., Perez-Ramirez, D., Toledano, C., Granados-Muñoz, M.J., Olmo, F.J., Alados-Arboledas, L., Aerosol properties over the western Mediterranean basin: Temporal and spatial variability, *Atmos. Chem. and Phys.*, **15** (5), 2473-2486, 2015.
- Mailler, S., Menut, L., Di Sarra, A.G., Becagli, S., Di Iorio, T., Formenti, P., Bessagnet, B., Briant, R., Gómez-Amo, J.L., Mallet, M., Rea, G., Siour, G., Sferlazzo, D.M., Traversi, R., Udisti, R., and Turquety, S.: On the radiative impact of aerosols on photolysis rates: comparison of simulations and observations in the Lampedusa island during the ChArMEx/ADRIMED campaign, *Atmos. Chem. Phys. Discuss.*, **15**, 7585-7643, doi:10.5194/acpd-15-7585-2015, 2015.
- Mallet, M., Roger, J.C., Despiau, S., Dubovik, O., and Putaud, J.P.: Microphysical and optical properties of aerosol particles in urban zone during ESCOMPTE, *Atmos. Res.*, **69**, 73-97, doi:10.1016/j.atmosres.2003.07.001, 2003.
- Mallet, M., Roger, J.C., Despiau, S., Putaud, J.P., and Dubovik, O.: A study of the mixing state of black carbon in urban zone, *J. Geophys. Res.*, **109**, D04202, doi:10.1029/2003JD003940, 2004.
- Mallet, M., Van Dingenen, R., Roger, J. C., Despiau, S., and Cachier, H.: In situ airborne measurements of aerosol optical properties during photochemical pollution events. *J. Geophys. Res.*, **110**, D03205, doi:10.1029/2004JD005139, 2005.
- Mallet, M., Pont, V., Lioussé, C., Roger, J.C., and Dubuisson, P.: Simulation of aerosol radiative properties with the ORISAM-RAD model during a pollution event (ESCOMPTE 2001), *Atmos. Environ.*, **40**, 7696–7705, doi:10.1016/j.atmosenv.2006.08.031, 2006.
- Mallet, M., Gomes, L., Solmon, F., Sellegri, K., Pont, V., Roger, J.C., Missamou, T., and Piazzola, J.: Calculations of key optical properties over the main anthropogenic aerosols over the Western French coastal Mediterranean Sea, *Atmos. Res.*, Vol. 101, doi:10.1016/j.atmosres.2011.03.008, 396-411, 2011.
- Mallet, M., Dubovik, O., Nabat, P., Dulac, F., Kahn, R., Sciare, J., Paronis, D., and Léon, J.F.: Absorption



- properties of Mediterranean aerosols obtained from multi-year ground-based remote sensing observations, *Atmos. Chem. Phys.*, 13, 9195-9210, 2013.
- Markowicz, K. M., Flatau, P. J., Ramana, M. V., Crutzen, P. J., and Ramanathan, V.: Absorbing Mediterranean aerosols lead to a large reduction in the solar radiation at the surface, *Geophys. Res. Lett.*, 29, 1968, doi:10.1029/2002GL015767, 2002.
- Mariotti, A., Zeng, N., Yoon, J., Artale, V., Navarra, A., Alpert, P., and Li, L.Z.X.: Mediterranean water cycle changes: transition to drier 21st century conditions in observations and CMIP3 simulations, *Environ. Res. Lett.*, 3, 044001, doi:10.1088/1748-9326/3/4/044001, 2008.
- Mariotti A., Pan, Y., Zeng, N., and Alessandri, A.: Long-term climate change in the Mediterranean region in the midst of decadal variability, *Clim. Dyn.*, 44, 1437-1456, doi:10.1007/s00382-015-2487-3, 2015.
- Martcorena, B. and Bergametti, G.: Modeling the atmospheric dust cycle 1. Design of a soil-derived dust production scheme, *J. Geophys. Res.*, 100, 16415–16430, 1995.
- McConnell, C. L., Formenti, P., Highwood, E. J., and Harrison, M. A. J.: Using aircraft measurements to determine the refractive index of Saharan dust during the DODO Experiments, *Atmos. Chem. Phys.*, 10, 3081–3098, doi:10.5194/acp-10-3081-2010, 2010.
- Meloni D., Di Sarra, A., DeLuisi, J., Di Iorio, T., Fiocco, G., Junkermann, W., and Pace, G.: Tropospheric aerosols in the Mediterranean: 2. Radiative effects through model simulations and measurements, *J. Geophys. Res.*, 108, 4317, doi:10.1029/2002JD002807, 2003.
- Meloni, D., Di Sarra, A., Di Iorio, T., and Fiocco, G.: Direct radiative forcing of Saharan dust in the Mediterranean from measurements at Lampedusa Island and MISR space-borne observations, *J. Geophys. Res.*, 109, D08206, doi:10.1029/2003JD003960, 2004.
- Meloni, D., Di Sarra, A., Pace, G., and Monteleone, F.: Aerosol optical properties at Lampedusa (Central Mediterranean). 2. Determination of single scattering albedo at two wavelengths for different aerosol types, *Atmos. Chem. Phys.*, 6, 715-727, 2006.
- Meloni, D., Di Sarra, A., Monteleone, F., Pace, G., Piacentini, S., and Sferlazzo, D.M.: Seasonal transport patterns of intense dust events at the Mediterranean island of Lampedusa, *Atmos. Res.*, 88, 134-148, doi:10.1016/j.atmosres.2007.10.007, 2008.
- Meloni, D., Junkermann, W., di Sarra, A., Cacciani, M., De Silvestri, L., Di Iorio, T., Estellés, V., Gómez-Amo, J.L., Pace, G., and Sferlazzo, D.M.: Altitude-resolved shortwave and longwave radiative effects of desert dust in the Mediterranean during the GAMARF campaign: indications of a net daily cooling in the dust layer, *J. Geophys. Res. Atmos.*, 120, doi:10.1002/2014JD022312, 2015.
- Meloni, M., di Sarra, A., Brogniez, G., Denjean, C., De Silvestri, L., Di Iorio, T., Formenti, P., Gomez-Amo, J.-L., Gröbner, J., Kouremeti, N., Mallet, M. and Pace, G.: Simulating vertically resolved SW and LW irradiances and infrared brightness temperatures measured at Lampedusa during the Charmex/ADRIMED campaign, in prep. for this special issue, 2015.
- Menut, L., Bessagnet, B., Khvorostyanov, D., Beekmann, M., Blond, N., Colette, A., Coll, I., Curci, G., Foret, G., Hodzic, A., Mailler, S., Meleux, F., Monge, J.-L., Pison, I., Siour, G., Turquety, S., Valari, M., Vautard, R., and Vivanco, M. G.: CHIMERE 2013: a model for regional atmospheric composition modelling, *Geosci. Model Dev.*, 6, 981-1028, doi: 10.5194/gmd-6-981-2013, 2013.
- Menut, L., Mailler, S., Siour, G., Bessagnet, B., Turquety, S., Rea, G., Briant, R., Mallet, M., Sciare, J., and Formenti, P.: Ozone and aerosols tropospheric concentrations variability analyzed using the ADRIMED measurements and the WRF-CHIMERE models, *Atmos. Chem. Phys. Discuss.*, 15, 3063–3125, doi: 10.5194/acpd-15-3063-20, 2015.
- Millán, M.M., Salvador, R., Mantilla, E., and Kallos, G.: Photooxidant dynamics in the Mediterranean basin in summer: Results from European research projects, *J. Geophys. Res.*, 102, 8811-8823, doi:10.1029/96JD03610, 1997.
- Moosmüller, H., Chakrabarty, R. K., and Arnott, W. P.: Aerosol light absorption and its measurement: A review, *Journal of Quantitative Spectroscopy & radiative transfer*, 100, 844-878, 2009.
- Mulcahy, J. P., O'Dowd, C. D., Jennings, S. G., and Ceburnis, D.: Significant enhancement of aerosol optical depth in marine air under high wind conditions, *Geophys. Res. Letters*, Vol. 35, L16810, doi:10.1029/2008GL034303, 2008.
- Nabat, P., Solmon, F., Mallet, M., Kok, J. F., and Somot, S.: Dust emission size distribution impact on aerosol budget and radiative forcing over the Mediterranean region: a regional climate model approach, *Atmos. Chem. Phys.*, 12, 10545-10567, doi:10.5194/acp-12-10545-2012, 2012.
- Nabat, P., Somot, S., Mallet, M., Chiapello, I., Morcrette, J. J., Solmon, F., Szopa, S., Dulac, F., Collins, W., Ghan, S., Horowitz, L. W., Lamarque, J. F., Lee, Y. H., Naik, V., Nagashima, T., Shindell, D., and Skeie, R.: A 4-D climatology (1979-2009) of the monthly tropospheric aerosol optical depth distribution over the

- Mediterranean region from a comparative evaluation and blending of remote sensing and model products, *Atmos. Meas. Tech.*, 6, 1287-1314, doi:10.5194/amt-6-1287-2013, 2013.
- Nabat, P., Somot, S., Mallet, M., Sanchez-Lorenzo, A., and Wild, M.: Contribution of anthropogenic sulfate aerosols to the changing Euro-Mediterranean climate since 1980, *Geophys. Res. Lett.*, 41, 5605-5611, doi:10.1002/2014GL060798, 2014.
- Nabat, P., Somot, S., Mallet, M., Sevault, F., Chiacchio, M., and Wild, M.: Direct and semi-direct aerosol radiative effect on the Mediterranean climate variability using a coupled regional climate system model, *Clim. Dyn.*, doi:10.1007/s00382-014-2205-6, 2015a.
- Nabat, P., Somot, S., Mallet, M., Michou, M., Sevault, F., Driouech, F., Meloni, D., Di Sarra, A., Di Biagio, C., Formenti, P., Sicard, M., Léon, J.-F., and Bouin, M.-N.: Dust aerosol radiative effects during summer 2012 simulated with a coupled regional aerosol-atmosphere-ocean model over the Mediterranean, *Atmos. Chem. Phys.*, 15, 3303-3326, doi:10.5194/acp-15-3303-2015, 2015b.
- Nicolas, J., Mallet, M., Roberts, G., Denjean, C., Formenti, P., Fresney, E., Sellegri, K., Borgniez, G., Bourrienne, T., Pigué, B., Torres, B., Dubuisson, P., and Dulac, F.: Aerosol direct radiative forcing at a regional scale over the western Mediterranean in summer within the ADRIMED project: airborne observations compared to GAME simulations, *Atmos. Chem. Phys. Discuss.*, in prep. for this special issue, 2015.
- Noilhan, J. and Mahfouf, J.-F.: The ISBA land surface parameterisation scheme, *Global Planet. Change*, 13, 145-159, doi:10.1016/0921-8181(95)00043-7, 1996.
- Ortiz-Amezcuca, P., Guerrero-Rascado, J. L., Granados-Muñoz, M. J., Bravo-Aranda, J. A., Alados-Arboledas, L.: Characterization of atmospheric aerosols for a long range transport of biomass burning particles from canadian forest fires over the southern iberian peninsula in July 2013, *Optica Pura y Aplicada*, 47, 43-49, 2014.
- Otto, S., Bierwirth, E., Weinzierl, B., Kandler, K., Esselborn, M., Tesche, M., Schladitz, A., Wendisch, M., and Trautmann, T.: Solar radiative effects of a Saharan dust plume observed during SAMUM assuming spheroidal model particles, *Tellus B*, 61, 270-296, doi:10.1111/j.1600-0889.2008.00389.x, 2009.
- Pace, G., Meloni, D., and di Sarra, A.: Forest fire aerosol over the Mediterranean basin during summer 2003, *J. Geophys. Res.*, 110, D21202, doi:10.1029/2005JD005986, 2005.
- Pace, G., Di Sarra, A., Meloni, D., Piacentino, S., and Chamard, P.: Aerosol optical properties at Lampedusa (Central Mediterranean). 1. Influence of transport and identification of different aerosol types, *Atmos. Chem. Phys.*, 6, 697-713, 2006.
- Papadimas, C. D., Hatzianastassiou, N., Matsoukas, C., Kanakidou, M., Mihalopoulos, N., and Vardavas, I.: The direct effect of aerosols on solar radiation over the broader Mediterranean basin, *Atmos. Chem. Phys.*, 12, 7165-7185, doi:10.5194/acp-12-7165-2012, 2012.
- Papayannis, A., Balis, D., Amiridis, V., Chourdakis, G., Tsaknakis, G., Zerefos, C., Castanho, A.D.A., Nickovic, S., Kazadzis, S., and Grabowski, J.: Measurements of Saharan dust aerosols over the Eastern Mediterranean using elastic backscatter-Raman lidar, spectrophotometric and satellite observations in the frame of the EARLINET project, *Atmos. Chem. Phys.*, 5, 2065-2079, 2005.
- Papayannis, A., Amiridis, V., Mona, L., Tsaknakis, G., Balis, D., Bösenberg, J., Chaikovski, A., De Tomasi, F., Grigorov, I., Mattis, I., Mitev, V., Müller, D., Nickovic, S., Pérez, C., Pietruczuk, A., Pisani, G., Ravetta, F., Rizi, V., Sicard, M., Trickl, T., Wiegner, M., Gerding, M., Mamouri, R. E., D'Amico, G., and Pappalardo, G.: Systematic lidar observations of Saharan dust over Europe in the frame of EARLINET (2000-2002), *J. Geophys. Res.*, 113, D10204, doi:10.1029/2007JD009028, 2008.
- Pappalardo, G., Amodeo, A., Mona, L., Pandolfi, M., Pergola, N., and Cuomo, V.: Raman lidar observations of aerosol emitted during the 2002 Etna eruption, *Geophys. Res. Lett.*, 31, L05120, doi:10.1029/2003GL019073, 2004.
- Pappalardo, G., Amodeo, A., Apituley, A., Comeron, A., Freudenthaler, V., Linné, H., Ansmann, A., Bösenberg, J., D'Amico, G., Mattis, I., Mona, L., Wandinger, U., Amiridis, V., Alados-Arboledas, L., Nicolae, D., and Wiegner, M.: EARLINET: towards an advanced sustainable European aerosol lidar network, *Atmos. Meas. Tech.*, 7, 2389-2409, doi:10.5194/amt-7-2389-2014, 2014.
- Péré, J.C., Mallet, M., Pont, V., and Bessagnet, B.: Impact of aerosol direct radiative forcing on the radiative budget, surface heat fluxes, and atmospheric dynamics during the heat wave of summer 2013 over western Europe: A modelling study, *J. Geophys. Res.*, 116, D23119, doi:10.1029/2011JD016240, 2011.
- Pérez, C., Sicard, M., Jorba, O., Comerón, A., and Baldasano, J.M.: Summertime re-circulations of air pollutants over the north-eastern Iberian coast observed from systematic EARLINET lidar measurements in Barcelona, *Atmos. Environ.*, 38, 3983-4000, 2004.
- Pérez, C., Nickovic, S., Baldasano, J.M., Sicard, M., Rocadenbosch, F., Cachorro, V.E.: A long Saharan dust event

- over the western Mediterranean: Lidar, sun photometer observations, and regional dust modeling, *J. Geophys. Res.*, **111**, D15214, doi:10.1029/2005JD006579, 2006.
- Petzold, A., Onasch, T., Kebedian, P., and Freedman, A.: Intercomparison of a Cavity Attenuated Phase Shift-based extinction monitor (CAPS PMex) with an integrating nephelometer Climate and a filter-based absorption monitor, *Atmos. Meas. Tech.*, **6**, 1141–1151, 2013.
- Piazzola, J., Tedeschi, G., and Demoisson, A.: A model for a transport of sea-spray Aerosols in the coastal zone, *Boundary Layer Meteorol.*, **155**:329-350, 2015.
- Ramanathan, V., et al.: Indian Ocean experiment: An integrated analysis of the climate forcing and effects of the great Indo-Asian haze, *J. Geophys. Res.*, **106**, 28371–28398, doi:10.1029/2001JD900133, 2001.
- Ravetta, F., Ancellet, G., Colette, A., and Schlager, H.: Long-range transport and tropospheric ozone variability in the western Mediterranean region during the Intercontinental Transport of Ozone and Precursors (ITOP-2004) campaign, *J. of Geophys. Res.*, **112**, doi:10.1029/2006JD007724, 2007.
- Rea, G., Turquety, S., Menut, L., Briant, R., Mailler, S., and Siour, G.: Source contributions to 2012 summertime aerosols in the Euro-Mediterranean region, *Atmos. Chem. Phys. Discuss.*, **15**, 8191–824, doi:10.5194/acpd-15-8191-20, 2015.
- Renard, J.-B., et al.: LOAC: a small aerosol optical counter/sizer for ground-based and balloon measurements of the size distribution and nature of atmospheric particles – Part 1: Principle of measurements and instrument evaluation, *Atmos. Meas. Tech. Discuss.*, **8**, 1203-1259, doi:10.5194/amtd-8-1203-2015, 2015a.
- Renard, J.-B., et al.: LOAC: a small aerosol optical counter/sizer for ground-based and balloon measurements of the size distribution and nature of atmospheric particles – Part 2: First results from balloon and unmanned aerial vehicle flights, *Atmos. Meas. Tech. Discuss.*, **8**, 1261-1299, doi:10.5194/amtd-8-1261-2015, 2015b.
- Roger, J.C., Mallet, M., Dubuisson, P., Cachier, H., Vermote, E., Dubovik, O., and Despiiau, S.: A synergetic approach for estimating the local direct aerosol forcing: application to an urban zone during the Experience sur Site pour Contraindre les Modèles de Pollution et de Transport d’Emission (ESCOMPTE) experiment, *J. Geophys. Res.*, **111**, D13208, doi:10.1029/2005JD006361, 2006.
- Royer, P., Raut, J.-C., Ajello, G., Berthier, S., and Chazette, P.: Synergy between CALIOP and MODIS instruments for aerosol monitoring: application to the Po Valley, *Atmos. Meas. Tech.*, **3**, 893-907, doi:10.5194/amt-3-893-2010, 2010.
- Ryder, C. L., Highwood, E. J., Rosenberg, P. D., Trembath, J., Brooke, J. K., Bart, M., Dean, A., Crosier, J., Dorsey, J., Brindley, H., Banks, J., Marsham, J. H., McQuaid, J. B., Sodemann, H., and Washington, R.: Optical properties of Saharan dust aerosol and contribution from the coarse mode as measured during the Fennec 2011 aircraft campaign, *Atmos. Chem. Phys.*, **13**, 303-325, doi:10.5194/acp-13-303-2013, 2013.
- Saha, A., Mallet, M., Roger, J.C., Dubuisson, P., Piazzola, J., and Despiiau, S.: One year measurements of aerosol optical properties over an urban coastal site: Effect on local direct radiative forcing, *Atmos. Res.*, **90**, 195-202, doi:10.1016/j.atmosres.2008.02.003, 2008.
- Sanchez-Gomez, E., Somot, S., and Mariotti, A.: Future changes in the Mediterranean water budget projected by an ensemble of regional climate models, *Geophys. Res. Lett.*, **36**, L21401, doi:10.1029/2009GL040120, 2009.
- Salameh, T., Drobinski, P., Menut, L., Bessagnet, B., Flamant, C., Hodzic, A., and Vautard, R.: Aerosol distribution over the western Mediterranean basin during a Tramontane/Mistral event, *Ann. Geophys.*, **25**, 2271-2291, 2007.
- Santese, M., Perrone, M.R., Zakey, A.S., De Tomasi, F., and Giorgi, F.: Modeling of Saharan dust outbreaks over the Mediterranean by RegCM3: case studies, *Atmos. Chem. Phys.*, **10**, 133–156, doi:10.5194/acp-10-133-2010, 2010.
- Sassen, K.: Lidar backscatter depolarization technique for cloud and aerosol research, in *Light Scattering by Nonspherical Particles: Theory, Measurements, and Applications*, edited by Mishchenko, M., Hovenier, J.W., and Travis, L.D., Academic Press, 393-417, 1999.
- Schepanski, K., Tegen, I., Laurent, B., Heinold, B., and Macke, A.: A new Saharan dust source activation frequency map derived from MSG-SEVIRI IR-channels, *Geophys. Res. Lett.*, **34**, 18803, doi:10.1029/2007GL030168, 2007.
- Sciare, J., Cachier, H., Oikonomou, K., Ausset, P., Sarda-Estève, R., and Mihalopoulos, N.: Characterization of carbonaceous aerosols during the MINOS campaign in Crete, July–August 2001: a multi-analytical approach, *Atmos. Chem. Phys.*, **3**, 1743-1757, doi:10.5194/acp-3-1743-2003, 2003.
- Sciare, J., Oikonomou, K., Favez, O., Liakakou, E., Markaki, Z., Cachier, H., and Mihalopoulos, N.: Long-term measurements of carbonaceous aerosols in the Eastern Mediterranean: evidence of long-range transport of biomass burning, *Atmos. Chem. Phys.*, **8**, 5551–5563, doi:10.5194/acp-8-5551-2008, 2008.
- Schicker, I., Radanovics, S., and Seibert, P.: Origin and transport of Mediterranean moisture and air *Atmos.*

- Chem. Phys., 10, 5089–5105, doi:10.5194/acp-10-5089-2010, 2010.
- Schroeder, W., Csiszar, I., Giglio, L., and Schmidt, C. C.: On the use of fire radiative power, area, and temperature estimates to characterize biomass burning via moderate to coarse spatial resolution remote sensing data in the Brazilian Amazon, *J. Geophys. Res.*, 115, D21121, doi:10.1029/2009JD013769, 2010.
- Sellegrì, K., Rose, C., Culot, A., Sauvage, S., Roberts, G., Marchand, N., Pey, J., Sciare, J., Bourriane, T., Mallet, M., and Dulac, F.: Spatial extent, occurrence and precursors of nucleation events over the western Mediterranean basin, in prep. for publication in this special issue, 2015.
- Sellitto, P., di Sarra, A., Corradini, S., Boichu, M., Herbin, H., Dubuisson, P., Sèze, G., Meloni, D., Monteleone, F., Merucci, L., Rusaleem, J., Salerno, G., Briole, P., and Legras, B.: Synergistic use of Lagrangian dispersion modelling, satellite- and ground-based remote sensing measurements for the investigation of volcanic plumes: the Mount Etna eruption of 25-27 October 2013, *Atmos. Chem. Phys. Disc.*, submitted to this special issue, 2015.
- Sicard, M., Rocadenbosch, F., Reba, M. N. M., Comerón, A., Tomás, S., García-Vázquez, D., Batet, O., Barrios, R., Kumar, D., and Baldasano, J. M.: Seasonal variability of aerosol optical properties observed by means of a Raman lidar at an EARLINET site over Northeastern Spain, *Atmos. Chem. Phys.*, 11, doi:10.5194/acp-11-175-2011, 2011.
- Sicard, M., Bertolín, S., Mallet, M., Dubuisson, P., and Comerón, A.: Estimation of mineral dust long-wave radiative forcing: sensitivity study to particle properties and application to real cases in the region of Barcelona, *Atmos. Chem. Phys.*, 14, 9213–9231, doi:10.5194/acp-14-9213-2014, 2014a.
- Sicard, M., Bertolín, S., Muñoz, C., Rodríguez, A., Rocadenbosch, F., and Comerón, A.: Separation of aerosol fine- and coarse-mode radiative properties: Effect on the mineral dust longwave, direct radiative forcing, *Geophys. Res. Lett.*, 41, doi:10.1002/2014GL060946, 2014b.
- Sicard, M., Barragan, R., Muñoz-Porcar, C., Comerón, A., Mallet, M., Dulac, F., Pelon, J., Alados-Arboledas, L., Amodeo, A., Boselli, A., Bravo-Aranda, J. A., D'Amico, G., Granados-Muñoz, M. J., Leto, Guerrero-Rascado, J. L., Madonna, F., Mona, L., Pappalardo, G., Perrone, M. R., Burlizzi, P., Rocadenbosch, F., Rodríguez-Gómez, A., Scollo, Spinelli, N., Titos, G., Wang, X., and Zanmar Sanchez, R.: Contribution of EARLINET/ACTRIS to the summer 2013 Special Observing Period of the ChArMEx project, *Óptica Pura y Aplicada*, submitted, 2015a.
- Sicard, M., Barragan, Dulac, F., Alados-Arboledas, L., and Mallet, M.: Aerosol Aerosol optical, microphysical and radiative properties at three regional background insular sites in the western Mediterranean Basin, *Atmos. Chem. Phys. Discuss.*, submitted in this special issue, 2015b.
- Solmon, F., Giorgi, F., and Liousse, C.: Aerosol modelling for regional climate studies: application to anthropogenic particles and evaluation over a European/African domain, *Tellus*, 58B, 51–72, doi:10.1111/j.1600-0889.2005.00155.x, 2006.
- Solmon, F., Mallet, M., Elguindi, N., Giorgi, F., Zakey, A., and Konaré, A.: Dust aerosol impact on regional precipitation over western Africa: mechanisms and sensitivity to absorption properties. *Geophys Res Lett* 35, L24705, doi:10.1029/2008GL035900, 2008.
- Spada, M., Jorba, O., Pérez Garcia-Pando, C., Janjic, Z., and Baldasano, J. M.: Modeling and evaluation of the global sea-salt aerosol distribution: sensitivity to emission schemes and resolution effects at coastal/orographic sites, *Atmos. Chem. Phys.*, 13, 11735–11755, doi:10.5194/acp-13-11735-2013, 2013.
- Tafuro, A.M., Barnaba, F., De Tomasi, F., Perrone, M. R., and Gobbi, G. P.: Saharan dust particle properties over the central Mediterranean, *Atmos. Res.*, 81, 67–93, 2006.
- Tafuro, A. M., Kinne, S., De Tomasi, F., and Perrone, M. R.: Annual cycle of aerosol direct radiative effect over southeast Italy and sensitivity studies, *J. Geophys. Res.*, 112, D20202, doi:10.1029/2006JD008265, 2007.
- Tanré, D., Kaufman, Y. J., Herman, M., and Mattoo, S.: Remote sensing of aerosol properties over oceans using the MODIS/EOS spectral radiances, *J. Geophys. Res.*, 102, 16971–16988, 1997.
- Tanré, D., Bréon, F. M., Deuzé, J. L., Dubovik, O., Ducos, F., Francois, P., Goloub, P., Herman, M., Lifermann, A., and Waquet, F.: Remote sensing of aerosols by using polarized, directional and spectral measurements within the A-Train: the PARASOL mission, *Atmos. Meas. Tech.*, 4, 1383–1395, doi:10.5194/amt-4-1383-2011, 2011.
- Tegen, I., Harrison, S. P., Kohfeld, K. E., and Prentice, I. C.: Impact of vegetation and preferential source areas on global dust aerosol: Results from a model study, *J. Geophys. Res.*, 107, 4576, doi:10.1029/2001JD000963, 2002.
- Thieuleux, F., Moulin, C., Bréon, F. M., Maignan, F., Poitou, J., and Tanré, D.: Remote sensing of aerosols over the oceans using MSG/SEVIRI imagery, *Ann. Geophys.*, 23, 3561–3568, doi:10.5194/angeo-23-3561-2005, 2005.
- Torres, B., Dubovik, O., Fuertes, D., Lapyonok, T., Toledano, C., Schuster, G.L., Goloub, P., Blarel, L., Barreto, A., Mallet, M., and Tanré, D.: Advanced characterization of aerosol properties from measurements of spectral optical thickness of the atmosphere, in prep. for this special issue, 2015.
- Turco, M., Llasat, M.C., Tudela, A., Castro, X., and Provenzale, A.: Decreasing fires in a Mediterranean region

- (1970-2010, NE Spain), *Nat. Hazards Earth Syst. Sci.*, 13, 649-652, doi:10.5194/nhess-13-649-2013, 2013.
- Turquety, S., Menut, L., Bessagnet, B., Anav, A., Viovy, N., Maignan, F., and Wooster, M.: APIFLAME v1.0: high-resolution fire emission model and application to the Euro-Mediterranean region, *Geosci. Model Dev.*, 7, 587-612, 2014.
- Vaishya, A., Jennings, S. G., and O'Dowd, C.: Wind-driven influences on aerosol light scattering in north-east Atlantic air, *Geophys. Res. Lett.*, 39, L05805, doi:10.1029/2011GL050556, 2012.
- Valenzuela, A., Olmo, F. J., Lyamani, H., Antón, M., Quirantes, A., Alados-Arboledas, L.: Aerosol radiative forcing during African desert dust events (2005-2010) over Southeastern Spain, *Atmos. Chem. and Phys.*, 12, 10331-10351, 2012.
- Vialard, J., et al.: Cirene: Air-sea interactions in the Seychelles-Chagos thermocline ridge region, *Bull. Am. Meteor. Soc.*, 90, 45-61, doi:10.1175/2008BAMS2499.1, 2009.
- Wang, Y., Sartelet, K. N., Bocquet, M., Chazette, P., Sicard, M., D'Amico, G., Léon, J. F., Alados-Arboledas, L., Amodeo, A., Augustin, P., Bach, J., Belegante, L., Binietoglou, V., Bush, X., Comerón, A., Delbarre, H., García-Vízcaíno, D., Guerrero-Rascado, J. L., Hervo, M., Iarlori, M., Kokkalis, P., Lange, D., Molero, F., Montoux, N., Muñoz, A., Muñoz, C., Nicolae, D., Papayannis, A., Pappalardo, G., Preissler, J., Rizi, V., Rocadenbosch, F., Sellegri, K., Wagner, F., and Dulac, F.: Assimilation of lidar signals: application to aerosol forecasting in the western Mediterranean basin, *Atmos. Chem. Phys.*, 14, 12031-12053, doi:10.5194/acp-14-12031-2014, 2014.
- Waquet, F., Cornet, C., Deuzé, J.-L., Dubovik, O., Ducos, F., Goloub, P., Herman, M., Lapyonok, T., Labonnote, L.C., Riedi, J., Tanré, D., Thieuleux, F., and Vanbauce, C.: Retrieval of aerosol microphysical and optical properties above liquid clouds from POLDER/PARASOL polarization measurements, *Atmos. Meas. Tech.*, 6, 991-1016, doi:10.5194/amt-6-991, 2013.
- Wolke, R., Schroeder, W., Schroedner, R., Renner, E.: Influence of grid resolution and meteorological forcing on simulated European air quality: A sensitivity study with the modeling system COSMO-MUSCAT. *Atmos. Environ.*, 53, 110-130, 2012.
- Yue, X., Liao, H., Wang, H.J., Li, S.L., and Tang, J.P.: Role of sea surface temperature responses in simulation of the climatic effect of mineral dust aerosol, *Atmos. Chem. Phys.*, 11, 6049-6062, doi:10.5194/acp-11-6049-2011, 2011.
- Zakey, A. S., Solmon, F., and Giorgi, F.: Implementation and testing of a desert dust module in a regional climate model, *Atmos. Chem. Phys.*, 6, 4687-4704, 2006.
- Zakey, A. S., Giorgi, F., and Bi, X.: Modeling of sea salt in a regional climate model: Fluxes and radiative forcing, *J. Geophys. Res.*, 113, D14221, doi:10.1029/2007JD009209, 2008.
- Zanis, P., Ntogras, C., Zakey, A., Pytharoulis, I., and Karacostas, T.: Regional climate feedback of anthropogenic aerosols over Europe using RegCM3, *Clim. Res.*, V52, 267-278, doi:10.3354/cr01070, 2012.
- Zhu, A., Ramanathan, V., Li, F., and Kim, D.: Dust plumes over the Pacific, Indian, and Atlantic oceans: Climatology and radiative impact, *J. Geophys. Res.*, 112, D16208, doi:10.1029/2007JD008427, 2007.